An Experimental and Analytical Study of Laminar Dust Flame Propagation

By

MEHDI BIDABADI

Department of Mechanical Engineering
McGill University
Montreal, Quebec, Canada.

A thesis submitted to the
Faculty of Graduate Studies and Research
in partial fulfillment of the requirements for the degree of
Doctor of Philosophy.

January, 1995

ISBN 0-612-05673-2

Canada

Abstract

The fundamental properties of dust flame propagation have been studied experimentally and theoretically. Experiments were carried out in a Pyrex tube having a 5 cm inside diameter and a length of 1.2 meters. The dust dispersion system in the present experiment has been demonstrated to produce a laminar flow with uniform dust concentration. It is observed that the propagating flame exhibits a truly laminar character of propagation. Propagation and quenching of dust-air flames were measured for aluminum dust for a relatively wide range of dust concentration. It was observed that the process of the dust flame propagation in the tube can be divided into three different stages: laminar flame, oscillating flame and turbulent accelerating flame. During the first stage, the flame propagates with approximately constant speed and the flame is laminar. This stage is about 1/3 to 1/2 of the tube length and the shape of the flame front during this phase is close to the usual parabolic shape. In the second stage, flame starts to oscillate. Bright regular flashes alternate with stages when the flame is almost invisible. The third stage of the flame propagation can be observed only if the dust concentration is close to or higher than stoichiometric. The quenching distance and flame velocity of an aluminum dust flame under different initial oxygen concentrations and with different inert gases such as helium and nitrogen were also measured. When the amount of the initial oxygen concentration decreases, both the quenching distance and the lean limit increase, while the flame velocity decreases. On the other hand, after using helium as the inert gas of the mixture, it was observed that the whole value of the quenching distance, the lean limit, and the flame velocity increase. However, the objective is to understand the mechanism of the dust flame propagation. Theoretical models have also been developed to correlate the data to achieve a better understanding of the propagation mechanism of the dust flame. A relatively simple analytical model for aluminum dust flames was developed to predict quenching distance and burning velocity. Another model is presented to describe the combustion of organic dust, which can be used for predicting quenching distance. As a step towards the evaluation of the role of radiation on dust flame propagation, some mathematical calculation and discussion on the effect of radiation is presented. Finally, conclusions and recommendations for future study are presented, and the future direction of research is also indicated.

Résumé

Les propriétés fondamentales de la propagation de flammes dans la poussière ont été étudiées tant expérimentallement que théoriquement. Les expériences ont été faites dans un tube de Pyrex de 5 cm de diamètre interne et d'une longueur de 1.2 mètre. Il fut prouvé que le système de dispersion de la poussière utilisée produit un écoulement d'air laminaire d'une concentration de poussière uniforme. Il fut observé que la flamme propagée avait un caractère de propagation réellement laminaire. La propagation et l'extinction des flammes de poussière-air ont été mesureés pour la poussière d'aluminium pour une vaste gamme de concentrations de poussière. Il fut observé que le procédé de propagation de la flamme de poussière. Pouvait être divisé en trois différentes étapes: une flamme laminaire, une flamme oscillante et une flamme turbulente accélérate. Dans la première étape, la flamme se propage à une vitesse approximativement constante et la flamme est laminaire. Cette étape correspond à 1/3-1/2 de la longueur du tube et la forme du front de la flamme est très près de la parabole habituelle. Dans la deuxième étape, la flamme commence à osciller. De brillants et réguliers éclats lumineux alterent avec des périodes où la flamme est presque invisible. La troisième étape ne peut être observée que si la concentration de poussière est près ou supérieure à la concentration stoechiométrique. La distance d'extinction et la vitesse de la flamme de poussière d'aluminium avec différentes concentrations initiales d'oxygène et avec différents gas inertes ont été aussi mesurées. Lorsque la quantité initiale d'oxygène est réduite, la distance d'extinction et la limite pauvre augmentent tandis que la vitesse de la flamme baisse. D'autre part, après avoir utilisé de l'hélium comme gaz inerte dans le mélange, il fut observé que la valeur complète de la distance d'extinction, de la limite pauvre et la vitesse de la flamme augmente. Cependant, l'objectif est de comprendre le méchanisme de propagation de la flamme. Des modèles théoriques ont été développés pour trouver une corrélation des données et avoir une meilleure compréhension du mécanisme de propagation de la flamme. Un modèle relativement simple fut développé pour prédire la distance d'extinction et la vitesse de combustion de la flamme de poussière d'aluminum. Un autre modèle est aussi présenté pour décrire la combustion de poussière organique qui peut être utilisé pour la prédiction des distances d'extinction. Dans une optique d'étude sur le rôle de la radiation sur la propagation de flammes de poussière, quelques calculs mathématiques et une discussion sur l'effect de la radiation sont présentés. Finalement, les conclusions et des recommendations pour de futures études sont présentées et la direction future de la recherche est aussi indiquée.

Acknowledgments

The author wishes to express his sincere appreciation to his supervisor, Prof. John Lee. The successful completion of this thesis was due, in large part, to his constant encouragement and many useful suggestions which arose from discussions throughout the course of this research.

This work could not have been completed without the understanding and patience of my wife, and my children. Their sacrifices were great; my gratitude is profound.

The acknowledgments are further extended to Dr. Samuel Goroshin, for his continuous help and advice.

A special thanks goes to Ms Michele Shemie for her editorial comments, and Mr Jean-Francois Viau who supplied the French version of the Abstract.

The last, but not least, the financial support provided by the Iranian Ministry of Culture and Higher Education is highly appreciated. In addition, I would like to thank the Canadian Space Agency, whose financial support to the laboratory in which I worked made the research possible.

Table of Contents

List of Figures

Nomenclature

A	Parameter characterizing rate of vaporization of fuel particles (constant)
B	Frequency factor characterizing rate of gas phase oxidation of gaseous fuel
b	$= y_{Ff}/\varepsilon$, Scaled mass fraction of fuel on the boundary between the reaction zone and the convection zone
b'	Heat loss coefficient
C_F	Molar concentration of fuel
C_p	Heat capacity
C_s	Heat capacity of a fuel particle
d	Distance between quenching plates
d_{32}	Sauter diameter
d_i	Diameter of the particle for each class
d_p	Diameter of the particle
d_q	Quenching distance
d_u	Particle size at initial conditions
D	Diffusion coefficient, Dust concentration
E	Activation energy
K	Kinetic reaction speed
K_a	Absorption coefficient
K_s	Scattering coefficient
K_t	Total attenuation coefficient
k	Absorptive index
I	Radiation intensity
K_o	Rate constant of the solid-gas heterogeneous reaction
K_1	Defined in Eq. 3.26
$K_\pm$	Defined in Eq. 3.41
L	Path length
Le	Lewis number
m	The time attenuation coefficient
n	Real refractive index, Temperature exponent characterizing rate of vaporization of fuel particles
n_i	Number of particles for each class
n_p	Number of particles per unit of volume

$P(\theta,\Phi)$	Phase function
P_e	Peclet number
Q	Heat release per unit mass of solid fuel consumed
Q_a	Absorption efficiency
Q_{ext}	Extinction factor
Q_v	Heat associated with vaporizing unit mass of fuel
Q_L	External heat loss from the preheat vaporization zone
q_r	Radiation heat transfer
R	gas constant
r	Radius of fuel particle
S	Flame velocity
T	Temperature
T_f	Flame temperature
t	Time
T_{si}^u	Particle ignition temperature based on ambient oxygen concentration
v	Velocity
v_v	Burning velocity calculated including heat of vaporization of fuel particles
W_F	Molecular weight of gaseous fuel
w_v	Rate of vaporization of fuel particles(mass of gaseous fuel vaporized per unit volume per second)
w_F	Reaction rate characterizing consumption of gaseous fuel (mass of gaseous fuel consumed per unit volume per second)
x	Position
x'	Spatial coordinate
Y	Mass fraction
Y_{Fu}	Gaseous fuel available in the particles in the ambient reactant stream
y	Defined in Eqs. 3.12, and 4.30
Y_{o_2}	Oxygen mass concentration
$Y_{o_2}^u$	Initial oxygen mass concentration
Z_e	Zeldovich number
z	Scaled independent variable
Z_-	Defined in Eq. 3.40

Greek Symbols

α	$= Y_{Fu}/Y_{Fc}$, Thermal diffusivity of the gas
δ	Flame zone thickness , Characteristic physical dimension
ε	$= 1/Z_e$ Emissivity
σ	Fuel mass concentration , The Stefan-Boltzman
γ	Stoichiometric reaction coefficient
η	Parameter of heat loss
κ	Dimensionless burning velocity
θ	Dimensionless gas temperature
θ_s	Dimensionless particle temperature
λ	Thermal conductivity , Wave length
ρ	Density , refraction term
ρ_s	Density of solid particle
υ	Defined in Eq. 3.12
ϕ	Equivalence ratio
Φ	Dimensionless oxygen concentration
τ	Transmissivity
τ_c	Characteristic combustion time
μ	Dimensionless heat productivity

Subscripts

a	Absorption
ad	Adiabatic condition
b	Conditions after completion of chemical reaction
c	Conduction, Critical condition
F	Gaseous fuel
f	Flame zone
g	Gas
i	Ignition
p	Particle
pf	Post flame zone
ph	Preheat zone
u	Condition in the ambient reactant stream
$\circ$	Initial state
o_2	Oxygen
r	Radiation
s	Solid fuel, scattering
st	Stoichiometric condition
t	Total attenuation

IN THE NAME OF GOD

Chapter 1

1. Introduction

1.1 Introduction

At the turn of the century it was already known that clouds of organic or metallic dust could generate an explosion. There is an inherent danger of a dust explosion when combustible dusts are handled in industry [68]. Dust explosions occur in coal mines, in agricultural handling and processing facilities, and in wood, sugar, metal, paper, chemical, and rubber industries. The interest in dust explosions was rejuvenated occasionally when a few major explosions occurred over a short time. This occurred in December of 1977 when five major agricultural dust explosions occurred within eight days, in the United States.

The main dust research was coal dust arising from the need to prevent coal mine explosions. A main hazard in handling coal is the ability of coal dust suspensions to form self-sustaining explosions [70]. Typically the source of an explosion in a coal mine is a pocket of a flammable methane-air mixture being ignited by a spark, hot surface or some other ignition source. The pressure waves and resulting flow generated by such local explosions entrain dust from the floor and other surfaces and create a coal dust-air suspension. If the concentration of dust is high enough, the flame can propagate through the coal dust-air mixture and the result can be extensive damage to the mine equipment, and death or injury to miners at the site of flame passage.

Miners are still killed or injured in explosions in underground coal mines even in the present day. During the years' 1976-1985, about 3500 miners are reported to have been involved in explosions in coal mines underground worldwide [2]. In the period 1962 to 1980 there were 485 explosions and 715 fires reported in the United Kingdom which involved flammable dusts. These resulted in 26 fatalities and 639 injuries [3]. The United States Department of Agriculture reported 31 accidents under its jurisdiction in 1977, resulting in 65 deaths and 876 injuries. During the years 1970-1978 in Poland, there were more than 20 explosions in the food and textile industries, while more than 400 dust explosions occurred in the Federal Republic of Germany and its neighboring countries, during the years 1960-1972 [4].

A significant number of similar dust explosions still occur in facilities designed for handling, processing of grain, grain products, and in coal mines around the world every year. These explosions cause loss of human life, injury, property damage, and loss of business. Thus, an accurate knowledge of the dust flame propagation is of great practical importance in assessing the fire and explosion hazards posed by dust in mining, agricultural, chemical, pharmaceutical, storage, transportation and other industrial environments.

On the other hand, the bulk of energy production in the industrialized world comes from the burning of fossil fuels [71]. A large part involves the direct combustion of solid (e.g., coal) or heavy liquid (e.g., bunker oil). Such fuels are invariably burnt in atomized form. The large value of specific surface allows dust combustion to reach the heat release rate up to intensity of gas phase reaction.

Efficient and environmentally clean combustion necessitates a fundamental understanding of the underlying mechanisms of such heterogeneous combustion to model the burning processes adequately. This direction of study has rapidly grown during last decade.

The current level of physical understanding of dust combustion phenomena is in a rudimentary state compared with the understanding of gas combustion processes. The reason for such a lack of fundamental understanding of dust combustion process is the complexity associated with multiphase combustion, difficulties in experimental investigations, and the enormous diversity of chemical-physical properties of solid fuels.

The present research work is concerned with the study heterogeneous combustion to achieve a better understanding of flame propagation mechanisms of dust-air mixtures.

1.2 Review of Dust Flame Studies

1.2.1 Difficulties of Dust Combustion

There are numerous systems in practical situations involving more than one phase. Examples are solid dust suspensions in a gas or liquid, or liquid droplets in a gas or vapor. Organic and metallic solids in the form of very fine particles form an explosive dust suspension in air or oxygen. Experiments indicate that self-sustained combustion waves can propagate through a dust mixture. The thermodynamics and fluid mechanics of heterogeneous systems are very complex. The basic equations that describe the fluid dynamics of such heterogeneous systems are not well found. Even fundamental properties

and transport coefficients of these heterogeneous systems are not well known. The combustion of dust mixtures has been studied for many years to determine the fundamental characteristics of the dust flame [72-106]. However, relatively little fundamental information is available on the properties of these combustion waves and on their mechanisms of propagation.

There exists no clear idea on the mechanism of flame propagation in a dust air mixture. Researchers have tried to understand the role of fundamental processes occurring during combustion, such as: radiation, heterogeneous reaction, emission of volatile components, diffusion or heat conduction. Direct detailed investigation of the flame structure in a heterogeneous mixture is difficult. For these reasons the dust flame propagation mechanism has not been understood yet. For gas flames the mechanism of propagation is known to be controlled by thermal and molecular diffusion. Radiation has no influence on gas flame propagation. However, for dust flames the role of radiation is not clear. The details of equilibrium thermal radiation in a heterogeneous multi phase reaction is a complex physical process. However due to both experimental and theoretical difficulties in obtaining the role of radiation as a mechanism of dust flame propagation, the analogy is not complete, and thus the role of radiation is not yet completely elucidated.

One of the main problems in the study of heterogeneous dust air mixtures is the difficulty in generating a uniform stationary dust suspension whereby controlled experiments on the propagation of laminar dust flames can be carried out. In the bulk of the research effort on dust combustion, this uniform stationary suspension is invariably achieved in one of two ways. The first of these is via the burner-stabilized flame technique in which the dust is convected with the air stream and the flame is anchored on the burner lip. The second method involves a freely propagating flame in a predispersed dust air medium in which a turbulence field maintains the dust suspension.

For burner stabilized flames, severe limitations are imposed on the range of laminar burning velocities that can be achieved. The flow velocity in the burner must exceed the gravitational settling velocity of the particulate, yet must be within the range of the blow-off limit of the mixture. Moreover, the reaction length scale of dust flames is at least an order of magnitude larger than that for homogeneous gas flames making it necessary to increase the burner scale and hence the flow Reynolds number. This in turn limits the range of laminar flow conditions that can be obtained. It has been demonstrated that dust flames are extremely difficult to stabilize. This is due to the requirement of substantial heat losses from the flame to the flame stabilizer, thereby resulting in a highly non-adiabatic condition. In certain cases, it is found necessary to use a downward flow burner where buoyant convective preheating and mixing of the unburned mixture by the hot products further complicates the initial conditions

of the combustion process. It is therefore very evident that earthbound stabilized flames in dust air mixtures, in which gravitational settling plays a strong role, are far from being clean experiments of fundamental value.

In the freely propagating flame case, it is extremely difficult to achieve an initial uniform quiescent dust mixture since some form of turbulence must be associated with maintaining the dust in suspension. A strong turbulence field with a turbulent velocity fluctuation of the order of the settling velocity of the particulate is necessary to maintain a suspension. Therefore, the turbulence intensity required to maintain a uniform dust suspension is of the order of the sedimentation velocity. The scale of the turbulence fluctuation must also be of the order of the mean particle spacing, which is of the order of fractions of a millimeter. Thus, very intense small scale turbulence is required to maintain a uniform dust suspension. This is difficult to realize experimentally. Large scale turbulence will simply swirl the dust particles around, creating large concentration inhomogeneities.

The roles of turbulence in the heat and mass transport phenomena are complex. Even in homogeneous gas flames, the role of turbulence is not understood quantitatively. In heterogeneous mixtures, turbulence influences the dust concentration field in addition to the complex role it plays in the heat and mass transport. Dust particles tend to migrate in the acceleration field of the turbulent eddies and the dust stratifies. Thus, unlike a homogeneous gas mixture, the fuel and oxidizer in a heterogeneous mixture tend to get 'unmixed' even though the mixture is initially uniform. Heterogeneous dust flames are also less sensitive than gas flames because of the additional time scales involved in heat and mass transfer processes between the solid particles and the gas environment. Hence, the length scale of the combustion zone is much larger than that of gas flames. Burning velocities are also lower than gas flames enhancing the influence of buoyancy. Larger length scales and slower burning velocities result in a stronger dependence on the apparatus and boundary conditions. It is perhaps of importance to review the existing techniques of dust dispersion, so that the need to develop a proper method of generating a uniform dust suspension can be appropriated.

1.2.2 Techniques of Dust Dispersion

Unlike homogeneous gas combustion, well controlled "clean" experiments in heterogeneous combustion are extremely difficult to carry out in an earthbound gravitational environment, because of the difficulty in generating a uniform dust cloud due to gravity

sedimentation. In a dust-air mixture the air is in gas phase but the dust particles are in solid phase, thus are strongly influenced by the force of gravity. Therefore, to achieve a uniform dust suspension is a major concern to experimenters in this field.

One of the most common dispersion systems, used is the Hartmann tube, which consists of a mushroom deflector and a dispersion cup developed by the Bureau of Mines. There are also other widespread pressure systems; an 8 liter device with the dispersion cone system, 5, 10, and 20 liter spherical devices with dispersion nozzles or a dispersion cone system [11].

Another area in which knowledge of the dust air mixture is employed, involves the fluidized bed. Initially Pioneered in the 1960s by the European chemical industry for various thermochemical processes, a fluidized bed employs an upward moving gas stream to partially suspend a bed of small particles that tend otherwise to settle under gravity forces. The work of Greene et al [14] is an example of fluidized beds in a combustion application. In their experiment, coal dust was extracted from a fluidized bed and dispersed into the secondary air stream by means of a turbulent mixture, and the resulting coal dust-air mixture was then introduced into the conical transition section. Another recent example of the fluidized bed in a combustion application is the work of Proust and Veyssiere [9, 64], in which pulverized dust in particle form is concurrently fed into the bed within a square section vertical glass tube.

Another method that can give satisfactory uniformity of suspension is the free fall system used by Palmer et al [12], consisting of a hopper and a screw device to feed the dust at the top of a long combustion tube. But this method has some difficulties. The creation of dust air mixtures in the free fall system is followed by sedimentation, agglomeration and recirculating phenomena that will affect of the flame propagation after the mixture is ignited.

E.P.S. is another method for generating dust suspension using an electrostatic field [10, 16, 69]. The underlying principle is one of charge repulsion by the electrostatic Coulomb force. If dust of finite permitivity is placed on the positive electrode in a two electrode configuration, and a voltage is applied between the two electrodes, the dust will acquire a positive charge, will be repelled by the positive electrode and will migrate to the opposite (negative or ground) electrode. However the electrostatic field may have an influence on the combustion phenomenon.

No one dispersion system is exclusively superior to the others, each of them should satisfy their experimental requirements. Therefore, a good dispersion system is a system satisfying vessel configuration, ignition timing, turbulence, the aims of the particular research program and the dust to be tested.

1.3 Dust Flame Quenching Distance Studies

1.3.1 Scientific Motivation

The main impetus for dust explosion research came with the need of accidental dust explosions. Extensive research has been carried out by the Department of Interior Bureau of Mines [5-7] in the United States, to index the explosive hazard of different dusts, and to determine the influence of chemical and physical variables on the initiation of dust explosions. The appreciable differences among data from different test equipment used can be traced to the lack of a consistent theoretical basis for doing the experiments and for understanding the mechanism of dust flame propagation.

A knowledge of the dynamic parameters (such as the flame thickness, burning velocity, minimum ignition energy, the quenching distance, the flammability limits and others) provides a valuable insight into the basic mechanisms of flame propagation in the mixture itself. The flame thickness and the laminar burning velocity, even for homogeneous premixed gas flames are difficult to measure precisely. Great care must be exercised to eliminate curvature effects, the complex flow field in the unburned medium ahead of the flame and heat losses to the walls of burners or vessels that render the flame non-adiabatic.

For dust flames, where the flame thickness is expected to be an order of magnitude or greater than for premixed gas flames, these problems would be severely aggravated. The minimum spark energy for ignition of a heterogeneous mixture will be difficult to measure as well as to interpret, in a fundamental sense, when attempting to correlate with the basic properties of the mixture. A corresponding appropriate ignition spark for heterogeneous mixtures would require joules of energy and millisecond duration. This would introduce other transport and combustion phenomena into the ignition process leading to a very complicated phenomenon. It is therefore difficult to interpret the minimum ignition data since it will be strongly dependent on the spark discharge properties and the electrode geometry.

Flammability limits, even for a homogeneous gas mixture, are difficult to define, measure and interpret as a fundamental parameter. Thus the quenching distance is left, appearing to be the most ideal fundamental parameter to be determined for heterogeneous mixtures. Quenching distance as a fundamental parameter, is directly proportional to the flame thickness [8]. Thus knowledge of the quenching distance provides a fundamental length scale of the combustion phenomenon. Comparison of the quenching distance for dusts with and without volatiles, or with solids that react in the liquid or solid phase can elucidate

the detailed mechanisms of the flame zone. The quenching distance is also related to the minimum ignition energy since conceptually the inability to ignite means that the flame is quenched due to losses. Based on previous work [8-9], it is evident that quenching distance is a fundamental parameter that can be readily measured experimentally. Therefore in view of its fundamental significance and experimental accessibility, it is proposed that concerted efforts be made to obtain the quenching distance for a variety of dusts reliably and accurately.

1.3.2 Background of Dust Flame Quenching Distance Studies

There is very little experimental data on the quenching distance of dust flames. The little experimental data that is available are not in agreement with each other. This is mainly due to the difficulties and limitations of having a uniform dust suspension inside the quenching gap. The few data that are presently available are insufficient for meaningful correlation with the properties of the mixture to be made. Also there is no comprehensive theoretical model for predicting the dust flame quenching distance. For these reasons the dust flame propagation mechanism has not yet been understood.

In 1966, Singer *et al.* [13] measured the quenching distance for flames of hybrid mixture of methane and coal dust. They used a vertical, rectangular tube with varying cross section through which the hybrid mixtures can flow upward. When the flow is interrupted, the flames flash back and propagate downward until it is quenched at the appropriate tube cross section. They observed that the quenching distances of hybrid mixtures are greater than those of methane-air mixtures of the same overall stoichiometry. However they did not carry out quenching distance measurements for pure dust air mixtures. Measurements of the quenching distances of dust-air mixtures were also made by Greene *et al.* [14]. In their experiment, coal dust was extracted from a fluidized bed and dispersed into the secondary air stream by means of a turbulent mixture. The resulting coal dust-air mixture is then introduced into the conical transition section and when the flow is interrupted, the quenching diameter was observed. They measured the quenching distance of coal-air mixtures with particle size between 10 and 20 μm. They found the minimum quenching distances of Pittsburgh, Sewell and Pocahontas coal and Lignite to be 7, 8, 22, and 32 mm, respectively.

In the early eighties, Ballal [15, 18] also measured the dust flame quenching distances. The quenching distance as determined by Ballal corresponds to the spatial separation between two glass discs that the dust-air flame is extinguished by during minimum ignition energy measurements. He found the minimum quenching distances of coal, graphite,

aluminum and magnesium dust in air to be 5, 6, 4, and 2 mm, respectively. He also pointed out the strong similarity between the quenching distances of dust clouds and that for liquid fuel mists.

Another measurement of the quenching distance was made by Jarosinski *et al.* [8]. A large cylindrical tube, containing a set of steel quenching plates in the middle of it, was used. The quenching distance of the dust-air flame, for a particular quenching gap setting, was determined by varying the fuel-air composition until the extinction concentration was observed. They found that the minimum quenching distances are 5.5 mm for cornstarch, 10.4 mm for aluminum, 25.0 mm for coal of fine particles (less than 5 μm), and about 190 mm for coal with coarse particles (less than 70 μm). They also mentioned that because the order of magnitude of the measured quenching distances in cornstarch and aluminum dust flames are the same as in gas flames, it is inferred that the processes controlling propagation in these flames should be similar.

More recent measurements of the quenching distance were also reported by Proust *et al.* [9]. They measured the quenching distance of starch particles in air and they found that the minimum quenching distance is 7 mm. Their experimental apparatus has been designed for studying the propagation of dust-air flames in tubes where the dust suspension is generated by a fluidized bed. For the determination of quenching distances, a set of square stainless steel plates were mounted inside the tube similar to Jarosinski's experiment. The main result of their study had been to show that among the different possible processes by which a flame propagates in a dust suspension, a process very close to that of premixed gaseous mixtures is the most likely.

The results from different investigators using different methods are not in agreement. This is largely due to the numerous parameters that affect dust combustion, and which are difficult to control between laboratories. Jarosinski *et al* [8] found the minimum quenching distance of cornstarch to occur at a concentration to be 3.4 times the theoretical stoichiometric one. On the contrary, Proust *et al.* [9] found that the minimum quenching distance corresponds to stoichiometry. The lean flammability limit of cornstarch exhibited by Proust *et al.* [9] experiment is 70 g/m^3, while Jarosinski *et al* [8] found a value 5.5 times higher. Also Ballal's value [18] for the aluminum dust quenching distance is almost half of that reported by Jarosinski *et al* [8], while the particle size used in the experiment of Jarosinski *et al* [8] is less than that of Ballal's experiment [18].

1.4 Basic Considerations and Thesis Objectives

The present research work is concerned with the study heterogeneous combustion to achieve a better understanding of the flame propagation mechanism of dust-gas mixtures. The overall objective is to obtain fundamental, i.e. apparatus independent characteristics of laminar flame propagation, such as quenching distance, which can be used to identify the processes controlling flame propagation in dust-gas mixtures.

As it was mentioned before, one of the main difficulties of studying dust combustion is the generation of a uniform dust suspension. As a result, from the experimental point of view, the objective is preparing an apparatus which can generate a uniform dust cloud. Chapter two (section 2.2.1 and 2.2.2) demonstrate the overall experimental setup. The dependence of fundamental characteristics of dust combustion on the particle size is quite strong. Therefore, there is a need to have accurate information about particle size. Section 2.2.3 shows the results of particle size measurement. One of the most important parameters in dust combustion is accurately measuring the dust concentration. The procedure of the dust concentration measurement by the light extinctiometer and its calibration are explained in section 2.2.4.

There is very little experimental data on quenching distances of dust flames. The few data that are presently available are insufficient for meaningful correlation with the properties of the mixture. In the present study, it has been attempted to measure fundamental characteristics of laminar flame propagation such as quenching distance accurately. However, the objective of the experimental work is to measure quenching distance and flame velocity of aluminum dust flames under different initial oxygen concentration and different inert gases such as helium and nitrogen. The results of the experimental work are discussed in section 2.3.

The main purpose is to understand the mechanisms of dust flame propagation. Theoretical models have been developed to correlate the data, in order to achieve a better understanding of the propagation mechanism of the dust flame. As a result, from the theoretical point of view, the purpose of this work is to develop models to predict the quenching distance and burning velocity of dust flames. A relatively simple analytical model for aluminum dust flames is presented in chapter three, and the experimental and theoretical results are compared. In chapter 4, another model is presented to describe the combustion of organic dust, which can use for the prediction of quenching distance. As a step towards the evaluation of the role of radiation on dust flame propagation, some mathematical calculation

and discussion on the effect of radiation is presented in chapter 5. From the results of chapter 5, it can thus be seen that the effect of radiation may be significant even for a small scale flame, depending on the type of fuel burned. Finally, conclusions and recommendations for future study are presented in chapter six.

Chapter 2

2. Experimental Considerations

2.1 Introduction

In the present study a new experimental apparatus has been designed to produce a uniform dust suspension with a well controlled, stable dust concentration. The overall objective of the present study is to obtain fundamental, i.e. apparatus independent, characteristics of the laminar flame propagation such as quenching distance, which can be used to identify the processes controlling flame propagation in dust-air clouds.

2.2 Experimental Details

2.2.1 Overall Experimental Setup

The dust combustion setup consists of four major units (Fig. 1): dust dispersion system, combustion tube assembly, venting system and optical diagnostics with video and high speed filming cameras. The dispersion system of this experiment has demonstrated the ability to produce a uniform dust flow. This confirms that the general approach to the design of the dust dispersion system as a combination of two parts: dust feeder and disperser is correct. The dispersion process starts when the piston begins to move and the dust is exposed to a high speed jet from the slot at the top of the cylinder. The variation of the dust concentration in the producing flow can be achieved by changing the linear speed of the piston and by using different gas flow rates. The combustion tube assembly is shown in Fig. 1. The design permits safe observation of the dust flame as well as the measurement of the quenching distance. In order to determine quenching distance in the laminar mode of the

flame propagation a set of thin (0.25 mm thickness) evenly spaced stainless-steel plates was installed in the upper third part of the tube to form a grid aligned with the flow direction. The design also allows quick and easy replacement of this grid. The flame propagates in the Pyrex flame tube, 1.2 m long and 5 cm ID. The ignition system is a tungsten wire which is installed in the top of the tube, and the dust is ignited at the upper open end of the tube, operated from the control panel. After achieving a stable flame, the air flow dispersing the dust is cut off by a solenoid valve and the flame starts to propagate downward inside the tube in the quiescent dust cloud. The working quenching plates assembly with variable quenching distance is installed at the upper part of the tube. The venting system filters and vents of the dust flow and combustion products outside the laboratory, through a window. In this experiment, the pressure difference is supported by the standard 400 W vacuum cleaner. The ventilation duct is connected to the combustion tube by a hood at the top of the tube.

2.2.2 Experimental design

The general scheme of the apparatus is shown in Figs. 1 and 2. The specially designed dust dispersion system can produce a uniform dust stream for 2 to 9 minutes (depend on the desired concentration). The dispersing system consists of two components: dust feeder and disperser. The feeding of the dust is carried out by the piston-cylinder device (20 cm long and 2.5 cm internal diameter). The linear speed of the piston (the mass rate of the dust supply) is controlled by a special electro-mechanical system to be in a range of $0.02 - 0.2 \quad cm/s$. Dust is dispersed at the base of the conical chamber by the impact of the high speed jet flow (flow rate $200 - 700 \quad cm^3/\text{sec}$) venting through the 20 - 40 micron circular slot. The Pyrex flame tube is connected to the dispersion system by a conical diffuser (angle 8°).

2.2.3 Particle Size

For this research, Aluminum Ampal Dust, (Ampal 637;) has been tested. The scanning electron microscopic picture, Fig. 20, shows the fact that the aluminum particles are not exactly spherical in shape, as expected. For the purpose of basic quantitative measurements, this dust was not ideal since one would like to have truly spherical shaped dust

particles. The size distribution analysis of the particle sizes is shown in Fig. 19 for this aluminum powder. For obtaining the particle size, we use the Sauter diameter, which is defined by the following formula

$$d_{32} = \frac{\sum_i n_i d_i^3}{\sum_i n_i d_i^2} \tag{2.1}$$

where n_i is the number of particles for each class of diameter d_i in the dust sample. After doing some statistical process on the particles based on the Fig. 19, we find $d_{32} \approx 5.4\ \mu m$ for the above aluminum powder.

2.2.4 Dust Concentration

The results have always shown that the dispersion, the entertainment and the homogenization of the dust were a critical problem. Moreover, the design of an optimal dispersion system requires a perfect understanding of the mechanism of the initial stage of the dispersion. Therefore, there was a real need to study and monitor the dust dispersion during an experiment. To measure the concentration of the dust in the dust-air cloud in the present study, the dust concentration has been determined by the light extinctiometer using expanded laser beam (d=12 mm) crossing the dust flow along the diameter near the upper rim of the glass tube (Fig. 3). The light attenuation τ (opacity, $\tau = I/I_\circ$), measured with the probes, can be converted to particle concentration σ, by using the following relation [19]

$$\sigma = \frac{2\, d_p\, \rho_s}{3\, Q_{ext}\, L} Ln\left(\frac{1}{\tau}\right) \tag{2.2}$$

where, d_p, ρ_s, Q_{ext}, and L are particle diameter, density of the particles, extinction factor, and path length, respectively. The light extinctiometer is calibrated by aspiration of the dust from flow through the pile of Berkshire BM 112 type filters (Baxter, Canlab, 96% filtration efficiency for 0.5 μm particles) (Fig. 4). A disk sampler consists of a vacuum pump that samples air at a certain flow rate for several seconds. The air is passed through a filter on which the dust collects. The filter is held by suction of the vacuum pump with a strong piece of screening to keep the flow uniform. The quantity of dust collected is weighed and the air output measured by a rotameter. This gives the dust concentration per unit volume of air.

Experiments have shown that the pile of 5 filters can absorb about 95% of the flow's dust during 5 second. There was an average of 73% collected dust in the first layer, 12% in the second layer, 6% in the third layer, 3% in the fourth layer, and 2% in the fifth layer. The measurements have shown that the designed dispersing system can produce dust flow with a stable mass concentration in a wide range of dust concentration during 5-9 minute (Fig. 5).

2.3 Experimental Results

In the present experiments it was observed that in general, the process of the dust flame propagation in the tube can be divided into three different stages: laminar flame, oscillating flame and turbulent accelerating flame. During the first stage after ignition, the flame, and is laminar propagates with approximately constant speed. In this stage, the flame propagates through 1/3 to 1/2 of the tube length, with the flame front close to the usual parabolic shape. The second stage of the flame propagation begins at approximately the middle of the tube (or earlier at large concentrations). In this second stage the flame starts to oscillate. Bright flashes alternate regularly with stages when the flame is almost invisible. The frequency of the flame oscillations is close to the basic acoustic mode of the tube showing that the nature of the oscillations is acoustic coupling between the gas pulsation in the tube and the rate of the burning. This phenomena is well known and has been studied in gas combustion [48]. It was experimentally studied by Goroshin et al. [49] in dust combustion and was also reported by Berlad et al. [50] during micro gravity dust combustion experiments. The third stage of the flame propagation can be observed only if the dust concentration is close to or higher than stoichiometric. After propagating for about 20-50 cm in the regular oscillating regime with increasing pulsating amplitude, the flame suddenly starts to experience irregular fast pulsation, becomes turbulent and then undergoes rapid acceleration. In this mode, the flame speed at the end of the tube can well exceed, 10 m/sec.

The measured laminar flame speed of aluminum dust air mixtures as a function of dust concentration in the laminar mode of flame propagation is shown in Fig. 10. To obtain the burning velocity we have to divide the value of flame speed on the ratio of the flame surface to the tube cross sectional area. This ratio is approximately equal to 2 and seems to be constant for the different dust concentrations. The burning velocity obtained is close to those measured in a dust cloud formed from fine aluminum dust by Ballal [15] (micro gravity flame propagation in tubes) and by Cassel [51] and Goroshin [52] (stabilized Bunsen and flat dust flames).

For determining the quenching distances of each dust mixture quenching plates were installed in the upper part of the tube where the flame is steady and laminar. These plates allow us to study the flame quenching process in a stable, laminar mode of flame propagation. The high speed movie shows that when a flame with a parabolic shape approaches the quenching plates the flame front becomes almost flat. Far from the quenching limit the flame penetrates into all the quenching channels and propagates with the same speed in each channel. Sometimes several cycles of the flame pulsation can be seen inside the quenching plates, with a frequency of pulsation close to the basic tube acoustic mode. If the fuel concentration is close to the quenching limit the flame usually propagates only through the one channel that is closest to the tube axis. The quenching distance of aluminum dust air mixtures as a function of dust concentration is shown in Fig. 6.

In comparison with experimental data of the previous researchers, the minimum quenching distance reported in the present work is much lower. The present values are almost half of those reported by Jarosinski et al. [8], (the only direct experimental measurement of the quenching distance of aluminum dust clouds available in the literature). The data reported by Jarosinski are also shifted (in comparison with the measurements of this study) in the region of rich concentrations by 300 g/m^3 . The lean limit of the flame propagation reported by Jarosinski in the wide tube is approximately 400 g/m^3 (stoichiometric concentration of aluminum dust is 310 g/m^3). This data contradicts the value of the lower concentration limit for constant pressure aluminum dust combustion found by Balal [15] (160 g/m^3), which corresponds well to the value obtained in the present work (154 g/m^3). Because no direct dust concentration measurements were performed in Jarosinski's experiments, the dust concentration was calculated with the assumption that the entire mass of the dust in the dispersion device was perfectly dispersed and uniformly distributed throughout the combustion volume. Agglomeration and deposition of the dust on the walls of the combustion chamber during dispersion by the pulse air jets make this assumption inaccurate.

To observe the effect of initial oxygen concentration on the dust flame propagation, two sets of experiments, (16% and 11% oxygen in the initial mixture) were considered. Figures 7 and 8 show the dependence of the experimentally obtained quenching distance on the dust concentration for two different initial oxygen concentrations, 16% and 11%, respectively. When the amount of the initial oxygen concentration decreases, both the quenching distance and the lean limit increase (Fig. 9), but the flame velocity decreases (Figures 11, 12, and 13). The data may support that a lower value of initial oxygen concentration corresponds to a higher value of the combustion time. As a result, for a smaller amount of initial oxygen concentration, the quenching distance increases and the flame velocity decreases.

To investigate of the effect of a different inert gas on the dust flame propagation, tests were carried out using helium instead of nitrogen. Figures 14 and 16 show the dependence of the experimental values of quenching distance and flame velocity on dust concentration, using helium as the inert gas instead of nitrogen in the dust-gas mixture. From figures 15 and 17, it is observed that using helium as the inert gas of the mixture causes the quenching distance, the lean limit, and the flame velocity to increase. The main reason for these effects comes from the higher value of thermal diffusivity of helium in comparison to thermal diffusivity of nitrogen.

Chapter 3

3. Theoretical Considerations

3.1 Introduction

To model a dust combustion system, it is recognized that many simultaneously occurring processes are involved, namely particle oxidation, gas-phase homogeneous reaction, and mass, momentum and energy transport. It has been underlined various times in the literature that the main difference between flames in homogeneous and heterogeneous mixtures is the possibility of radiation heat transfer from the combustion to the preheat zone in dust cloud flames [9, 34, 66, 63, 67]. What is usually neglected is that different mechanisms of particle combustion in the flame zone can also make a strong difference. This is known because of two asymptotic regimes of particle combustion [37]. In the first case or so-called "kinetic regime", the single particle combustion burning rate is determined by the rate of heterogeneous (or homogeneous) reaction on (or near) the particle surface. In this case, the structure of the deflagration wave in the dust cloud does not greatly differ from that of homogeneous gas mixtures [38]. In the second case or the so-called "diffusion regime", it is assumed that the rate of reaction after ignition is controlled by the rate of oxygen diffusion from the surrounding gas to the particle surface (or to a zone close to the particle surface). Although the phenomenon of particle combustion in a dust flame can be in reality very complicated due to the fact that the reaction speed is controlled by diffusive mass exchange between the particle and the gas, this phenomenon can by itself be enough to predict several important consequences.

In the present model, after considering the diffusion regime for particle combustion, explicit algebraic equations are obtained for predicting the burning velocity of the flame as a function of the initial particle size, concentration and the external heat loss term. Quenching distances are obtained from the curve of variation of flame velocity at the points of stable and unstable solution.

3.2 Formulation

Combustion of metallic dust (aluminum in particular) is of interest in the present formulation. Very little detailed information has been reported to date on the combustion mechanism of aluminum particles in oxidizing atmospheres, and there is no universally accepted view point on the detailed mechanism of aluminum ignition. According to the ideas of several investigators, ignition occurs due to the heterogeneous reaction of liquid aluminum with the oxidant through an oxide film, while combustion takes place in the gas phase where aluminum vapor reacts with the oxidant [39]. In the present formulation, it is assumed that the combustion reaction occurs in the gas phase, forming a spherical diffusion flame around the fuel particle.

In the present formulation, a model of aluminum dust combustion is developed. A one-dimensional, two-phase combustible mixture consisting of uniformly distributed fuel particles in air is assumed to pass through a planar heat source, perpendicular to the flow direction. To model the external heat loss, it is assumed that the loss term is linearly proportional to the temperature. This represents loss through heat conduction from the dust-air mixture to the wall, which is assumed to be maintained at a constant upstream temperature. In the analysis, gradients of all dependent variables including that of the temperature and concentration in the direction parallel to the flame front are neglected. It is further assumed that the particle velocity is equal to the gas velocity.

The initial concentration and the initial particle size are presumed to be known. All external forces including gravitational effects are assumed to be negligible. Another approximation introduced is that the heat transport by radiation is negligible. In the analysis it is assumed that the chemical reaction that controls the combustion process is localized on or near particle surface.

The combustion process is modeled as a one-step overall reaction, with the rate constant written in the diffusion form. Figures 21 and 22 illustrate the presumed flame structures for lean and rich mixtures respectively. The assumed flame structure consists of a preheat zone, reaction zone, and convection zone for lean mixtures and a preheat and reaction zone for rich mixtures.

3.3 Governing Equations

For low Mach number flow, the governing equations can be written as follows:

Mass conservation:

$$\rho v = \text{const.} \tag{3.1}$$

Energy conservation:

$$\rho v C \frac{dT}{dx} = \lambda_u \frac{d^2T}{dx^2} + w_F \frac{\rho_u}{\rho} Q - \frac{b'\lambda}{d^2} \frac{\rho_u}{\rho} (T - T_u) \tag{3.2}$$

Oxygen conservation:

$$\rho v \frac{dY_{o_2}}{dx} = \rho_u D_u \frac{d^2Y_{o_2}}{dx^2} - \gamma_F^{-1} w_F \frac{\rho_u}{\rho} \tag{3.3}$$

Equation of state:

$$\rho T = \text{const.} \tag{3.4}$$

The independent variable x is related to the spatial coordinate x' as:

$$x = \int_0^{x'} \left(\frac{\rho}{\rho_u} \right) dx' \tag{3.5}$$

The reaction zone is presumed to be located at $x = 0$. The thermal conductivity of the mixture, λ, is proportional to T and the diffusion coefficient D is proportional to T^2. The heat capacity C appearing in Eq. 3.2 is the combined heat capacity of the gas, C_p, and of the particle, C_s, and can be evaluated from the expression

$$C = \begin{cases} C_p & \text{for} \quad \phi < 1 \\ C_p + \dfrac{\sigma C_s}{\rho} & \text{for} \quad \phi > 1 \end{cases} \tag{3.6}$$

where σ is mass fuel concentration. The reaction rate w_F appearing in Eqs. 3.2 and 3.3 can be written as

$$w_F = \begin{cases} \dfrac{\sigma}{\tau_c} & \text{for} \quad \phi < 1 \\ \dfrac{3}{2}\dfrac{\sigma}{\tau_c}\Phi & \text{for} \quad \phi > 1 \end{cases} \tag{3.7}$$

where Φ and τ_c are respectively: the ratio of oxygen concentration and the combustion time of an individual particle, which is assumed to have a weak dependence on temperature.

$$\Phi = \frac{Y_{o_2}}{Y^u_{o_2}} \tag{3.8}$$

$$\tau_c = \frac{r^2 \rho_s}{2 D \sigma_{st}} \tag{3.9}$$

The heat exchange between the particles and the gas in the preheat zone can be written as:

$$\left(\frac{4}{3}\pi r^3 \rho_s C_s\right) v \frac{dT_s}{dx} = \left(4\pi r^2\right)\frac{\lambda}{r}\frac{\rho_u}{\rho}\left(T - T_s\right) \tag{3.10}$$

with boundary conditions:

$$x = -\infty \qquad T = T_s = T_u;\ Y_{o_2} = Y^u_{o_2}$$

$$x = 0 \qquad T = T_i;\ T_s = T_{si}$$

$$x = +\infty \qquad T = T_u \tag{3.11}$$

3.4 Non dimensionalization of Governing Equations:

Non dimensional quantities:

$$\theta = \frac{T}{T_u}; \qquad \theta_s = \frac{T_s}{T_u}; \qquad y = \frac{x}{v_u \tau_c};$$

$$\kappa^2 = \frac{v^2 \tau_c}{\alpha}; \qquad Le = \frac{\alpha}{D}; \qquad \eta = b' \frac{\alpha \tau_c}{d^2};$$

$$\zeta = \frac{3}{2} \frac{Le}{\upsilon}; \qquad \upsilon = \frac{C_s \sigma_{st}}{C \rho}; \qquad \phi = \frac{\sigma}{\sigma_{st}};$$

$$\Phi = \frac{Y_{o_2}}{Y^u_{o_2}}; \qquad \mu = \frac{\sigma_{st} Q}{\rho C_p (T_{si} - T_u)} \tag{3.12}$$

The combustion time , τ_c, in these expressions is the combustion time of a single particle with heterogeneous surface reaction. The above dimensionless parameters have a clear physical meaning. The dimensionless flame speed κ is the ratio of combustion zone thickness to the thickness of preheat zone; η is the parameter of heat loss, which is the ratio of characteristic time of heat transfer in the channel to the particle combustion time; μ is the parameter that characterizes the heat productivity of combustion and is the ratio of maximum possible adiabatic temperature to the ignition temperature, etc. After applying the above dimensionless parameters, the final dimensionless governing equations can be written as follows:

$$\frac{d^2\theta}{dy^2} - \kappa^2 \beta_1 \frac{d\theta}{dy} = \kappa^2 \eta(\theta - 1) - \beta_2 \mu \phi \kappa^2 (\theta_{si} - 1) \tag{3.13}$$

$$\frac{d^2\Phi}{dy^2} - \kappa^2 Le \frac{d\Phi}{dy} = \beta_2 \phi \kappa^2 Le \tag{3.14}$$

$$\frac{d\theta_s}{dy} = \zeta(\theta - \theta_s) \tag{3.15}$$

where

$$\beta_1 = \begin{cases} 1 & \text{for} \quad \phi < 1 \\ 1 + \phi\upsilon & \text{for} \quad \phi > 1 \end{cases} \quad \text{and} \quad \beta_2 = \begin{cases} 1 & \text{for} \quad \phi < 1 \\ \frac{3}{2}\Phi & \text{for} \quad \phi > 1 \end{cases} \tag{3.16}$$

with boundary conditions:

$$y = -\infty \qquad \theta = \theta_s = \Phi = 1$$

$$y = 0 \qquad \theta = \theta_i ; \quad \theta_s = \theta_{si}$$

$$y = +\infty \qquad \theta = 1 \tag{3.17}$$

3.5 Lean Mixture:

It is considered that the flame propagates in a mixture with considerable oxygen excess (equivalence ratio less than one). For lean mixtures, we can distinguish three zones: preheat zone, reaction zone, and post flame zone. The first zone is preheat zone $(x < 0)$ where the temperature of particles is lower than the ignition temperature and the rate of reaction is equal to zero. The second zone is the reaction zone, $0 < x < v_u \tau_c$, where the particles burn in the diffusive regime, and the particle temperature remains approximately constant. It is assumed that all the heat produced by reaction goes directly to the combustion zone. The third zone is the post flame zone, $x > v_u \tau_c$, where the temperature of the combustion products decreases asymptotically to the ambient temperature at infinity. Because of oxygen excess, the decreasing of oxygen concentration in the flame is small and the combustion time of particles in the reaction zone is the same as that for a single particle under initial oxygen concentration. However, based on the above mentioned assumption for lean mixtures we have:

3.5.1 Preheat Zone:

$$\frac{d^2\theta}{dy^2} - \kappa^2 \frac{d\theta}{dy} = \kappa^2 \eta(\theta - 1) \tag{3.18}$$

$$\frac{d\theta_s}{dy} = \zeta(\theta - \theta_s) \tag{3.19}$$

Boundary conditions:

$$y \to -\infty \quad \Rightarrow \quad \theta = \theta_s = 1$$

$$y \to 0^- \quad \Rightarrow \quad \theta = \theta_i \,;\, \theta_s = \theta_{si} \tag{3.20}$$

3.5.2 Combustion Zone:

$$\frac{d^2\theta}{dy^2} - \kappa^2 \frac{d\theta}{dy} = \kappa^2 \eta(\theta - 1) - \mu\,\phi\,\kappa^2(\theta_{si} - 1) \tag{3.21}$$

Boundary conditions

$$y \to 0^+ \quad \Rightarrow \quad \theta^+ = \theta^- \,;\quad \left.\frac{d\theta}{dy}\right)_{0^+} = \left.\frac{d\theta}{dy}\right)_{0^-}$$

$$y \to 1^- \quad \Rightarrow \quad \theta^+ = \theta^- \,;\quad \left.\frac{d\theta}{dy}\right)_{1^+} = \left.\frac{d\theta}{dy}\right)_{1^-} \tag{3.22}$$

3.5.3 Post Flame Zone:

$$\frac{d^2\theta}{dy^2} - \kappa^2 \frac{d\theta}{dy} = \kappa^2 \eta(\theta - 1) \tag{3.23}$$

Boundary conditions:

$$y \to 1^{+} \quad \Rightarrow \quad \theta^{+} = \theta^{-}; \quad \left.\frac{d\theta}{dy}\right)_{1^{+}} = \left.\frac{d\theta}{dy}\right)_{1^{-}}$$

$$y \to 1 \quad \Rightarrow \quad \theta = 1 \tag{3.24}$$

Because of the linearity of the above differential equations, they can easily be solved and the eigenvalue combustion speed can be obtained by the term of continuity of the heat flux on the border between the combustion and preheat zones. The non-linear equation obtained for combustion speed can be written in the following form:

$$\frac{1}{\mu\phi} = \frac{\zeta}{K_1(\zeta + K_1)} \frac{1 - Exp(-K_1)}{\sqrt{1 + 4.\frac{\eta}{\kappa^2}}} \tag{3.25}$$

where

$$K_1 = \frac{\kappa^2}{2}\left(1 + \sqrt{1 + 4\frac{\eta}{\kappa^2}}\right) \tag{3.26}$$

From Eq. 3.25 the value of the equivalence ratio at the lean limit for the adiabatic condition can be obtained as $\phi = 1/\mu$. This equality is actually the expression for the condition of adiabatic flame temperature: $(T_{ad} - T_u) > (T_{si} - T_u)$. If T_{ad} goes to T_{si}, $(\phi \to 1/\mu)$ then the flame speed goes to zero.

3.6 Rich Mixture:

In the present study, it can be assumed that the particle radius is constant and the rate of diffusive combustion in rich mixtures is determined only by oxygen depletion in the reaction zone. On the other hand, because of the large value of combustion time, unlike in lean mixtures, there is no post flame zone in the rich mixture flame structure. The equation of heat and oxidizer transfer can be written in the following dimensionless form:

3.6.1 Preheat Zone:

$$\frac{d^2\theta}{dy^2} - \kappa^2(1+\upsilon\phi)\frac{d\theta}{dy} = \kappa^2\eta(\theta-1) \tag{3.27}$$

$$\frac{d\theta_s}{dy} = \zeta(\theta-\theta_s) \tag{3.28}$$

$$\frac{d^2\Phi}{dy^2} - \kappa^2 Le\frac{d\Phi}{dy} = 0 \tag{3.29}$$

Boundary conditions:

$$\begin{aligned} &y\to-\infty \quad\Rightarrow\quad \theta=\theta_s=\Phi=1 \\ &y\to 0^- \quad\Rightarrow\quad \theta=\theta_i\,;\,\theta_s=\theta_{si}\,;\,\Phi=\Phi_\circ \end{aligned} \tag{3.30}$$

3.6.2 Combustion Zone:

$$\frac{d^2\theta}{dy^2} - \kappa^2(1+\upsilon\phi)\frac{d\theta}{dy} = \kappa^2\eta(\theta-1) - \frac{3}{2}\mu\phi\kappa^2(\theta_{si}-1)\Phi \tag{3.31}$$

$$\frac{d^2\Phi}{dy^2} - \kappa^2 Le\frac{d\Phi}{dy} = \frac{3}{2}\phi\kappa^2 Le\Phi \tag{3.32}$$

Boundary conditions:

$$\begin{aligned} &y\to 0^+ \quad\Rightarrow\quad \theta^+=\theta^- \qquad ;\quad \left.\frac{d\theta}{dy}\right)_{0^+} = \left.\frac{d\theta}{dy}\right)_{0^-} \\ &\qquad\Rightarrow\quad \Phi^+=\Phi^-=\Phi_\circ\,;\quad \left.\frac{d\Phi}{dy}\right)_{0^+} = \left.\frac{d\Phi}{dy}\right)_{0^-} \end{aligned} \tag{3.33}$$

$$y\to+\infty \quad\Rightarrow\quad \theta=1\,;\Phi=0$$

The concentration of oxygen on the boundary between the preheat and reaction zones, Φ_*, could be considerably lower than the initial value and depends on the flame speed. Therefore, because of dependence of particle ignition temperature on the oxygen concentration, it is a function of combustion speed in rich mixtures. The particle ignition temperature with surface one step reaction is defined by the following equation [37]:

$$\frac{3\,Q\,E}{C\,R\,T_{si}}\frac{r\,\rho_s}{3\,\lambda}K_0\,Y_{o_2}^{\nu}\,Exp\left(-\frac{E}{RT_{si}}\right)=\frac{1}{e} \tag{3.34}$$

For ignition temperature under two different oxygen concentrations from Eq. 3.34, follows $(\nu=1)$:

$$\left(\frac{T_{si}}{T_{si}^u}\right)^2 Exp\left(\frac{E}{RT_{si}}-\frac{E}{RT_{si}^u}\right)=\frac{Y_{o_2}\big|_{\gamma=0}}{Y_{o_2}^u}=\Phi\big|_{\gamma=0}=\Phi_0 \tag{3.35}$$

If the temperatures T_{si} and T_{si}^u are not significantly different, we can use the exponential approximation of power function [47]:

$$\left(T_{si}/T_{si}^u\right)^2=e^2\,Exp\left(-2\,T_{si}^u/T_{si}\right) \tag{3.36}$$

and Eq. 3.35 takes a form:

$$\frac{\theta_{si}-1}{\theta_{si}^u-1}=\left(\frac{2\,T_{si}^u-\frac{E}{R}}{2-\frac{E}{RT_{si}^u}-Ln(\Phi_0)}-T_0\right)\left(\frac{1}{T_{si}^u-T_0}\right) \tag{3.37}$$

After solving Eq. 3.32 with its boundary condition in Eq. 3.33, the oxygen concentration on the boundary between the combustion and preheat zones will be obtained as:

$$\Phi_*=\frac{2}{1+\sqrt{1+6\frac{\phi}{\kappa^2\,Le}}} \tag{3.38}$$

The differential Eqs 3.27-3.33 are linear and again we can find the algebraic equation for flame speed by matching the solutions in each of zones on the boundary. The flame speed is:

$$\frac{3}{2}\mu\frac{\zeta}{\zeta+K_+}\frac{\theta_{si}-1}{\theta_{si}^u-1}=(K_+-K_-)(K_+-Z_-)(\kappa^2-Z_-)\left(\frac{\phi}{\kappa^2}\right) \tag{3.39}$$

where

$$Z_-=\frac{\kappa^2\,Le}{2}-\sqrt{\left(\frac{\kappa^2\,Le}{2}\right)^2+\frac{3}{2}\kappa^2\phi\,Le} \tag{3.40}$$

$$K_\pm=\frac{(1+\upsilon\phi)\,\kappa^2}{2}\pm\sqrt{\left(\frac{(1+\upsilon\phi)\,\kappa^2}{2}\right)^2+\kappa^2\eta} \tag{3.41}$$

The algebraic Eq 3.39 with expressions 3.37 and 3.38 do not include unknown parameters and completely define the rich fuel mixtures flame speed. However, the application of the above solution is limited from the side of very high values of fuel equivalence ratio. For very rich mixtures, the oxygen concentration on the border of preheat zones is so low that ignition does not lead to the full value of the stationary diffusive regime of particle combustion.

3.7 Ratio of Quenching Distance to Flame Thickness:

The flame thickness may be defined as follows:

$$\delta_f=\delta_p+\delta_c \tag{3.42}$$

where δ_p and δ_c are preheat zone thickness and combustion zone thickness respectively, and which can be obtained from the following expressions

$$\begin{aligned}\delta_p&=\alpha/v\\ \delta_c&=v_u\,\tau_c^*\end{aligned} \tag{3.43}$$

where

$$\tau_c^* = \begin{cases} \tau_c & \text{for} \quad \phi < 1 \\ (-Z_-)\tau_c & \text{for} \quad \phi > 1 \end{cases} \tag{3.44}$$

After applying the above equations 3.42-3.44 and η_c from Eq 3.12, it can be found that

$$\frac{d_q}{\delta_f} = \frac{\sqrt{b'/\eta_c}}{A\kappa + 1/\kappa} \tag{3.45}$$

where d_q is the quenching distance, and

$$A = \begin{cases} 1 & \text{for} \quad \phi < 1 \\ (-Z_-) & \text{for} \quad \phi > 1 \end{cases} \tag{3.46}$$

3.8 Results and Discussion

Typical numerical results that illustrate the effects of the principal parameters on the burning velocity and quenching distance are presented in this section. Consider a uniformly distributed cloud of aluminum fuel particles in air.

Calculations were performed with $\rho_s = 2707 \ \ kg/m^3$, $C_s = .896 \ \ kJ/(kg\,^\circ K)$, [41] $b' = 8$ [56], $\lambda_u = .02624 \ \ W/(m\,^\circ K)$, $\rho_u = 1.1774 \ \ kg/m^3$, $C_p = 1.0057 \ \ kJ/(kg\,^\circ K)$, $D_u = .206E-4 \ \ m^2/\text{sec}$, [44], $E/R = 21100\,^\circ K$, [43], $\tau_c/d_p^2 = 4E+6 \ \text{sec}/m^2$, [42], $T_{si}^u = 2200\,^\circ K$, [39], $Q = 30945 \ \ kJ/kg$, [40], $d_p = 5.4 \ \ \mu m$, and $T_u = 300\,^\circ K$.

At first the value of the heat loss term η is considered to be zero (adiabatic condition). The dimensionless flame velocity is calculated at adiabatic conditions and then calculations are performed for heat losses by increasing the value of η to its critical value. For each value of η the quenching condition is obtained from the curve of dimensionless flame velocity at stable and unstable solutions.

Figures 23 and 24 show the dependence of the dimensionless flame speed κ on the fuel equivalence ratio ϕ, for different values of heat loss parameters for lean and rich mixtures respectively. In the present results, similar to those of gas flame quenching [45-46, 55-61, 65] when the amount of heat loss is greater than zero, in general two values of flame speed are possible, however the lower one is unstable. The mechanism of flame quenching in a dust is

similar to that of homogeneous mixtures, i.e. feedback between the flame speed and the heat losses [47].

The burning velocity at different equivalence ratios is predicted numerically to determine the effect of particle concentration. Fig. 30 shows the experimental and theoretical results of the burning velocity. As it is seen, the predicted burning velocity does not correspond very well with the experimental value. It is lower than the experimental value. One reason for this discrepancy comes from the experimental evaluation of the burning velocity. To obtain the burning velocity, one must consider the effect of the flame surface area, which is difficult to measure accurately.

The dependence of the burning velocity on the particle size is quite strong. Experimentally, it is extremely difficult to sustain flame propagation in a suspension of large particle size. From the result of the burning velocity calculation, it is found that the burning velocity is lower than that of a methane gas flame. For larger particle size, the burning velocity is lower than that for smaller particle size. These results are due to the physical structure of the dust flame. The burning velocity of a dust-air mixture in the reaction zone is governed by the total surface area available within the reaction zone, which depends on the particle size. Small particles have more surface area per unit volume than larger ones, thus more fuel available in the reaction zone and consequently a higher value of burning velocity.

As mentioned above, the quenching condition occurs by definition at the critical point of the dimentionless flame velocity curve. As a result, for each value of equivalence ratio, the critical heat loss parameter can be obtained. The quenching distance at different equivalence ratios is predicted numerically to see the effect of particle concentration, and compared with the experimental value (Fig. 29). It is seen that the trend of both the experimental and theoretical curves are the same, and the quenching distance does not change for a relatively wide range of dust concentration. From the present model, it is clear that the weak dependence of the diffusive combustion rate on temperature can explain the phenomenon of weak dependence of quenching distance on dust concentration in a rich mixture.

From the results of the quenching distance calculation it is found that the quenching distance of a dust flame is greater than that of a methane gas flame. From the theory it can also be seen that for larger particle size, the quenching distance is larger than that of smaller particle size. These results are physically meaningful because the burning time of a dust flame is typically greater than the burning time of a gas flame. As well, the burning time of a large particle is greater than that of a smaller one. Also, a large value of burning time corresponds to a thicker flame, and as a result a larger value of quenching distance.

After calculating the quenching distance, from the ratio of quenching distance to flame thickness (Eqs. 3.45 and 3.46), it is found that the flame thickness is about one to two millimeters for a wide range of dust concentration $(300 \text{ to } 600 \ g/m^3)$.

The theoretical value of the lean flammability limit is obtained from the burning velocity curve(Fig. 30), as 68 g/m^3. This value is much lower than the experimentally obtained value of 157 g/m^3. The discrepancy is mainly due to the complexity of dust combustion. A more realistic numerical model that solves the balance equations for each of the gas and particle phases in the system should be adopted for a better estimation of the combustion characteristics.

Figures 25 and 27 show the dependence of the theoretically calculated quenching distance and burning velocity on dust concentration for different values of initial oxygen concentration in the mixture. When the initial oxygen concentration decreases, the quenching distance increases and the burning velocity decreases. These phenomena come from the effect of dimensionless heat productivity (μ) and combustion time (τ_c) on the quenching distance and the burning velocity. When the initial oxygen concentration decreases, heat productivity decreases and the combustion time increases. From the theory it can be seen that a small value of μ corresponds to a small value of the heat loss parameter (η) and dimensionless burning velocity (κ). Therefore from the definitions of quenching distance and burning velocity based on expressions of Eq. 3.12, it is found that smaller values of η and κ , and larger values of combustion time correspond to a larger value of quenching distance and smaller value of burning velocity.

Figures 26 and 28 show the dependence of the theoretical quenching distance and burning velocity on the dust concentration for two different inert gases, nitrogen and helium respectively. After changing the inert gas of the mixture, both the values of quenching distance and burning velocity change due to different values of mass diffusivity, thermal diffusivity, and combustion time. In the case of helium, the quenching distance increases, due to higher value of Lewis number (Le) and $\alpha \tau_c$ (where α is thermal diffusivity). The burning velocity also increases, due to a higher value of α/τ_c.

Chapter 4

4. Theory of Flame Quenching Distance for Organic Dust

4.1 Introduction

There is no comprehensive theoretical model for predicting the quenching distance in a dust flame. For this reason the dust flame propagation mechanism has not yet been understood. Recently, Seshadri *et al.* [53] successfully studied the structure of premixed particle-cloud flames based on a model that the particles vaporize completely and combustion occurs in the gas phase. His analysis was performed in the asymptotic limit, where the value of the characteristic Zeldovich number $\left(Z_e = E/RT_f\right)$ based on the gas phase oxidation of the gaseous fuel, is large, and values of $\phi_u > 1.0$, where ϕ_u is the equivalence ratio based on the fuel available in the fuel particles. In the present study, after following Seshadri's model, explicit algebraic equations are obtained for predicting the burning velocity of the flame as a function of the initial size, number density of the particles and the external heat loss term. Quenching distances are obtained from the curve of variation of flame temperature versus the external heat loss term.

4.2 Governing Equations

A one-dimensional, two-phase combustible mixture consisting of uniformly distributed volatile fuel particles in air is assumed to pass through a planar heat source located perpendicular to the flow direction. To model the external heat loss in the problem, it is assumed that the loss term is proportional to $\left(T - T_u\right)$. This represents loss via heat conduction from the dust-air mixture to the wall, which is assumed to be maintained at the constant upstream temperature $\left(T_u\right)$.

The assumed flame structure consists of a broad preheat-vaporization zone, a thin reaction zone, and a broad convection zone. For simplicity we also assume that external heat loss occurs only in the upstream region of $x_{-\infty}$ to 0 (preheat-vaporization zone). In the analysis it is assumed that the fuel particles vaporize to form a known gaseous compound which is then oxidized. Thus in the flame zone surface reactions are neglected. Seshadri [53] has formulated a mathematical problem for an adiabatic laminar dust flame and this formulation will be followed closely. The most important difference is the addition of a heat loss term to the energy equation.

It is assumed that the fuel and oxidizer reaction is described by an overall one-step reaction model. The rate constant of the overall reaction is written in the Arrhenius form and the characteristic Zeldovich number (Williams, [45]) is assumed to be large. The initial number density of the particles, n_u (number of particles per unit volume) and the initial radius, r_u , are presumed to be known. All external forces including gravitational effects are assumed to be negligible. Another approximation introduced is that heat transport via radiation is negligible.

Distinction is made between the quantities ϕ_u and ϕ_g, where ϕ_g is the effective gas phase stoichiometriy at the reaction zone. Analysis shows that even though $\phi_u > 1.0$, for certain cases the calculated value of ϕ_g is less than unity (Seshadri, [53]) due to incomplete vaporization. In the analysis it is presumed that the fuel particles vaporize to form a known gaseous compound that is then oxidized. Thus surface reactions are neglected in the present model. For simplicity it is assumed that the particle temperature is approximately equal to the gas temperature.

The analysis is primarily focused on those cases where the overall gas phase stoichiometry at the reaction zone is fuel lean. Consequently, excess oxygen would leak from the reaction zone into the convection zone. Since vaporization of the fuel particles can be expected to continue in the convection zone, chemical reaction will occur in this zone between the vaporized gaseous fuel and oxygen. Since the convection zone is presumed to be broad, the diffusive terms in the conservation equations are presumed to be small in comparison with the convective terms and the terms representing the gas phase chemical reaction and vaporization of the fuel particles. In the thin reaction zone the convective and vaporization terms are assumed to be small in comparison with the diffusive and reactive terms. The burning velocity is determined from analyzing the structure of this zone. However, the comments on these assumptions were generally discussed in the previous study by Seshadri [53].

Because of the particular assumptions that are considered, the following dust flame quenching distance formulation is useful for those kinds of dust particles that mainly consist of volatile components within the particle, such as organic dust.

For low Mach number flow, the governing equations can be written as follows:

Mass conservation:

$$\rho v = const. \tag{4.1}$$

Energy conservation:

$$\rho v c \frac{dT}{dx} = \lambda_u \frac{d^2T}{dx^2} + w_F \frac{\rho_u}{\rho} Q - w_v \frac{\rho_u}{\rho} Q_v - \frac{\rho_u}{\rho} Q_L \tag{4.2}$$

Gaseous fuel conservation:

$$\rho v \frac{dY_F}{dx} = \rho_u D_u \frac{d^2Y_F}{dx^2} - w_F \frac{\rho_u}{\rho} + w_v \frac{\rho_u}{\rho} \tag{4.3}$$

The equation governing the mass fraction of the particles:

$$\rho v \frac{dY_s}{dx} = -w_v \frac{\rho_u}{\rho} \tag{4.4}$$

Equation of state:

$$\rho T = const. \tag{4.5}$$

where:

$$w_v = A n_s 4\pi r^2 T^n$$

$$w_F = \nu_F M_F c_F B \exp(-E/RT) \tag{4.6}$$

$$c = c_p + \frac{4\pi r^3 c_s \rho_s n_s}{3\rho} \tag{4.7}$$

$$Q_L = K(T - T_u) \tag{4.8}$$

$$K = \frac{b'\lambda}{d^2} \tag{4.9}$$

The independent variable x is related to the spatial coordinate x' as

$$x = \int_0^{x'} \left(\frac{\rho_u}{\rho}\right) dx'$$

The boundary conditions are:

$$x = -\infty \qquad Y_F = 0,\ T = T_u,\ Y_s = Y_{FU} \tag{4.10}$$

$$x = 0 \qquad T = T_f < T_f' \tag{4.11}$$

$$x = +\infty \qquad Y_F = finite,\ T = T_b < T_b' \tag{4.12}$$

At the adiabatic condition we have:

$T_f = T_f'$ and $T_b = T_b'$

4.3 Non dimensionalization of Governing Equations

The non dimensional quantities:

$$\theta = \frac{T - T_u}{T_f - T_u}\ ;\ y_f = \frac{Y_F}{Y_{FC}}\ ;\ y_s = \frac{Y_S}{Y_{FC}}$$

$$m = \frac{\rho v}{\rho_u v_u}\ ;\ z = \frac{\rho_u v_u c}{\lambda_u} x \tag{4.13}$$

where

$$Y_{FC} = \frac{c}{Q}\left(T_f - T_u\right) \tag{4.14}$$

Introducing the definitions shown in Eq. 4.13 into Eqs. 4.1-4.4 and using 4.14 the following non dimensional equations are obtained

$m = const.$

$$m\frac{d\theta}{dz} = \frac{d^2\theta}{dz^2} + \omega\frac{\rho_u}{\rho} - q\ \gamma\ y_s^{2/3}\theta^n - \kappa\theta$$

$$m\frac{dy_f}{dz} = \frac{d^2y_f}{dz^2} - \omega\frac{\rho_u}{\rho} + \gamma\ y_s^{2/3}\theta^n \tag{4.15}$$

$$m\frac{dy_s}{dz} = -\gamma\ y_s^{2/3}\theta^n$$

where the radius r has been rewritten in terms of y_s using the relation $y_s = 4\pi\ r^3 n_s\ \rho_s\ \left(3\rho Y_{FC}\right)$ and for simplicity it is assumed that the Lewis number $\lambda/(\rho cD) = 1$. Also we define,

$$\omega = \frac{\lambda_u w_F}{\left(\rho_u v_u\right)^2 c Y_{FC}} \qquad \gamma = \frac{4.836 A n_u^{1/3}\lambda_u\left(T_f - T_u\right)^n}{v_u^2\rho_u^{4/3} c Y_{FC}^{1/3}\rho_s^{2/3}}$$

$$q = \frac{Q_v}{Q} \qquad \kappa = b' Pe^{-2} = \frac{b'\lambda\lambda_u}{\rho_u\rho v_u^2 c^2 D^2} \tag{4.16}$$

Boundary conditions for Eq. 4.15 are:

$$z = -\infty \qquad \theta = 0\ ;y_f = 0\ ;y_s = \alpha = \frac{Y_{FU}}{Y_{FC}}$$

$$z = 0 \qquad \theta = 1 \tag{4.17}$$

$$z = +\infty \qquad \theta = \theta_b = \frac{T_b - T_u}{T_f - T_u}\ ;y_f = finite$$

In the analysis, q, the ratio of the heat required to vaporize the fuel particles to the overall heat release in the flame, is presumed to be small. If θ° represents the non dimensionalized temperature for $q = 0$, then Eqs. 4.15 with $m = 1$ can be written as

$$\frac{d\theta^\circ}{dz} = \frac{d^2\theta^\circ}{dz^2} + \omega\frac{\rho_u}{\rho} - \kappa\theta^\circ$$

$$\frac{dy_f}{dz} = \frac{d^2y_f}{dz^2} - \omega\frac{\rho_u}{\rho} + \gamma y_s^{2/3}(\theta^\circ)^n \qquad (4.18)$$

$$\frac{dy_s}{dz} = -\gamma y_s^{2/3}(\theta^\circ)^n$$

Asymptotic solution to Eq. 4.16 will be obtained in the limit of $Z_e \to \infty$, with γ presumed to be of O(1).

4.4 Asymptotic Analysis

4.4.1 Preheat-Vaporization Zone With External Heat Loss

In the limit of $Z_e \to \infty$, chemical reaction between the gaseous fuel and oxidizer is negligible in the region where $z < 0$. Hence, the first expression in Eq. 4.18 yields to the leading order,

$$\frac{d\theta^\circ}{dz} = \frac{d^2\theta^\circ}{dz^2} - \kappa\theta^\circ \qquad -\infty < z < 0$$

$$\theta^\circ = 0 \text{ at } z = -\infty \quad \text{and} \quad \theta^\circ = 1 \text{ at } z = 0 \qquad (4.19)$$

For simplicity, after assuming $\kappa \neq \kappa(\theta^\circ)$, from integration the result:

$$\theta^\circ = \exp(\kappa' z) \qquad -\infty < z < 0 \qquad (4.20)$$

is obtained, where

$$\kappa' = \frac{1+\sqrt{1+4\kappa}}{2} \tag{4.21}$$

Introducing Eq. 4.20 into the third expression of Eq. 4.18 and integrating using the boundary condition shown in Eq. 4.17, yields

$$y_s = \left\{\alpha^{1/3} - a\ \exp(\kappa' nz)\right\}^3 \tag{4.22}$$

where:

$$a = \frac{\gamma}{3\kappa' n} \tag{4.23}$$

Introducing Eqs. 4.20 and 4.22 into the second expression of Eq. 4.18 and

$$\frac{dy_f}{dz} = \frac{d^2 y_f}{dz^2} + \gamma\left[\alpha^{1/3} - a\ \exp(\kappa' nz)\right]^2 \exp(\kappa' nz) \qquad -\infty < z < 0^-$$

$$\frac{dy_f}{dz} = 0\ ; y_f = 0 \quad at \quad z = -\infty \tag{4.24}$$

$$y_f = y_{Ff} \qquad at \quad z = 0^-$$

and integrating once between the limits $z = -\infty$, to $z = 0^-$ where the superscript - denotes conditions on the interface between the preheat vaporization zone and the reaction zone, yields the result

$$-\left[\frac{dy_f}{dz}\right]_{0^-} = \left(3a\alpha^{2/3} - 3a^2\alpha^{1/3} - y_{Ff}\right) \tag{4.25}$$

4.4.2 Convection Zone

The diffusive terms in the conservation equations are presumed to be of lower order than the convective-reactive and vaporization terms. Also, we assume that there is no heat loss term in this zone.

$$\xi = \varepsilon z \tag{4.26}$$

where, ε is a small quantity. It follows that at $z = 0^+$ the quantities $d\theta^\circ/dz$ and dy_f/dz are of order ε, where the superscript (+) denotes conditions at the interface between the convection zone and reaction zone. Thus

$$\frac{d\theta^\circ}{dz} = O(\varepsilon) \quad \text{and} \quad \frac{dy_f}{dz} = O(\varepsilon) \quad \text{at} \quad z = 0^+ \tag{4.27}$$

4.4.3 Reaction Zone

In the reaction zone the convective terms and the vaporization terms in the Eqs. 4.18 are assumed to be small in comparison to the diffusive terms and the reactive terms. Also it is assumed that there is no heat loss from this zone. Thus

$$\frac{d^2\theta^\circ}{dz^2} + \omega\frac{\rho_u}{\rho} = 0$$

$$\frac{d^2y_f}{dz^2} - \omega\frac{\rho_u}{\rho} = 0 \tag{4.28}$$

$$\frac{dy_s}{dz} = O(\varepsilon)$$

Boundary conditions for Eqs. 4.28 are:

$$\frac{d\theta^\circ}{dz} = 0 \; ; \frac{dy_f}{dz} = 0 \quad \text{at} \quad z = 0^+$$

$$\frac{d\theta^*}{dz} = \left[\frac{d\theta^*}{dz}\right]_{0^-} \qquad \text{at} \quad z = 0^- \tag{4.29}$$

To analyze the structure of this zone the expansions

$$z = \varepsilon\eta$$

$$y_f = \varepsilon(b + y) \tag{4.30}$$

$$\theta^* = 1 - \varepsilon t$$

are introduced, where $b = y_{Ff}/\varepsilon$ and $\varepsilon = 1/Z_e$ is the expansion parameter, which is presumed to be small. Now for obtaining the boundary conditions we introduce Eq. 4.30 into the first line of equation 4.29 :

$$\frac{dt}{d\eta} = \frac{dy}{d\eta} = 0 \qquad \text{at} \qquad z = 0^+ (or\ \eta \to +\infty) \tag{4.31}$$

From preheat zone we have:

$$\frac{dt}{d\eta} = -\kappa' \qquad \text{at} \qquad \eta \to +\infty \tag{4.32}$$

Now, introducing the expressions of Eq. 4.30 into the first and second expressions in Eq. 4.18 and using Eqs. 4.16 and 4.7 yields in the limit $\varepsilon \to 0$, the equations:

$$\frac{d^2t}{d\eta^2} = \Lambda(b + y)\exp(-t) \tag{4.33}$$

$$\frac{d^2(t - y)}{d\eta^2} = 0 \tag{4.34}$$

where the quantity Λ which is presumed to be of order unity is defined as

$$\Lambda = \frac{\nu_f \lambda_u B \varepsilon^2}{\rho_u v_u^2 c} \exp\left(-\frac{E}{RT_f}\right) \tag{4.35}$$

From Eqs. 4.34 and 4.31, it follows that $t = y$. Therefore Eq. 4.33 become

$$\frac{d^2t}{d\eta^2} = \Lambda(b+t)\ \exp(-t) \tag{4.36}$$

Boundary conditions for Eq. 4.37 are:

$$\begin{aligned} &\frac{dt}{d\eta} = 0 \qquad \text{at} \qquad \eta \to +\infty \\ &\frac{dt}{d\eta} = -\kappa' \quad \text{at} \qquad \eta \to -\infty \end{aligned} \tag{4.37}$$

After integration Eq. 4.36 and using the boundary conditions Eq. 4.37 yields the result

$$2(1+b)\Lambda = (\kappa')^2 \tag{4.38}$$

4.5 Evaluation of the Burning Velocity

Introducing Eq. 4.38 into Eq. 4.35 yields

$$v_u^2 = \frac{2(1+b)\nu_f \lambda_u B\varepsilon^2}{(\kappa')^2 \rho_u c} \exp\left(-\frac{E}{RT_f}\right) \tag{4.39}$$

Eq. 4.39 can be used to calculate v_u if b and T_f are known. To determine these quantities it is necessary to analyze the structure of the convection zone. For sufficiently high values of T_f, it is reasonable to set $y_{Ff} = 0$, which implies that $b = 0$. The value of T_f can be determined by requiring the gradients of θ° and y_f to satisfy the following jump conditions across the reaction zone

$$\left[\frac{d\theta^\circ}{dz}\right]_{0^+} + \left[\frac{dy_f}{dz}\right]_{0^+} = \left[\frac{d\theta^\circ}{dz}\right]_{0^-} + \left[\frac{dy_f}{dz}\right]_{0^-} \tag{4.40}$$

Introducing Eqs. 4.20 and 4.25 into Eq. 4.40 with $y_{Ff} = 0$, and assuming that the gradients at 0^+ are of order ε, yields

$$3a\,\alpha^{2/3} - 3a^2\alpha^{1/3} + a^3 - \kappa' = 0 \tag{4.41}$$

Eqs. 4.14, 4.39, and 4.41 can be used to calculate the quantities Y_{FC}, T_f and v_u. The quantities γ, κ' and a appearing in these equations can be calculated using Eqs. 4.16 and 4.23. Equation 4.39 shows that v_u is proportional to $\exp\left(-E/2RT_f\right)$. If v_u represents the calculated burning velocity including the influence of the heat of vaporization of the fuel particles, then v_u will be proportional $\exp\left(-E/2RT_{fv}\right)$, where $T_{fv} = T_f - q\left(T_f - T_u\right)$.Hence for a small q it follows that:

$$v_v = v_u\,\exp\left(-qZ_e/2\right) \tag{4.42}$$

4.6 Results and Discussion

A spatially uniform mixture of volatile fuel particles in air was considered. Sample calculations were performed assuming that the gaseous fuel that evolves from the fuel particle is methane. To illustrate the influences of external heat loss a previous study is followed [53] for various equivalence ratios and particle sizes. Numerical calculations were performed for values of $\phi_u > 1.0$, for a combustible mixture of fuel particles and air, where the fuel particles vaporize to yield methane. From the result of the calculation of ϕ_g. it is seen that although the value of ϕ_u is greater than unity, the corresponding value of ϕ_g is less than unity [53].

In order to compare the results of the present calculations with those of a previous study [53], the value of the heat loss term κ' is considered equal to one, representing an adiabatic condition. As a result, the calculated flame temperature and the flame velocity at adiabatic conditions are almost identical to those of the previous study [53]. After increasing the value of κ' to its critical value, the quenching condition is obtained. In Fig. 31 the calculated flame temperatures in the reaction zone, T_f, are plotted as a function of the equivalence ratio, ϕ_u, for the adiabatic condition.

From the results of the flame temperature calculation, it is found that the dust flame temperature is lower than that of methane gas flames. Also, the flame temperature is lower in clouds of larger particle size. The value of the flame temperature in the reaction zone is governed by the amount of gaseous fuel vaporized within the preheat zone. For constant ϕ_u, the amount of gaseous fuel that is vaporized depends on the particle size. For a constant value of dust concentration, smaller particles have more surface area per unit volume than larger particles, thus, more fuel is available in the reaction zone and consequently the value of the flame temperature is higher.

The same analysis can be done for the flame velocity. In Fig. 32 the values of the burning velocity, v_u, are plotted as a function of ϕ_u for adiabatic conditions. The burning velocity for $d_u = 20\mu m$ is typically about half the value for homogeneous gas flames and is in accord with experimental observations that dust flames are typically slower than gas flames. The dependence of the burning velocity on the particle size is quite strong. Experimentally, it is found that in suspensions of particles of diameter greater than $100\mu m$, it is extremely difficult to sustain flame propagation.

In Fig. 33, variation of the flame temperature as a function of heat loss is shown for $\phi_u = 2$ and for different particle size. It is seen that the flame temperature decreases with increasing heat loss, reaches a minimum at a certain value of κ' and then increases again. This is physically unacceptable, and thus as a result the quenching condition is defined to be at this critical point. On the basis of this critical value the quenching distance is obtained. The critical value of the heat loss term increases with increasing particle size. The quenching distance is roughly proportional to the heat loss term, and therefore increasing the value of the heat loss term corresponds to an increase in the quenching distance. The results of quenching distance calculations are plotted in Fig. 34 for different particle sizes as a function of ϕ_u. This figure shows that for a given value of ϕ_u the quenching distance decreases with decreasing value of particle size. It will approach the value of a purely gaseous combustible mixture in the limit where the particle size goes to zero.

For comparing the results of the calculation with the experimental data of the quenching distance of methane at stoichiometric conditions, the quenching distance was obtained for the smallest value of the particle size. This value of quenching distance is $1.7mm$ and it is comparable with the experimental value of $2mm$ [54]. From the result of the quenching distance calculation it can be found that the quenching distance of dust flames is greater than that of gas flames. Also quenching distance is larger in dust flames of larger particle size. This result is physically acceptable because the burning time of a dust flame typically is greater than the burning time of gas flame. As well, the burning time of a large

particle is greater than that of a small one. A large value of burning time corresponds to a thicker flame, and as a result a larger value of quenching distance.

Chapter 5

5. The Role of Radiation in Premixed Laminar Dust Flames

5.1 Introduction

Light scattering by particles has received considerable attention in such diverse fields as "astrophysics, meteorology, physics, colloid chemistry, and dust combustion." [36]. Radiation in dust-air mixture such as coal combustors is one example of a wide class of problems in which the radiative heat transfer is occurring in an absorbing medium. Where multiple scatter is important within such a scattering-absorbing medium, the intensity of radiation is a function of position and direction.

It must be realized that scattering by real coal particles is much more complex than can realistically be calculated. For radiative heat transfer in dust combustion, several coefficients and parameters must be defined. Some of these parameters are fundamental definitions, others involve experimental coefficients which are obtained from data of various properties of the materials.

The complexities of the radiative heat transfer process in dust air mixtures are due mainly to the participating medium. In general, the system in combustors and gasifiers consist of non uniform, emitting, absorbing, reflecting, solid surfaces that are in complex geometrical configurations and surround a multi phase, nonuniform, emitting, absorbing, transmitting, scattering particle laden fluid that is also generating heat. The problem of finding the equilibrium conditions at every point in this system is complex.

In addition to the mathematical difficulty, one of the more serious problems is the lack of knowledge of the radiative properties of the materials involved in the system. For example, fundamental radiative properties of coal particles exist for only a very few selected coal types. Further, the properties of the particles are changing as they undergo chemical reaction, changing from mostly carbon particles to mostly ash.

The complete solution to Maxwell's equations discussed so far (Mie theory) is only applicable to spherical particles of constant composition. It is obvious that many assumptions have to be made to include radiative heat transfer in a dust combustion application[1]. In practice any kind of dust contains a range of particle sizes of different geometry and shape. Due to many difficulties, both experimental and theoretical, obtaining the role of radiation as a mechanism of dust flame propagation, and the role of radiation, is not yet completely elucidated.

In the present formulation, after following the thermal theory of premixed laminar dust flame propagation, some mathematical relationships are obtained for evaluating the role of radiation. For obtaining the role of radiation, $f = \Delta T_c / \Delta T_r$ is defined. This is the general expression for the ratio of heat transfer by conduction to that of radiation from the flame zone to the preheat zone.

5.2 Energy Equation:

A one-dimensional, laminar, combustible mixture consisting of uniformly distributed, spherical and monodisperse fuel particles in air is assumed. To write the energy equation through the preheat zone, it is assumed that no chemical reaction occurs and there is no temperature difference between the particles and gas. It then follows that:

$$\rho C_p \frac{dT}{dt} = \frac{d}{dx}\left(\lambda \frac{dT}{dx}\right) + q_r(t) \tag{5.1}$$

where

$$\rho C_p = \sigma C_{p_p} + \rho_g C_{p_g} \tag{5.2}$$

The above differential equation is a function of both space and time. As they have to be solved simultaneously, it is convenient to reduce it to a function of time only. As the system is in steady state, we may write:

$$\frac{d}{dx} = \frac{d}{dt}\frac{dt}{dx} = \frac{1}{S}\frac{d}{dt} \tag{5.3}$$

and if λ is constant, Eq. 5.1 becomes

$$\rho C_p \frac{dT}{dt} = \frac{\lambda}{S^2}\frac{d^2T}{dt^2} + q_r(t) \tag{5.4}$$

5.3 Radiation Intensity

The general equation of radiation transfer is

$$\frac{dI}{dx} = +K_a I + K_s I - K_a I_b - \frac{K_s}{4\pi}\int_{4\pi} I(\Omega)P(\theta,\Phi)d\Omega \tag{5.5}$$

All quantities are positive in this equation since I decays in the negative x direction. However, due to the integral differential nature of the equation of radiative transfer, the equation does not lend itself well to solution by numerical methods consistent with the methods used to solve for the fluid mechanics and chemistry of combustion. The main area of difficulty in the above equation is the last term on the right-hand side. This term is in integral form and must be reduced to a differential form to simplify the problem. The above equation is an integral-differential equation generally known as the transport equation. The integral term in the above equation introduces the contribution of multiple scattering. If we assume negligible multi-scattering contribution and emission of the medium along the path length within the preheat zone, only absorbed energy flux is converted into stored internal, thus

$$q_r = K_a I \tag{5.6}$$

where

$$K_a = K_{ag} + K_{ap} \tag{5.7}$$

The absorption coefficient K_{ag} may be related to the particle size (of diameter d_p), and to particle density (by number n_p); we assume that the fractional absorption of monotropic radiation passing through a very thin element of the cloud is the ratio of projected solid area of particles to the total area of the containing element. We then have for the absorption coefficient:

$$K_{ap} = \frac{3}{2} Q_a \frac{\sigma}{\rho_p d_p} \tag{5.8}$$

Where, Q_a, is absorption efficiency, and it depends on the three dimensionless quantities: (I) the complex refractive index $[n - ki]$, (II) the ratio of the characteristic particle dimension to wave length of radiation which is sometimes called the particle size parameter $(\pi d/\lambda)$, (III) a particle shape, (see next Section).
For obtaining K_{ag} , we can use Eq. 5.5. For gas, it is known that:

$$\frac{dI}{dx} = -K_{ag} I \tag{5.9}$$

After integrating, we obtain

$$\frac{I}{I_o} = e^{-K_{ag}\delta} = \tau_g \tag{5.10}$$

In general,

$$\alpha + \rho + \tau = 1 \tag{5.11}$$

We know for gas, $\rho \approx 0$, and $\alpha \approx \varepsilon$, emissivity; therefore

$$\varepsilon_g = 1 - \tau_g = 1 - e^{-K_{ag}\delta} \tag{5.12}$$

or

$$K_{ag} = -\frac{1}{\delta} Ln\left(1 - \varepsilon_g\right) \tag{5.13}$$

After using Eqs. 5.13 and 5.8, Eq. 5.7 will be

$$K_a = -\frac{1}{\delta} Ln\left(1 - \varepsilon_g\right) + \frac{3}{2} Q_a \frac{\sigma}{\rho_p d_p} \tag{5.14}$$

Now, for obtaining radiation intensity as a function of distance (or time), we can use Eq 5.5. If we can assume that the second and third term in Eq 5.5 are negligible, we will obtain:

$$\frac{dI}{dx} = +K_t I \tag{5.15}$$

where

$$K_t = K_a + K_s \tag{5.16}$$

and

$$K_s = \frac{3}{2} Q_s \frac{\sigma}{\rho_p d_p} \tag{5.17}$$

Where Q_s is the scattering efficiency (see next section). After using Eq. 5.3, we will have

$$\frac{dI}{dt} = +K_t S I \tag{5.18}$$

$$= mI \tag{5.19}$$

where

$$m = K_t S \tag{5.20}$$

Because the time-attenuation coefficient m is independent of space and time, Eq. 5.19 may now be integrated independently. Taking limits; $I = I$ at $t = t$; and $I = I_f$ at $t = 0$, we get

$$I = I_f e^{mt} \tag{5.21}$$

After substituting Eq. 5.21 into Eq. 5.6, we get

$$q_r = K_a I_f e^{mt} \tag{5.22}$$

$$= \frac{K_a}{K_t} \frac{m}{S} I_f e^{mt} \tag{5.23}$$

It is clear that for obtaining K_a and K_t, one must know Q_a and Q_t (or Q_s). Therefore in the next section, some basic principles for obtaining absorption and scattering efficiencies will be shown.

5.4 Absorption and Scattering Efficiencies

The formal solution of the problem of light scattering by homogeneous spheres of arbitrary radius was worked out by Mie (1908) [19]. The interaction of a particle with radiation incident upon it depends on three dimensionless quantities: (I) the complex refractive index; (II) the ratio of characteristic particle dimension to wavelength of radiation which is sometimes called the particle size parameter; and (III) a particle shape. The relationship among these three particle parameters and the incident radiation may be determined by solving Maxwell's equations with the appropriate boundary conditions corresponding to the different particle parameters [19]. In practice, such solutions are only available for a very limited number of particle parameters. However, the scattering properties of a sphere of diameter d_p for plane polarized radiation of wavelength λ may be determined in terms of the parameters [20]

$$\alpha = \pi d/\lambda \tag{5.24}$$

$$m = n - ik = \sqrt{K - 2i\sigma\lambda/c} \tag{5.25}$$

The complex index of refraction is the sole physical parameter which determines the absorption and scattering of an electromagnetic wave by a spherical particle with a given ratio of radius to wavelength. In the above equation, n and k are respectively the refractive and absorptive indices. The magnitude of the complex part of the complex refractive index (k), is an indication of the absorption strength of the material while the real part (n) is a measure of it scattering ability [24]. K is the dielectric constant and σ is the electrical conductivity of the particle material (For example, for graphite $\sigma = 1.2E15(Sec)^{-1}$ and $K = 2$, [20]), and c is the velocity of light, equal to $2.99793E10(Cm/s)$, [20] and α is the dimensionless size parameter.

After definition of the following quantities which may be computed from the Mie theory:

C_{sca} =cross-section for removal of incident energy from forward beam by scattering. (5.26)

C_{abs} =cross-section for removal of incident energy by true absorption. (5.27)

The above cross section not only depends upon the particle size, but upon the material of the particle body and state of the radiation (i.e. wavelength, polarization, coherence [1]). In addition, we define efficiency factors as:

$$Q_{sca} = C_{sca} \Big/ \pi \frac{d^2}{4}$$
$$Q_{abs} = C_{abs} \Big/ \pi \frac{d^2}{4} \qquad (5.28)$$
$$Q_{ext} = Q_{sca} + Q_{abs}$$

With the above efficiency factors for absorption and scattering coefficients, the problem of obtaining the proper coefficients for any of the above mentioned models is reduced to obtaining absorption and scattering efficiencies for all particles of interest to the dust combustion. These coefficients are based on properties of the surface and molecules themselves. The optical properties for the particulate involved in the dust combustion can be obtained from a solution of the Maxwell equations based on Mie theory if the refractive index of the particle is known [1]. The Mie formula give us

$$Q_{sca} = \frac{2}{\alpha^2} \sum_{n=1}^{\infty} (2n+1) \left[|a_n|^2 + |b_n|^2 \right] \qquad (5.29)$$

$$Q_{ext} = \frac{2}{\alpha^2} \sum_{n=1}^{\infty} (2n+1) \mathrm{Re}(a_n + b_n) \qquad (5.30)$$

where

$$a_n = \frac{\alpha \psi_n'(\beta) \psi_n(\alpha) - \beta \psi_n'(\alpha) \psi_n(\beta)}{\alpha \psi_n'(\beta) \zeta_n(\alpha) - \beta \zeta_n'(\alpha) \psi_n(\beta)} \qquad (5.31)$$

$$b_n = \frac{\beta \psi_n'(\beta) \psi_n(\alpha) - \alpha \psi_n'(\alpha) \psi_n(\beta)}{\beta \psi_n'(\beta) \zeta_n(\alpha) - \alpha \zeta_n'(\alpha) \psi_n(\beta)} \qquad (5.32)$$

with

$$\beta = m\alpha \tag{5.33}$$

The function $\psi_n(z)$, $\zeta_n(z)$ occurring in Eqs. 5.31 and 5.32 are the Riccati-Bessel functions defined in terms of J_n as follows:

$$\psi_n(z) = \left(\frac{\pi z}{2}\right)^{\frac{1}{2}} J_{n+\frac{1}{2}}(z) \tag{5.34}$$

$$\zeta_n(z) = \left(\frac{\pi z}{2}\right)^{\frac{1}{2}} \left[J_{n+\frac{1}{2}}(z) + i(-1)^n J_{-n-\frac{1}{2}}(z) \right] \tag{5.35}$$

where $J_{n+\frac{1}{2}}$ and $J_{-n-\frac{1}{2}}$ are Bessel function of the positive and negative half-orders.

Some physical significance can be attached to the amplitude functions a_n and b_n . a_1 and b_1 represent the contributions of electric dipoles respectively. a_2 and b_2, the contributions of the electric and magnetic quadrupoles, and the higher values of m the contribution of the corresponding multipoles [21]. For small non magnetic particles, only a_1 is significant and gives a solution identical to the Rayleigh equation, but as the particle size is increased the higher values of m contribute significantly. Therefore for small particle size, Eqs. 5.29 and 5.30 can be written as follows [19]:

$$Q_s = \frac{8}{3}\alpha^4 \left| \frac{m^2 - 1}{m^2 + 2} \right|^2 \tag{5.36}$$

$$Q_a = -4\alpha \,\mathrm{Im}\left(\frac{m^2 - 1}{m^2 + 2} \right) \tag{5.37}$$

Therefore, after using Eq. 5.25, we will find

$$Q_s = \frac{8}{3}\alpha^4 \frac{\left\{ \left[n^2(1-k^2) - 1 \right]\left[n^2(1-k^2) + 2 \right] + 4n^4k^2 \right\}^2 + 36n^4k^2}{\left\{ \left[n^2(1-k^2) + 2 \right]^2 + 4n^4k^2 \right\}^2} \tag{5.38}$$

$$Q_a = \frac{24n^2k\alpha}{\left[n^2(1-k^2)+2\right]^2 + 4n^4k^2} \tag{5.39}$$

and for two limited conditions, we have

$$\left.\frac{Q_s}{Q_a}\right|_{k\to 0} = \left[\alpha^3(n^2-1)^2/(9n^2k)\right] \tag{5.40}$$

$$\left.\frac{Q_s}{Q_a}\right|_{k\to \infty} = \alpha^3 n^2 k^3/9 \tag{5.41}$$

For small particles ($(\pi d/\lambda) < 0.6$), the absorption coefficient is proportional to the total particle volume and, for gray material, inversely proportional to wavelength. The scatter coefficient is proportional to the sum of the squares of the volumes of the particles and for gray materials, inversely proportional to the fourth power of the wavelength. The emissivity of a fine particle cloud (the luminosity of a sooty flame, for example) is therefore proportional to the volume fraction of space occupied by the particles and independent of their size or size distribution. On the other hand, because of the weighting by the square of particle volume, the distribution and magnitude of the scattered radiation may be representative of a few large particles, in some cases present in amounts of only a few particles per thousand smaller ones [21].

For large particle size, the absorption efficiency can be obtained from the following formula [22]:

$$Q_a = 2(1-A)\left[G(4k\alpha) + G(B) - G(4k\alpha + B)\right] \tag{5.42}$$

where

$$G(u) = \frac{1}{2} + \frac{e^{-u}}{u} + \frac{e^{-u}-1}{u^2} \tag{5.43}$$

$$B = \frac{2n\left[1+2/(n^2+k^2)\right]}{1-A} \tag{5.44}$$

$$A = R + (A-1)\exp\left[\frac{-2n\left(1+\frac{2}{n^2+k^2}\right)}{1-A}\right] \tag{5.45}$$

$$R = \left[\frac{(n-1)^2+k^2}{(n+1)^2+k^2}\right] \tag{5.46}$$

It can be concluded that Eq. 5.42 constitutes a useful approximation for large spheres. On the other hand, in the limit of $\alpha \to \infty$, it can be shown that:

$$Q_a = 2(1-A)G(B) \tag{5.47}$$

The incident radiation is attenuated by an amount proportional to $\pi d^2/4$. Depending on the particle size and angle of collection the effective cross-sectional area for attenuation can vary from $\pi d^2/4$ to $2(\pi d^2/4)$ [23]. The intercepted radiation will be reflected, refracted, and absorbed to an extent which can be calculated by applying the laws of geometrical optics. If the difference between the diffracted energy and the transmitted energy is one, a large particle diffracts a quantity of energy equal to that falling on an aperture with the same cross section as the particle, and in consequence has efficiency factors for capture and for diffraction of one each, or a total extinction efficiency Q_t of two. As a result, for large particle size, the scattering coefficient can be find as follows:

$$Q_s \approx 2 - Q_a \tag{5.48}$$

The essential physical parameter which enters into the previous equations is the complex index of refraction. The real and imaginary parts of the index of refraction are indicated by n and k respectively, where $m = n - ik$. However, it is clear that for obtaining absorption and scattering efficiencies from equations, 5.29 and 5.30 (for intermediate particle size) or 5.38 and 5.39 (for small particle size) or 5.42 and 5.48 (for large particle size), one must know about the optical properties of the particles.

5.5 Optical Properties

It is hardly necessary to emphasize the importance of the determination of the optical constants of materials, and of the methods to evaluate them. In general, for a given dust particle, the value of m is not known. Many measurements of the optical constants of materials have been made. In general to determine the optical constants n and k of the material two independent measurements related to optical constants are required, and these can be obtained in a variety of ways. It has been found that the measurement scheme and method of evaluation play a vital role in limiting the accuracy of the derived optical constants [25]. The complex part of the index of refraction can be obtained by an elementary calculation from the measured absorption coefficient [26]. However, the values of refractive indices of Al [27,28,29,33], Al_2O_3 [30,31,26], Mg [33], Mgo [30], Ti [27], Coal [32], Fe [27] have been reported by several investigators.

5.6 Approximate Values of Absorption Efficiencies

From the result of investigation of the section four (absorption and scattering efficiencies), we can conclude that one of the most important parameters to take into account in absorption efficiency calculation is the particle size. For calculating the numerical value of absorption efficiency, based on the value of the particle size, we can use the equations 5.39, 5.30, and 5.42, for small, intermediate and large particle size, respectively.

In thermal radiation heat transfer, wavelengths in the range of 0.1-100 μm are of interest [21]. In combustion processes, the most significant contributions to thermoenergy arrive from radiation having wavelengths between 0.5 and 10 μm [1]. On the other hand, from the spectroscopy of flames, we can conclude that the dominant wavelength of flames of Al and Mg are $0.44 < \lambda\ (\mu m) < 0.53$ and $0.49 < \lambda\ (\mu m) < 0.52$, respectively [35]. Thus, for example, for the particle diameter of 20 μm, the particle size has the order of magnitude of 100. Therefore for the first approximation, one can use Eq. 5.42 (large particle size), for obtaining the value of absorption efficiencies of such a dust flame. However, based on the optical properties that we have from the previous section, and after using Eq. 5.42, the absorption efficiencies of C, Fe, Cu, Ni, Ti, Al, and Mg are 0.8, 0.43, 0.40, 0.39, 0.38, 0.09, and 0.08, respectively.

5.7 Temperature Profile

For obtaining temperature profiles, we have to solve Eq. 5.1 with its boundary conditions. After using Eq. 5.23, we can write

$$\rho C_p \frac{dT}{dt} = \frac{\lambda}{S^2}\frac{d^2T}{dt^2} + \frac{K_a}{K_t}\frac{m}{S} I_f e^{mt} \tag{5.49}$$

Boundary conditions:

$$\begin{aligned} t &= t_i \qquad T = T_\bullet \\ t &= 0 \qquad T = T_i \end{aligned} \tag{5.50}$$

It will be assumed that the medium is gray, and that the absorption and scattering coefficients of the medium are independent of temperature. Therefore, from the above differential equation, one can find

$$(T - T_\bullet) = \frac{(T_f - T_\bullet)}{\frac{\delta_f}{\lambda}\rho C_p S} \frac{e^{\frac{\rho C_p S^2}{\lambda} t} - e^{\frac{\rho C_p S^2}{\lambda} t_i}}{1 - e^{\frac{\rho C_p S^2}{\lambda} t_i}} + \frac{K_a}{K_t}\frac{I_f}{\rho C_p S}\left(e^{mt} - e^{mt_i}\right) \tag{5.51}$$

It is easily observed from either of these equations that the total heat flux is represented as the sum of heat transfer by pure conduction and heat transfer by pure radiation. Hence, the total heat transfer corresponds to the superposition of the two separate modes of heat transfer as if each were occurring independently of the other.

5.8 The Ratio of Temperature Increase

We define the ratio of the temperature increase as:

$$f(t)=\frac{\Delta T_c(t)}{\Delta T_r(t)} \tag{5.52}$$

Substituting ΔT_c and ΔT_r from Eq 5.51 into Eq.5.52,we get

$$f(t)=\frac{\dfrac{\left(T_f-T_\infty\right)}{\dfrac{\delta_f}{\lambda}\rho C_p S}\dfrac{e^{\frac{\rho C_p S^2}{\lambda}t}-e^{\frac{\rho C_p S^2}{\lambda}t_i}}{1-e^{\frac{\rho C_p S^2}{\lambda}t_i}}}{\dfrac{K_a}{K_t}\dfrac{I_f}{\rho C_p S}\left(e^{mt}-e^{mt_i}\right)} \tag{5.53}$$

If we want to obtain the value of $f(t)$ at the end of preheat zone, we have to consider $t=0$, thus

$$f=\left(T_f-T_\infty\right)\left[\frac{K_{a_{ph}}}{K_{t_{ph}}}\frac{\delta_f}{\lambda}\left(1-e^{-K_{t_{ph}}\delta_{ph}}\right)I_f\right]^{-1} \tag{5.54}$$

From the above equation, it is clear that f is a measure of the relative importance of conduction versus radiation. One finds that as $f\to\infty$, this limit corresponds to negligible radiation within the media. In the above equation the radiation intensity at flame front, I_f, is

$$I_f=\left(\varepsilon_f+\varepsilon_{pf}e^{-K_{tf}\delta_f}\right)\sigma T_f^{\,4} \tag{5.55}$$

where

$$\varepsilon_f=1-e^{-K_{af}\delta_f} \tag{5.56}$$

$$\varepsilon_{pf}=1-e^{-K_{apf}\delta_{pf}} \tag{5.57}$$

5.9 The Role of Radiation in Thin Flames

For a thin flame, or $\delta \approx$ very small, we get

$$\begin{aligned} \varepsilon_f &\approx K_{a_f}\delta_f \\ \varepsilon_{pf} &\approx K_{a_{pf}}\delta_{pf} \\ e^{-K_{t_f}\delta_f} &\approx 1 \\ 1-e^{-K_{t_{ph}}\delta_{ph}} &\approx K_{t_{ph}}\delta_{ph} \end{aligned} \tag{5.58}$$

Substituting Eq.5.58 into Eqs. 5.55 and 5.54, we get

$$f=\left(T_f-T_\infty\right)\left[K_{a_{ph}}\frac{\delta_f}{\lambda}\delta_{ph}\left(K_{a_f}\delta_f+K_{a_{pf}}\delta_{pf}\right)\sigma T_f^{\,4}\right]^{-1} \tag{5.59}$$

where

$$K_a=-\frac{1}{\delta}Ln\left(1-\varepsilon_g\right)+\frac{3}{2}Q_a\frac{\sigma}{\rho_p d_p} \tag{5.60}$$

For a thin zone, $\varepsilon_g \ll 1$, thus

$$-Ln\left(1-\varepsilon_g\right)\approx\varepsilon_g \tag{5.61}$$

After using Eq. 5.61 into Eq. 5.60,we get

$$\delta K_a=\varepsilon_g+\frac{3}{2}Q_a\frac{\sigma}{\rho_p d_p}\delta \tag{5.62}$$

For thin flame. In the case of

$$\varepsilon_g \ll \frac{3}{2}Q_a\frac{\sigma}{\rho_p d_p}\delta \tag{5.63}$$

the absorption coefficient can be found from the following expression

$$K_a \approx \frac{3}{2} Q_a \frac{\sigma}{\rho_p d_p} \delta \tag{5.64}$$

Now in the case of $K_{a_f} \approx K_{a_{ph}}$, $K_{a_H} \approx 0$, $\delta_f \approx \delta_{ph}$, and $T_f >> T_.$, Eq. 5.59 can be written as follows:

$$f = \left[\lambda^{-1} \delta_f^{\,3} K_a^{\,2} \sigma T_f^{\,3}\right]^{-1} \tag{5.65}$$

where f is the conduction-radiation parameter (or Stark number [17]) based on the flame temperature. Therefore, the relative role of heat transfer by conduction to that by radiation is indicated by the above parameter. The radiation term vanishes for the limiting case of a transparent ($K_a \approx 0$) medium. On the other hand, for $f \to \infty$, heat transfer within the medium is only by conduction. The opposite extreme of $f \to 0$ corresponds to the case in which heat transfer is solely due to radiation.

5.10 Numerical Example and Conclusions

From the experimental data, for stoichiometric conditions of several dust air mixtures [15] , we have

	Mg	Al	Ti	C	
T_f	3000	3270	3200	1950	$°K$
σ	422	312	416	210	gr/m^3
ρ_p	1740	2700	4500	2000	kg/m^3
d_p	10	10	10	10	μm
δ_f	2	3	4	5	mm
Q_a	0.08	0.09	0.38	0.80	----

After using Eqs. 5.64 and 5.65 and using the values of $\lambda_{air} = 0.06525\,(W/m^{\circ}K)$ and $\sigma = 5.67E-8\,(W/m^{2\circ}K^{4})$, we find:

	Mg	Al	Ti	C	
K_a	2.91	1.56	5.27	12.6	$1/m$
$K_a\delta$	0.00582	0.00468	0.02108	0.063	----
f	629	501	20	8	----

As we can see from the above table, for a thin dust flame in a Mg-air mixture at stoichiometric conditions, radiation has no influence. For graphite at the same conditions however, the radiation heat transfer can have a relatively important role. In the case of graphite the ratio of the heat transfer term (f) is not far from one. Therefore the amount of heat transfer by radiation is comparable to that of by conduction from the flame to the unburned mixture. This means that the mechanism of the flame propagation for this kind of dust flame can be both radiation and conduction.

For obtaining the role of radiation on the premixed laminar dust flame, one must therefore be concerned about flame emissivity and dust absorbtivity. On the other hand, to get a basic idea about the role of radiation, one can use the three important parameters which are the absorption coefficient, flame thickness, and flame temperature, and apply them to Eq. 5.65. That resultant value can illustrate the general role of radiation.

Chapter 6

6. Concluding Remarks

The present work has been undertaken to obtain an improved physical understanding of the mechanism of dust flame propagation. An experimental and theoretical study has been carried out at atmospheric pressure on the flame propagation and quenching of aluminum powder.

A new experimental apparatus has been designed. The advantages of this apparatus are that a highly uniform particulate cloud is generated and this permits the experiment to be carried out under an approximately stationary initial condition. In contrast, a Hartmann type test tube relies on a transient testing method utilizing aerodynamics to create the suspension.

A light extinctiometer, accurately calibrated by complete aspiration of the dust from the flow through a set of filters, was used to measure the particle concentration. Because of direct measurement of dust concentration and its accuracy, the present data for the quenching distance of aluminum dust-air mixtures are more accurate than the previous data reported by Jarosinski, *et al.* [8].

High speed pictures taken at 2000 frames per second were used to observe the flame propagation behavior of dust clouds, the quenching conditions, and the flame velocity.

Theoretical studies were performed to predict the quenching distance and burning velocity of the aluminum dust flames, and compared with the experimental data. The study includes the effects of particle concentration, initial oxygen concentration, and the type of inert gas in the mixture. Good agreements between the theoretical and experimental values of the quenching distance of aluminum dust-air mixture are obtained.

6.1 Summary

The following results summarize important characteristics and behavior of dust flames studied in the course of this research:

- The minimum quenching distance of an aluminum dust flame increases as the initial oxygen concentration decreases, and generally the lean flammability limit appears to increase as the initial oxygen concentration decreases.

- In general the quenching distance of an aluminum dust flame decreases as the particle concentration increases until it reaches a minimum. Above this concentration, the quenching distance remains almost constant.

- Based on the analytical formulation for aluminum dust flames of the present study, the weak dependence of the diffusive combustion rate on temperature can explain the phenomenon of the weak dependence of the quenching distance on dust concentration in rich mixtures.

- Because the order of magnitude of the measured quenching distance in aluminum dust flames is the same as in gas flames, it can be concluded that processes controlling the flame propagation in aluminum dust flames should be similar to that of gas flames.

- A rich flammability limit does not exist or is very difficult to find.

- The shape of the flame velocity versus particle concentration curve is concave downward, contrary to the quenching distance versus particle concentration curve.

- The minimum quenching distance for aluminum dust flames ($d_{32} = 5.4\ \mu m$) is $5\ mm$ for air (or $21\%O_2, 79\%N_2$), $6\ mm$ for $16\%O_2, 84\%N_2$, $15\ mm$ for $11\%O_2, 89\%N_2$, and $7.5\ mm$ for $21\%O_2, 79\%He$.

- The quenching distance of an aluminum dust flame in standard air is much lower than that of the quenching distance in an 11% initial oxygen concentration mixture for the same particle concentration.

• The flame velocity of an aluminum dust flame in air mixture is much faster than that of it in the mixture of 11% initial oxygen concentration for the same particle concentration.

• The lower value of initial oxygen concentration corresponds to the higher value of the combustion time. As a result, for smaller amounts of initial oxygen concentration, the quenching distance increases and the flame velocity decreases.

• After using mixtures with different inert gases (nitrogen and helium), both values of the quenching distance and the burning velocity change, due to different values of mass diffusivity, thermal diffusivity, and combustion time.

• The aluminum combustion model is very efficient, and it provides useful rough estimates for predicting the effect of various parameters on laminar dust flame propagation.

• The predicted quenching distances of aluminum-air flames are slightly lower than the experimental data, but the effect of particle concentration is well predicted by this model.

• The mathematical model of aluminum combustion predicts burning velocity values lower than the experimental values, but the trends are the same. This discrepancy comes from the experimental evaluation of the burning velocity. To obtain the burning velocity, one should consider the effect of the flame surface area, which is difficult to measure accurately.

• In general, the process of dust flame propagation in the tube can be divided into three different stages: laminar flame, oscillating flame and turbulent accelerating flame.

• The effect of radiation may be significant even for a small scale dust flame, depending on the fuel burned.

The present study shows that quenching distance and flame velocity of an aluminum dust flame are influenced by particle concentration, initial oxygen concentration, and the type of inert gas in the mixture.

6.2 Contributions to Knowledge

The contributions to knowledge resulting from this study are:

- The author of the present thesis has developed a systematic method for accurately measuring fundamental characteristics of laminar dust flame propagation such as quenching distance.

- A further contribution consists, for the first time, of a systematic study of the effects of initial oxygen concentration and the type of inert gas in the mixture on the quenching distance of dust flames.

- The experiments show that a rich propagation limit does not exist up to an equivalence ratio of about four.

- In the present thesis, for the first time, theories of dust flame quenching distances for two kinds of dust particles have been developed.

- The author has clarified the role of radiation in the dust flame propagation mechanism. In particular, radiation has little influence on the propagation of flames in Al and Mg dust cloud.

6.3 Recommendations for Future Work

To further clarify the phenomena and to extend the investigation, the following recommendations are suggested:

- A refinement of the particle transport system on the particle burner is needed, so that burning velocities measured with this method and the burner method can be compared.

- A new two or three dimensional model of flame quenching must to be developed for better prediction of the quenching distance and flame propagation behavior of particulate fuels.

- Measuring of quenching distances for different particle sizes.

- Several tests need to be conducted at various pressures and at higher initial oxygen concentration to investigate these effects on the quenching distance and flame velocity.

- From the fact that the quenching distance can be used to identify the controlling processes in laminar dust flames, it is highly recommended to continue the present work by measuring quenching distance for different types of dust such as: Mg, Fe, etc. by using the present apparatus.

References

[1].Smoot, L.D., Smith, P.J., "Coal Combustion and Gasification", Plenum Press, New York, (1985)

[2]. Michelis, J., Margenburg, B., Müller, G., and Kleine, W., "Investigations into the Buildup and Development Conditions of Coal Dust Explosions in a 700-m Underground Gallery", Industrial Dust Explosions, pp. 124-137, (1986).

[3]. Alan R. Abrahamsen, "The U.K. Approach to Dust Explosibility Assessment and Its Relevance to Explosion Prevention and Protection", Industrial Dust Explosions, pp. 60-73, (1986).

[4]. Makris, A., "Lean Flammability Limits of Dust-Air Mixtures", M.S. Thesis, Mc Gill University, Canada, (1988)

[5]. Hartmann, I., Cooper, A.R. and Jacobson M., "Recent Studies on the Explosibility of Cornstarch", U.S. Bureau of Mines, Report of Investigation, RI 4725, (1951).

[6]. Nagy, J., Conn, J.W., and Verakis, H.C., "Explosion Development in Spherical Vessels", U.S. Bureau of Mines, Report of Investigation, RI 7279, (1969).

[7]. Nagy, J., Seiler, E.C., Conn, J.W., and Verakis, H.C., "Explosion Development in Closed Vessels", U.S. Bureau of Mines, Report of Investigation, RI 7507, (1971).

[8]. Jarosinski, J., Lee, J.H., Knystatutas, R. and Crowley, J.D., "Quenching of Dust-Air Flames", Proc. 21st Symp. (International) on combustion, pp. 1917-1924, (1986).

[9]. Proust, C., Veyssiere, B., "Fundamental Properties of Flames Propagating in Starch Dust-Air Mixtures", Combust. Sci. and Tech., Vol. 62, pp. 149-172 (1988).

[10]. Lee, J.H., F. Zhang and R. Knystautas, "Propagation Mechanisms of Combustion Waves in Dust-Air Mixtures", Powder Technology, Vol. 71, pp. 153-162 (1992).

[11]. Hartmann, I., Nagy, J. and Brown, H. R., "Inflammability and Explosibility of Metal Powders", U.S. Bureaw of Mines, Report of Investigation 37722 (1943).

[12]. Palmer, K.N. and Tonkin, P.S., "Coal Dust Explosions in a Large-Scale Vertical Tube Apparatus", Combustion and Flame, 17, pp. 159-170, (1971).

[13]. Singer, J.M., Bruszak, A.E., and Grumer, J., "Equivalence of Coal Dust and Methane at Lower Quenching Limits of Flames of Their Mixture," Bureau of Mines, Reported of Investigation 6761 (1966).

[14]. Greene, F.T., and O'Donnell, J.E., "Quenching Behavior of Coal Dust-Air Mixtures," Bureau of Mines, open file report 4-83 (Aug. 1981).

[15]. Ballal, D.R., "Flame Propagation through Dust Clouds of Carbon, Coal, Aluminum, and Magnesium in an Environment of Zero Gravity", Proc. Roc. Soc., A385, pp. 21-51 (1983).

[16]. Lee, J.H., Knystatutas, R., Proposal for Research Submitted to NASA, McGill University, Dept. of Mech. Eng., (1990).

[17]. Sparrow, E.M., Cess, R.D., "Radiation Heat Transfer", Washington: Hemisphere Pub. Corp., pp. 560-561 (1978).

[18]. Ballal, D.R., Proc. Roc. Soc., "Further Studies on the Ignition and Flame Quenching of Quiescent Dust Clouds", A385, pp. 1-19 (1983).

[19]. Van de Hulst, H.C., "Light Scattering by Small Particles", Wiley New York, (1957).

[20]. Wickramasinghe, N.C., "Light scattering Functions for Small Particles", New York: Wiley, (1973).

[21]. Hottel, H.C., Sarofim, A.F., "Radiative Transfer", McGraw-Hill, Inc., (1967).

[22]. Levine, P.H., "Absorption Efficiencies for Large Spherical Particles: a New Approximation", Applied Optics, Vol. 17, No. 24, pp. 3861-3862, (1978).

[23]. Gray, W.A., Kilham, J.K., Muller, R., "Heat Transfer from Flames", Paul Elek (Scientific Books) Ltd., London, (1976).

[24]. Guruz, K., Mehnet, Y., "A Theoretical Study of the Effect of Scattering on Radiative Heat Transfer", Archivum Combustionis, Vol. 3, No. 3, pp. 193-210, (1983).

[25]. Nagendra, C.L., Thutupalli, G.K.M., "Determination of Optical Properties of Absorbing Materials: a Generalized Scheme", Applied Optics, Vol. 22, No. 4, pp. 587-591, (1983).

[26]. Plass, G.N., "Temperature Dependence of the Mie Scattering and Absorption Cross Sections for Aluminum Oxide", Applied Optics, Vol. 4, No. 12, pp. 1616-1619, (1965).

[27]. Ordal, M.A., Long, L.L., Bell, R.J., Bell, S.E., Bell, R.R., Alexander, R.W., Jr., and Ward, C.A., "Optical Properties of the Metals Al, Co, Cu, Au, Fe, Pb, Ni, Pd, Pt, Ag, Ti, and W in the Infrared and far Infrared", Applied Optics, Vol. 22, No. 7, pp. 1099-1119, (1983).

[28]. Shiles, E., Sasaki, T., Inokuti, M., Smith, D.Y., "Self-Consistency and Sum-Rule Tests in the Kramers-Kronig Analysis of Optical Data: Applications to Aluminum", Physical Review B, Vol. 22, No. 4, pp. 1612-1628, (1980).

[29]. Skobel'tsyn, A.D.V., "Optical Properties of Metals and Intermolecular Interactions", Proceeding (Trudy) of the P.N. Lebedev Physics Institute, Vol. 55, (1973).

[30]. Plass, G.N., "Mie Scattering and Absorption Cross Sections for Aluminum Oxide and Magnesium Oxide", Applied Optics, Vol. 3, No. 7, pp. 867-872, (1964).

[31]. Malitson, I.H., "Refraction and Dispersion of Synthetic Sapphire", J. Opt. Soc. A., Vol. 52, No. 12, pp. 1377-1379, (1962).

[32]. Gouesbet, G., Grehan, G., Maheu, B., "Single Scattering Characteristics of Volume Elements in Coal Clouds", Applied Optics, Vol. 22, No. 13, pp. 2038-2050, (1983).

[33]. O'Bryan, H.M., "The Optical Constants of Several Metals in Vacuum", J. Opt. Soc. A., Vol. 26, pp. 122-127, (1936).

[34]. Essenhigh, R.H., Csaba, J., "The Thermal Radiation Theory for Plane Flame Propagation in Coal Dust Clouds", 9th Symposium (Int.) on Combustion, pp. 111-125, (1962).

[35]. Gaydon, A.G., "The Spectroscopy of Flame", London: Chapman and Hall, (1974).

[36]. Chromey, F.C., "Evaluation of Mie Equations for Colored Spheres", J. Opt. Soc. A., Vol. 50, No. 7, pp. 730-737, (1960).

[37]. Frank - Kamenetskii, "Diffusion and Heat Transfer in Chemical Kinetics", Plenum Press, New York, (1969).

[38]. King, M.K., "Prediction of Boron Dust Cloud Flame Speeds", 22th JANNAF Combustion Meeting, CPIA Publ., Vol. 1, pp. 361-376, (1985).

[39]. Merzhavov, A.G., Grigorjev, Yu.M., and Gal'chenko, Yu.A., "Aluminum Ignition", Combustion and Flame, Vol. 29, pp. 1-14, (1977).

[40]. Maham, B.H., "Elementary Chemical Thermodynamics", New York: W.A. Benjamin, (1964).

[41]. Kothandaraman, C.P., and Subramanyan, S., "Heat and Mass Transfer", New York: Wiley, (1977).

[42]. Pohil, D.F., Belyaev, A.F., Frolov, Y.V., Logachev, V.S., Korotkov, A.I., "Combustion of Powdered Metals in Active Gases", Moscow, Nauka, pp 178-179, (in Russian), (1972).

[43]. Cassel, H.M., and Liebman, I., "The Cooperative Mechanism in the Ignition of Dust Dispersions", Combustion and Flame, Vol. 3, pp. 467-475, (1959).

[44]. Holman, J.P., "Heat Transfer", 7th ed., New York, Mc Graw-Hill, (1990)

[45]. Williams, F.A., "Combustion Theory", 2nd ed., Menlo Park, Calif., Benjamin / Cummings Publishing Company, Inc., (1985).

[46]. Spalding, D.B., "A Theory of Inflammability Limits and Flame Quenching", Pro. Roy. Soc. A, Vol. 240, pp. 83-100, (1957).

[47]. Zeldovich, Ya.B., Barenblatt, G.I., Librovich, V.B., Makhviladze, G.M., "The Mathematical Theory of Combustion and Explosions", New York, Consultants Bureau, (1985).

[48]. Marcsteine, G.H., "Non steady Flame Propagation", Macmillan, NY, p. 328 (1964).

[49]. Groshin, S., Shevchuk, V.G., and Ageev, N.D., "Oscillatory Combustion of Gaseous Suspensions", Combustion Explosion and Shock Wave, 17(6), pp. 595-601, (1982).

[50]. Berlad, A.L., Ross, H., Facca, L., and Tangirala, V., "Particle Cloud Flames in Acoustic Fields", Combustion and Flame, Vol. 82, p. 448, (1990).

[51]. Cassel, H.M., "Some Fundamental Aspects of Dust Flames", US Dept. Interior Bureau of Mines, RI No. 6551, (1964).

[52]. Ageyev, N.D., Groshin, S.V., Zolotko, A.N., Poletayev, N.I., Shoskin, Y.L., "Flame Speed of Self-Sustaining Flame in Aluminum Dust Clouds", Combustion of Heterogeneous and Gas System, Chernogolovka, pp. 83-85, and pp. 160-167, (1989), (in Russian).

[53]. Seshadri, K., Berlad, A.L., and Tangirala, V., "The Structure of Premixed Particle Cloud Flames", Combustion and Flame, Vol. 89, pp. 333-342, (1992).

[54]. Jarosinski, J., "Flame Quenching by a Cold Wall", Combustion and Flame, Vol. 50, pp. 167-175, (1983).

[55]. Potter, A.E., "Flame Quenching", Proc. Comb. Sci. and Technology, pp. 145-181, (1960).

[56]. Jarosinski, J., "A Survey of Recent Studies on Flame Extinction", Prog. Energy Combust. Sci., Vol. 12, pp. 81-116, (1986).

[57]. Berlad, A.L., Yang, C.H., "A Theory of Flame Extinction Limits", Combustion and Flame, Vol. 4, pp. 325-333, (1960).

[58]. Mayer, E., "A Theory of Flame Propagation Limits Due to Heat Loss", Combustion and Flame, Vol. 1, pp. 438-452, (1957).

[59]. Adler, J., "One Dimensional Laminar Flame Propagation with Distributed Heat Losses: Thin Flame Theory", Combustion and Flame, Vol. 7, pp. 39-49, (1963).

[60]. Jarosinski, J., "Heat Transfer Between Hot Combustion Gases and a Cold Wall in Narrow Channels for Limit Flames", Int. Heat Mass Transfer, Vol. 27, No. 7, pp. 1113-1116, (1984).

[61]. Yang, C.H., "Burning Velocity and the Structure of Flames near Extinction Limits", Combustion and Flame, Vol. 5, pp. 163-174, (1961).

[62]. Ballal, D.R., Lefebver, A.H., "The Influence of Flow Parameters on Minimum Ignition Energy and Quenching Distance", 15th Symposium (Int.) on Combustion, pp. 1473-1481, (1974).

[63]. Essenhigh, R.H., "Combustion and Flame Propagation in Coal Systems: A Review", 16th Symposium (Int.) on Combustion, pp. 353-387, (1977).

[64]. Proust, C., Veyssiere, B., "New Experimental Apparatus for Studying the Propagation of Dust Air Flames", Progress in Astronautics and Aeronautics, AIAA., Vol. 113, pp. 43-61, (1988).

[65]. Buckmaster, J., "The Quenching of Deflagration Waves", Combustion and Flame, Vol. 26, pp. 151-162, (1976).

[66]. Bhaduri, D., Bandyopadhay, S., "Combustion in Coal Dust Flames", Combustion and Flame, Vol. 17, pp. 15-24, (1971).

[67]. Essenhigh, R.H., Woodhead, D.W., "Speed of Flame in Slowly Moving Clouds of Cork Dust", Combustion and Flame, Vol. 2, pp. 365-382, (1958).

[68]. Palmer, K.N.., "Dust Explosions and Fires", London, Chapman and Hall, (1973).

[69]. Lee, J.H.S., Knystautas, R., "Measurement of the Quenching Distance for Dust-Air Mixtures in a Micro gravity Environment", McGill University, Dept. of Mech. Eng., (1990).

[70]. Smoot, L.D., Horton, M.D., "Propagation of Laminar Pulverized Coal-Air Flames", Prog. Energy Combust. Sci., Vol. 3, pp. 235-258, (1977).

[71]. Smoot, L.D., Hedman, P.O., and Smith, P.J. "Pulverized Coal Combustion Research at Brigham Young University", Progress Energy Combustion Science, Vol. 10, pp. 359-441, (1984).

[72]. Ballal, D.R., "Ignition and Flame Quenching of Quiescent Dust Clouds of Solid Fuels", Proc. R. Soc. Lond. A, Vol. 369, pp. 479-500, (1980).

[73]. Jarosinski, J., Pu, Y.K., Bulewicz, E.M., Kauffman, C.W., Johnson, V.G., "Some Fundamental Characteristics of Cornstarch Dust-Air Flames", Dynamics of Heterogeneous Combustion and Reacting Systems, AIAA, Vol. 152, pp. 119-135, (1993).

[74]. Cassel, H.M., Liebman, I., Mock, W.K., "Radiative Transfer in Dust Flames", 6th Symposium (Int.) on Combustion, pp. 602-605, (1956).

[75]. Cassel, H.M., Gupta, A.K., Guruswamy, S., "Factors Affecting Propagation through Dust Clouds", 3rd Symposium on Combustion, Flame and Explosion Phenomena, pp. 185, (1949).

[76]. Powell, F., "The Effect of Inert Dust on the Combustion Limits of Lycopodium Spores Dispersed in Air", Combustion and Flame, Vol. 6, pp. 75-76, (1962).

[77]. Magutie, B.A., Slack, C., William, A.J., "The Concentration Limits for Coal Dust-Air Mixtures for Upward Propagation of Flame in a Vertical Tube", Combustion and Flame, Vol. 6, pp. 287-294, (1962).

[78]. Mason, W.E., Wilson, M.J.G., "Laminar Flames of Lycopodium Dust in Air", Combustion and Flame, Vol. 11, pp. 195-200, (1967).

[79]. Singer, J.M., Liebman, I., "Spherical Flames of Spark Ignited Dust Clouds", Combustion and Flame, Vol. 12, pp. 506-509, (1968).

[80]. Smoot, L.D., Horton, M.D. William, G., "Propagation of Laminar Pulverized Coal-Air Flames", 16th Symposium (Int.) on Combustion, pp. 375-387, (1977).

[81]. Bradley, D., Lee, J.H.S., "On the Mechanism of Propagation of Dust Flames", Presented at the First International Colloquium on Explosibility of Industrial Dust, Baranow, Poland, Nov. 8-10, (1984).

[82]. Horton, M.D., Goodson, F.P., Smoot, L.D., "Characteristics of Flat, Laminar Coal-Dust Flames", Combustion and Flame, Vol. 28, pp. 187-195, (1977).

[83]. Slezak, S.E., Fitch, D.J., Krier, H., Buckius, R.O., "Coal Dust Flame Propagation in a Laboratory Flammability Tube", Combustion and Flame, Vol. 54, pp. 103-119, (1983).

[84]. Bond, J.F., Knystaustas, R., Lee, J.H., "The Infuence of Turbulence on Dust and Gas Explosions in Closed Vssel", Dynamics of Explosions, Progress in Astronautics and Aeronautics, Vol. 106, pp. 571, (1986).

[85]. Eckhoff, R.K., "Towards Absolute Minimum Ignition Energies for Dust Clouds", Combustion and Flame, Vol. 24, pp. 53-64, (1975).

[86]. Lee, J.H.S., Knystautas, R., "Micro gravity Combustion of Dust Clouds", Final Progress Report, McGill University, Dept. of Mech. Eng., (1991).

[87]. Hertzberg, M., Conti, R.S., Cashdollar, K.L., "Spark Ignition Energies for Dust-Air Mixtures: Temperature and Concentration Dependence", 20th Symposium (Int.) on Combustion, pp. 1681-1690, (1984).

[88]. Jarosinski, J., Lee, J.H., Knystaustas, R., Crowley, J.D., "Quenching Distance of Self-Propagating Dust-Air Flames", Archivum Combustionis, Vol. 7, pp. 267-278, (1987).

[89]. Lee, J.H.S., Pu, Y.K., Knystautas, R., "Influence of Turbulence on Closed Volume Explosion of Dust-Air Mixtures", Archivum Combustionis, Vol. 7, No. 3-4, pp. 279-297, (1987).

[90]. Lee, J.H.S., Peraldi, O., Knystautas, R., Thirsk, R., "Micro gravity Combustion of Dust Suspension in a Spherical Chamber", Presented at the 2nd Japan-Canada Space Workshop, Tokyo, Jan. 23-24, (1992).

[91]. Essenhigh, M.A., "Predicted Burning Times of Solid Particles in an Idealized Dust Flame", J. Inst. Fuel., Vol. 34, pp. 239-244, (1961).

[92]. Veyssiere, F.R., Mouilleau, Y., Proust, C., "Experiments on Turbulent Flame Propagation in Dust-Air Mixtures", Dynamics of Heterogeneous Combustion and Reacting Systems, AIAA, Vol. 152, pp. 211-231, (1993).

[93]. Hertzberg, M., Zlochower, I.A., Cashdollar, K.L., "Metal Dust Combustion: Explosion Limits, Pressures, and Temperatures", 24th Symposium (Int.) on Combustion, pp. 1827-1835, (1992).

[94]. Hertzberg, M., Cashdollar, K.L., Zlochower, I.A., Green, G.M., "Explosives Dust Cloud Combustion", 24th Symposium (Int.) on Combustion, pp. 1837-1843, (1992).

[95]. Zhang, D.K., Wall, T.F., "An Analysis of the Ignition of Coal Dust Clouds", Combustion and Flame, Vol. 92, pp. 475-480, (1993).

[96]. Glassman, I., "Comment on: The Combustion Phase of Burning Metals, by T.A. Steinberg, D.B. Wilson, and F. Benz", Combustion and Flame, Vol. 93, pp. 338-342, (1993).

[97]. Mintz, K.J., "Upper Explosive Limit of Dusts: Experimental Evidence for Its Existence Under Certain Circumstances", Combustion and Flame, Vol. 94, pp. 125-130, (1993).

[98]. Ogle, R.A., Beddow, J.K., Vetter, A.F. "A Thermal Theory of Laminar Premixed Dust Flame Propagation", Combustion and Flame, Vol. 58, pp. 77-79, (1984).

[99]. Gieras, M., Wolanski, P., "Flame Propagation and Extinction in the Hybrid Mixtures at Micro gravity and Normal Gravity Conditions", Archivum Combustionis, Vol. 12, No. 1-4, pp. 109-123, (1992).

[100]. Austin, P.J., Kauffman, C.W., Sichel, M. "Combustion of Single Non spherical Cellulose particles", Dynamics of Heterogeneous Combustion and Reacting Systems, AIAA, Vol. 152, pp. 136-154, (1993).

[101]. Klements, R., "Mechanism of Flame Propagation in Dust-Air and Hybrid Mixtures", Dynamics of Heterogeneous Combustion and Reacting Systems, AIAA, Vol. 152, pp. 155-177, (1993).

[102]. Kordylewski, W., Wach, J., "Inferred Temperature of Pulverized-Coal Flames", archivum combustionis, Vol. 12, No. 1-4, pp. 125-131, (1992).

[103]. Bartlett, R.W., Ong, J.N., Fassell, W.M., Papp, C.A., "Estimating Aluminum Particle Combustion Kinetics", Combustion and Flame, Vol. 7, pp. 227-232, (1963).

[104]. Friedman, R., Macek, A., "Ignition and Combustion of Aluminum Particles in Hot Ambient Gases", Combustion and Flame, Vol. 6, pp. 9-19, (1962).

[105]. Ballal, D.R., Lefebver, A.H. "Ignition and Flame Quenching of Flowing Heterogeneous Fuel-Air Mixtures", Combustion and Flame, Vol. 35, pp. 155-168, (1979).

[106]. Proust, C., "Contribution a´ le´tude des me´canismes de propagation des flammes dans les me´langes he´te´rogenes gaz-particules solides", The´se de Docteur-Inge´nier, ENSMA, Poitiers, France, (1988).

Appendix A

Experimental Technique and Procedure

As it was mentioned before, the objectives of the experiment in present study are to obtain the fundamental data of the process of laminar flame propagation in a quiescent dust clouds such as: quenching distance. Following these objectives the typical test procedure in the experiment will be the next:

1. Installation of the combustion tube assembly.
2. Loading of the cylinder with the sample of dust in dispersion system.
3. Starting the ventilation
4. Starting the experiment
5. High speed flow is venting through dispersion
6. The piston with dust sample starts to move
7. Registration of the processes with video camera.
8. Measuring concentration
9. Ignition
10. Solenoid valves are closed
11. Turn off the DC motor.

After each experiment the whole apparatus should be cleaned. The registration of the process of dust flame propagation and quenching will be carried out by the Panasonic PV-S770-K Camcorder and high-speed 16 mm camera at framing rate of 2000 frames per second.

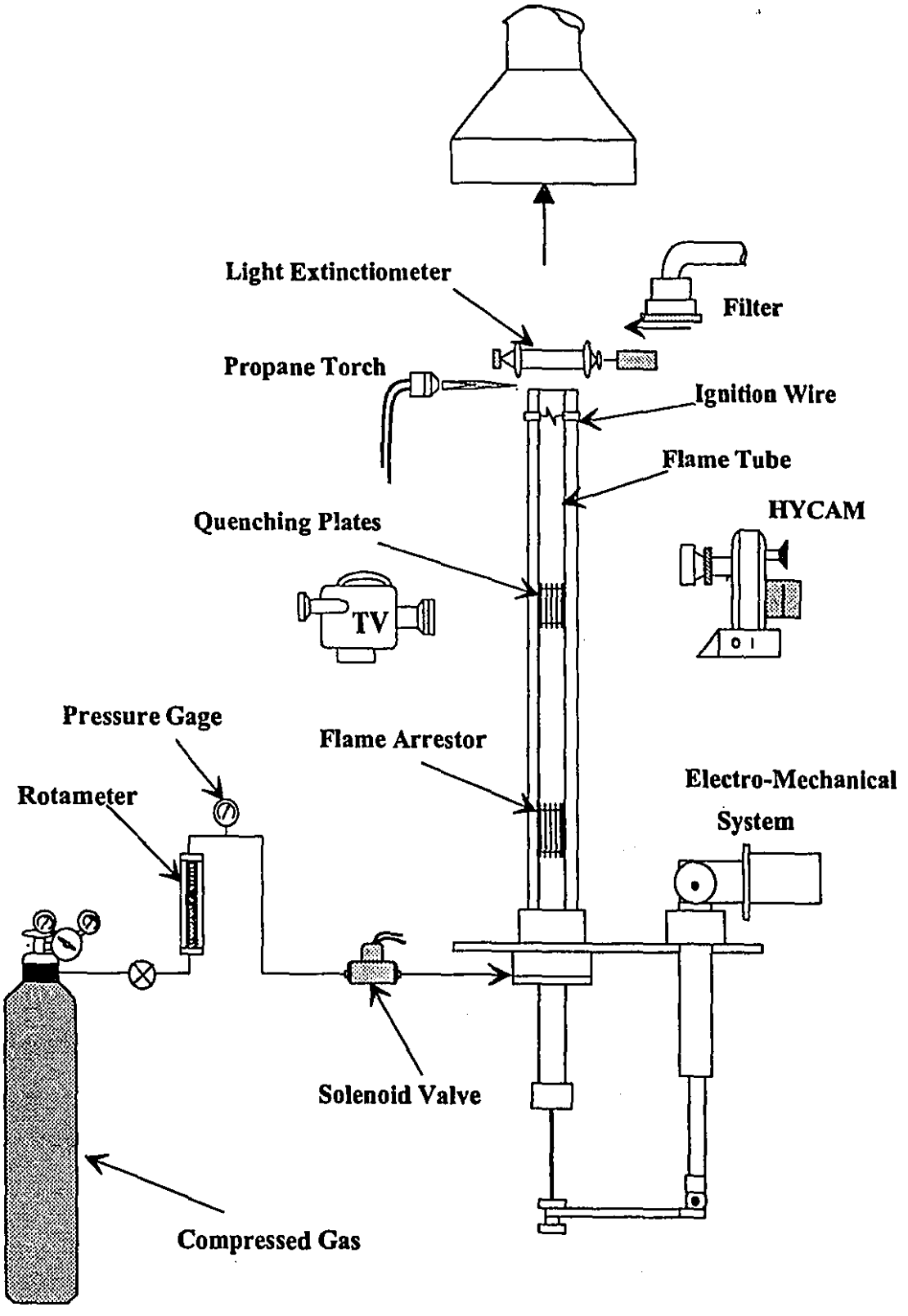

Figure 1: The general scheme of the experimental setup.

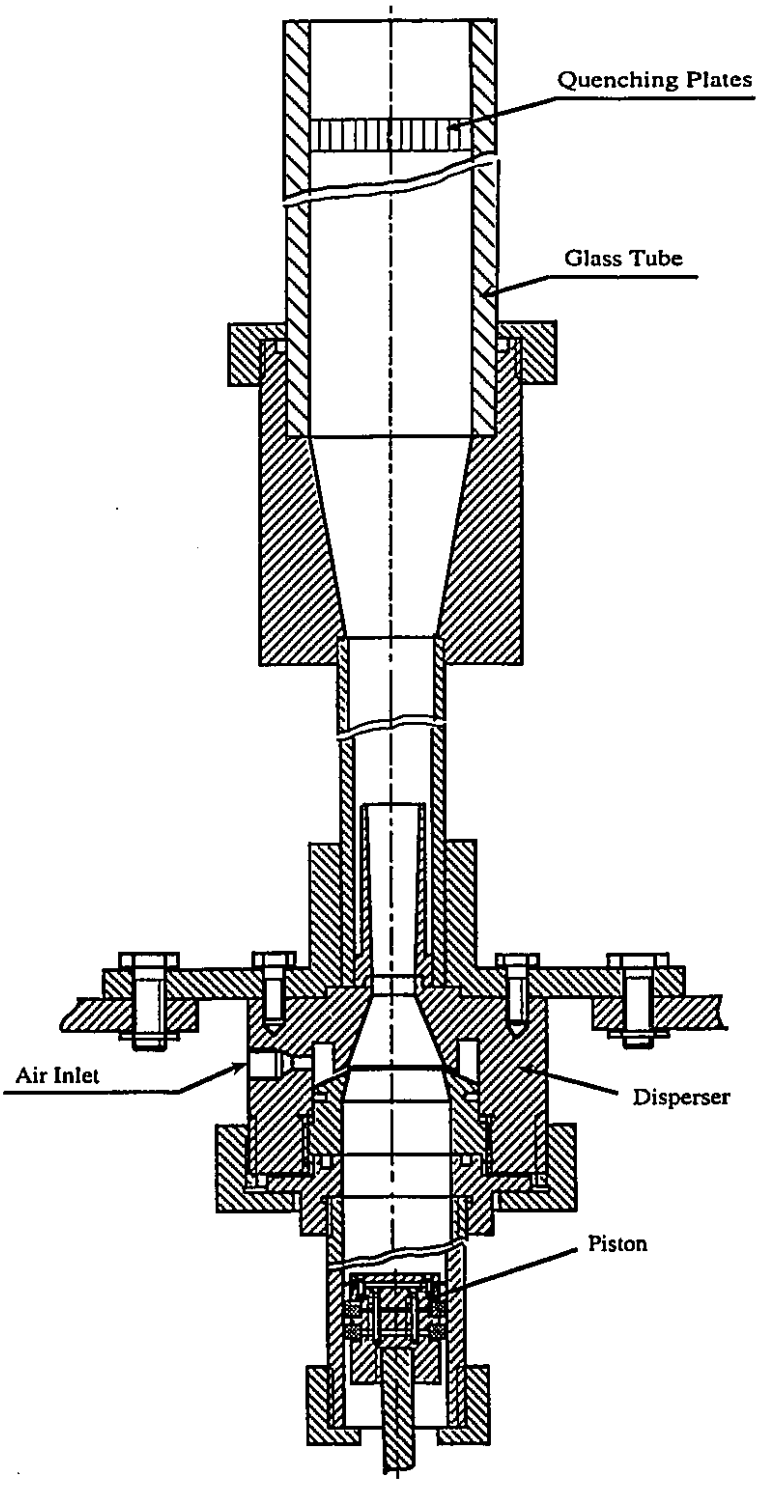

Figure 2: Schematic diagram of present experimental apparatus

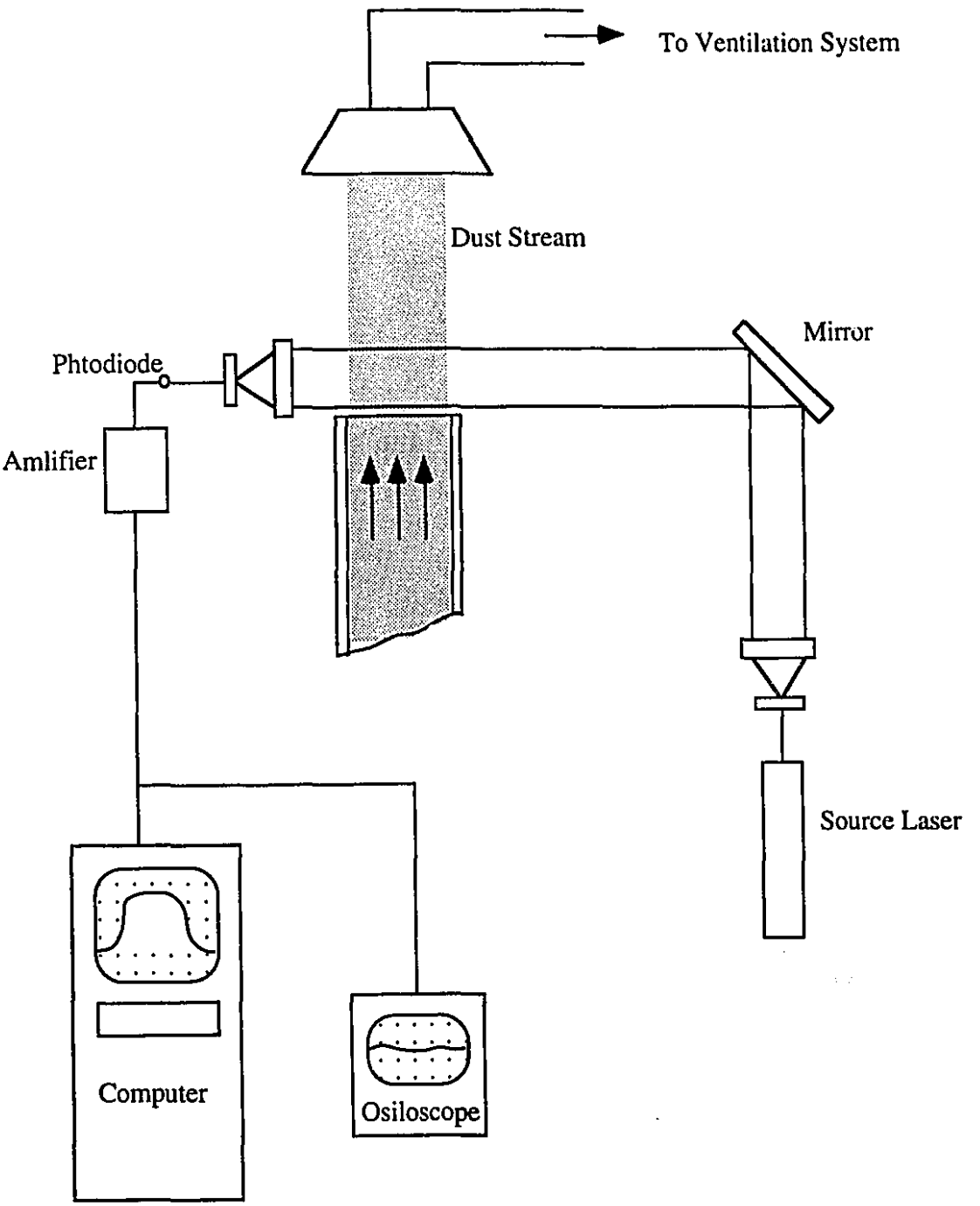

Figure 3: Optical arrangement of light transmission measurement of dust concentration

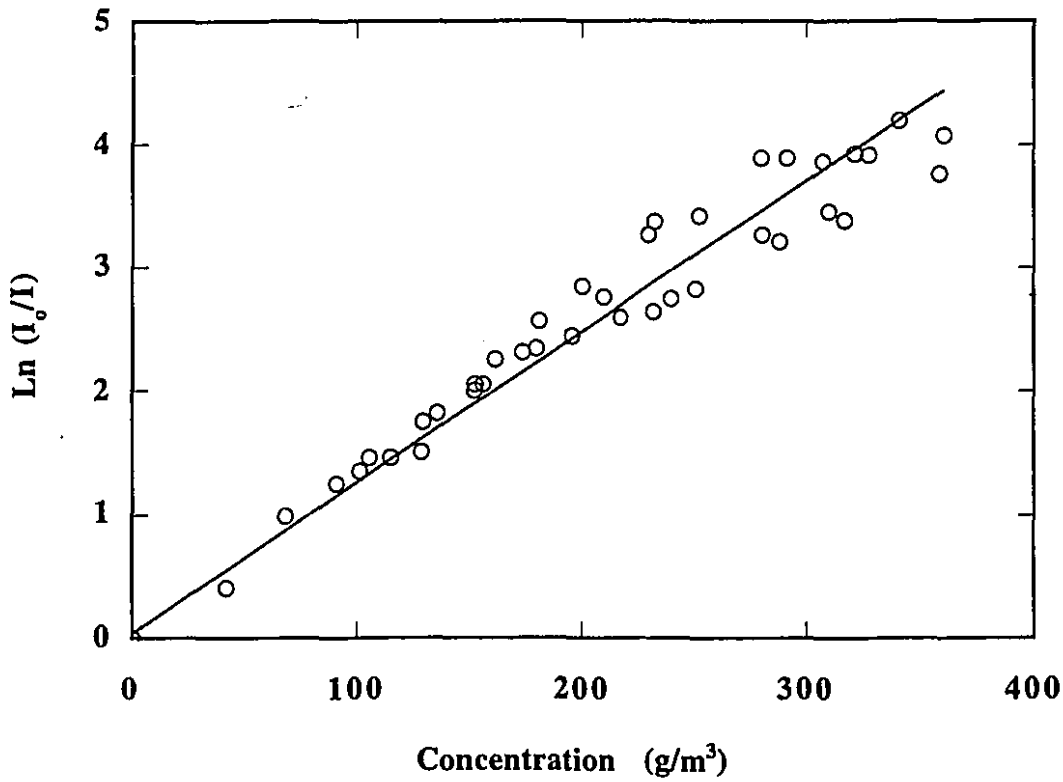

Figure 4: Calibration curve of dust concentration measurement

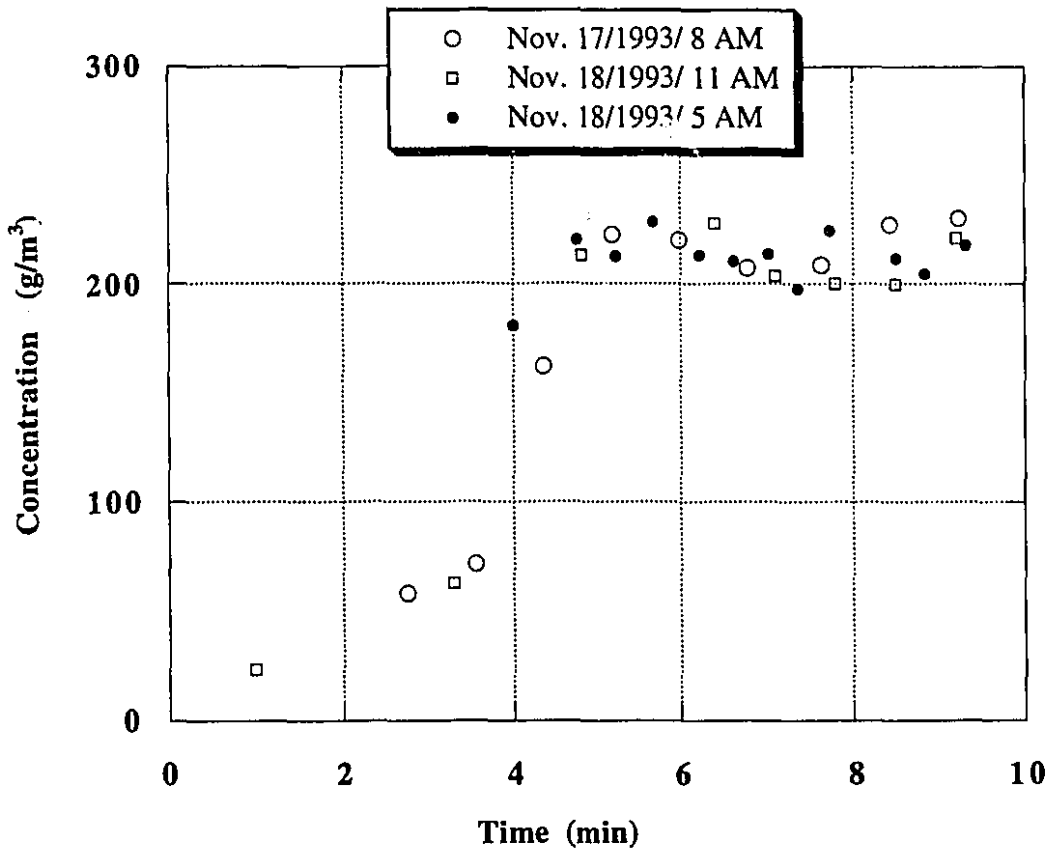

Figure 5: Time history of dust concentration (flow rate = 460 cm^3/s , and the speed of piston = 1.5 cm/s)

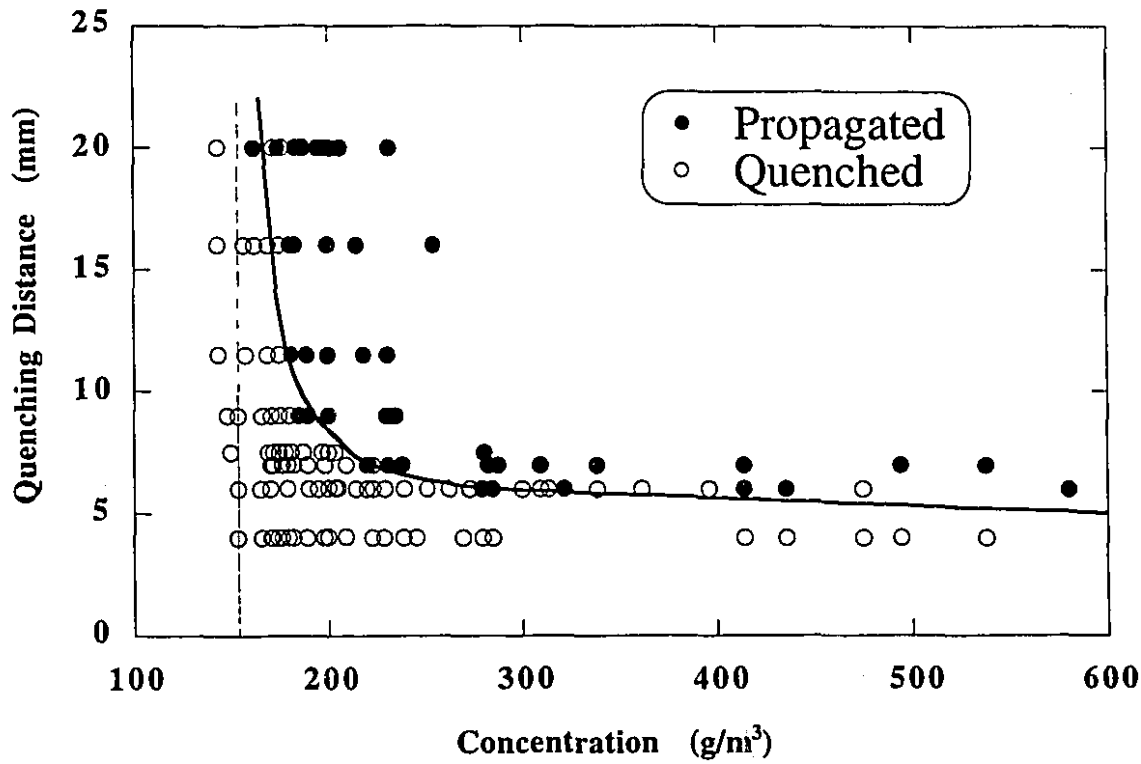

Figure 6: **Experimental result of aluminum dust-air flame quenching distance as a function of dust concentration.**

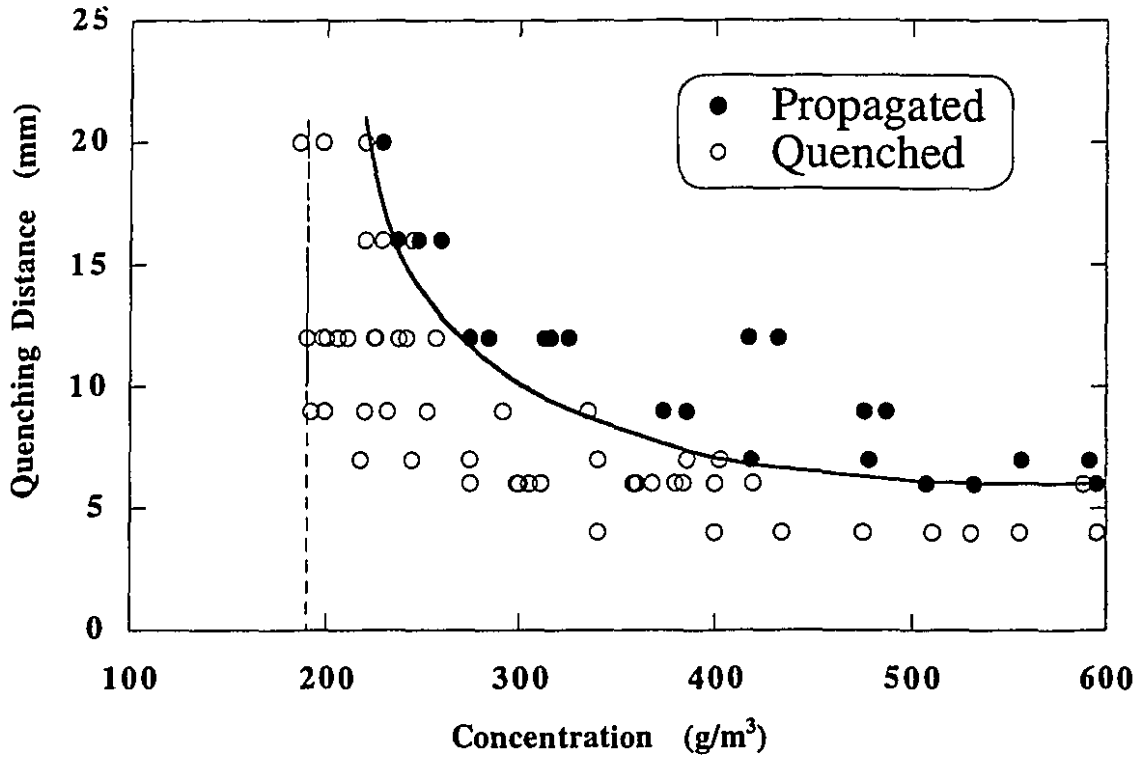

Figure 7: Experimental results of aluminum dust flame quenching distance for 16% initial oxygen concentration as a function of dust concentration.

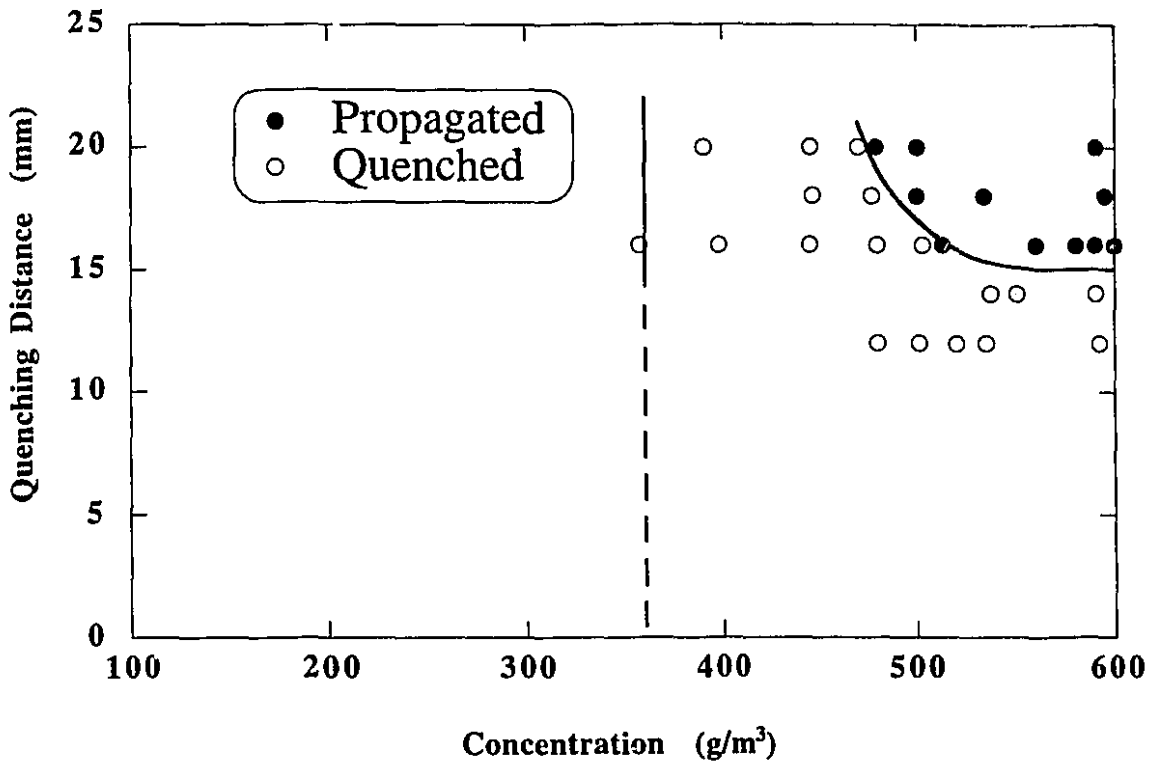

Figure 8: Experimental results of aluminum dust flame quenching distance for 11% initial oxygen concentration as a function of dust concentration.

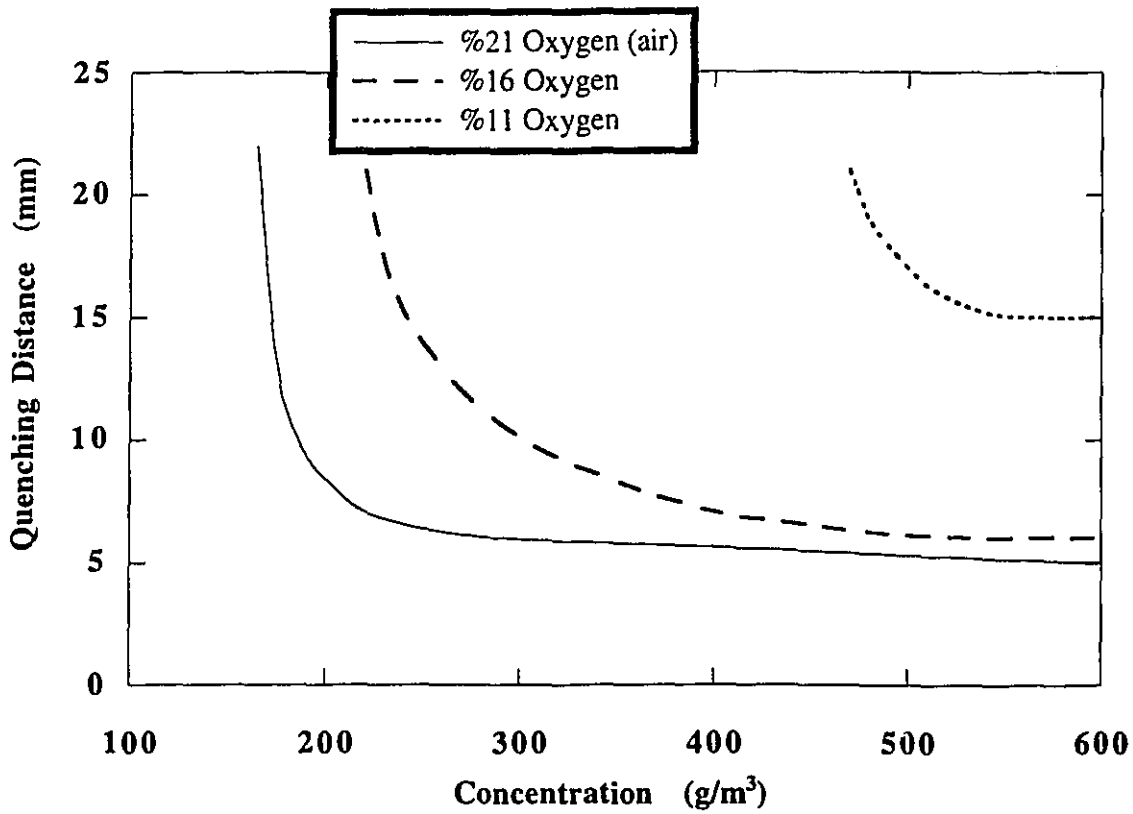

Figure 9: **Experimental results of aluminum dust flame quenching distance for different initial oxygen concentrations as a function of dust concentration.**

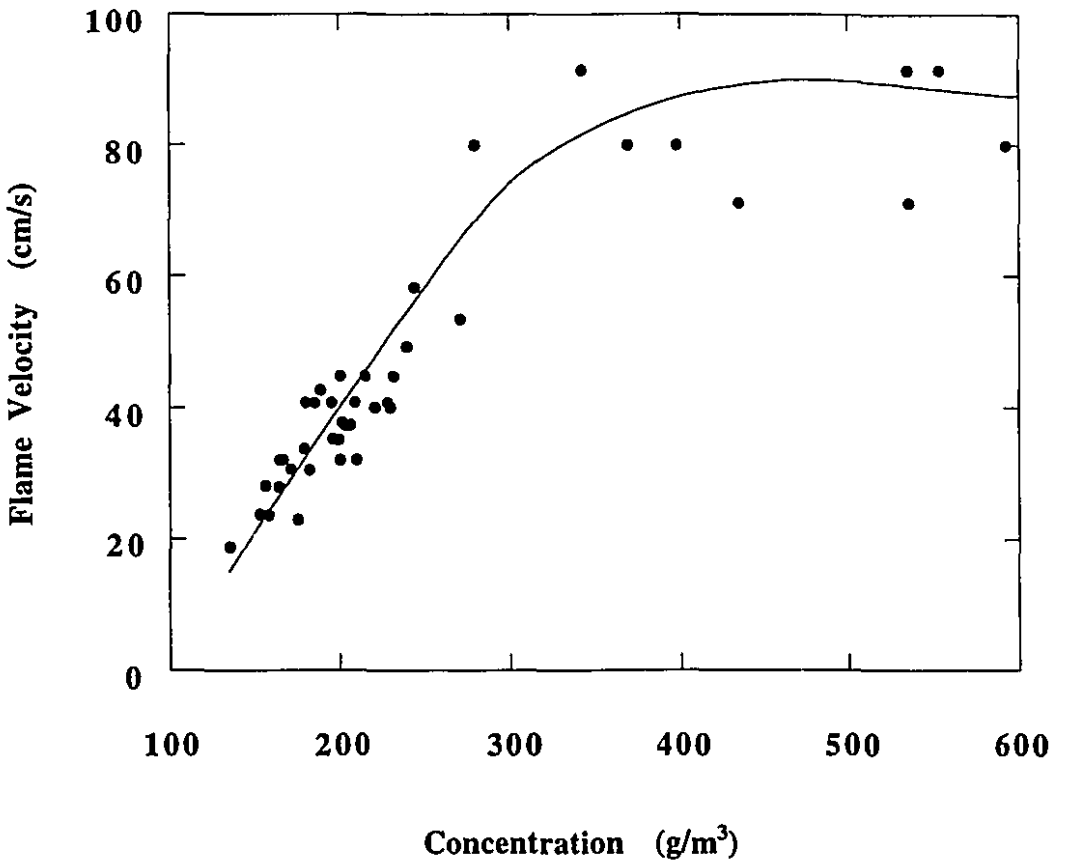

Figure 10: Experimental results of aluminum dust-air flame velocity as a function of dust concentration.

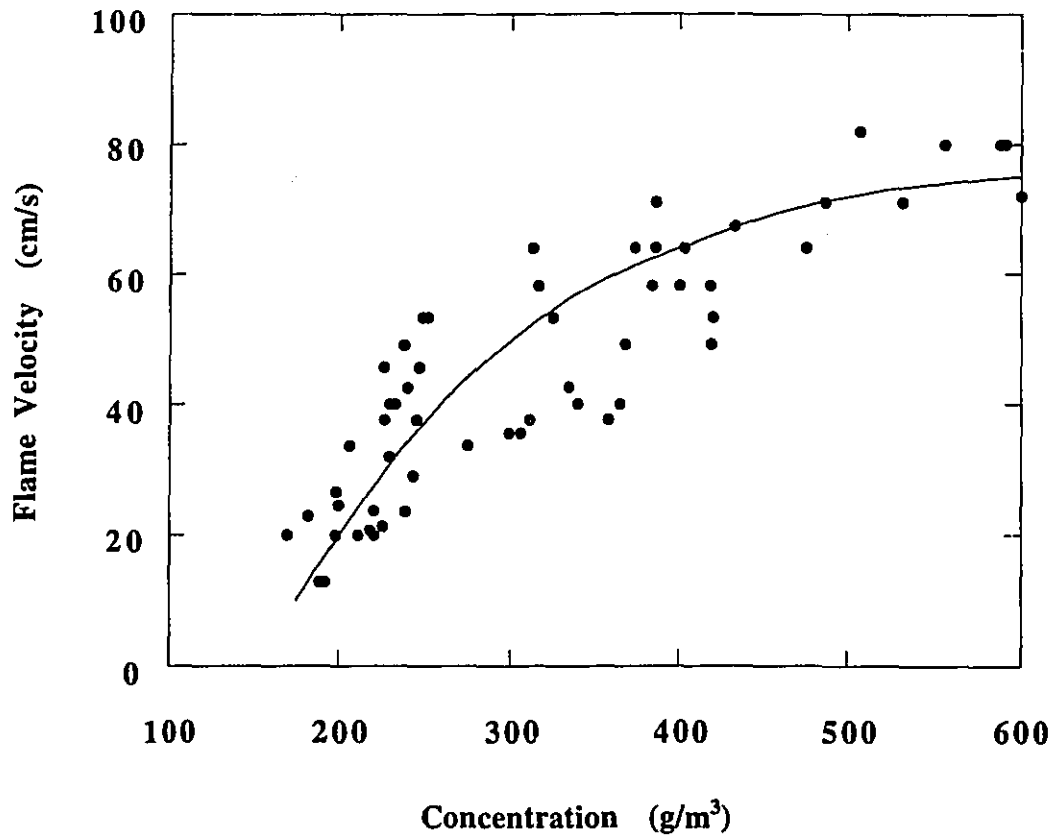

Figure 11: **Experimental results of aluminum dust flame velocity for 16% initial oxygen concentration as a function of dust concentration.**

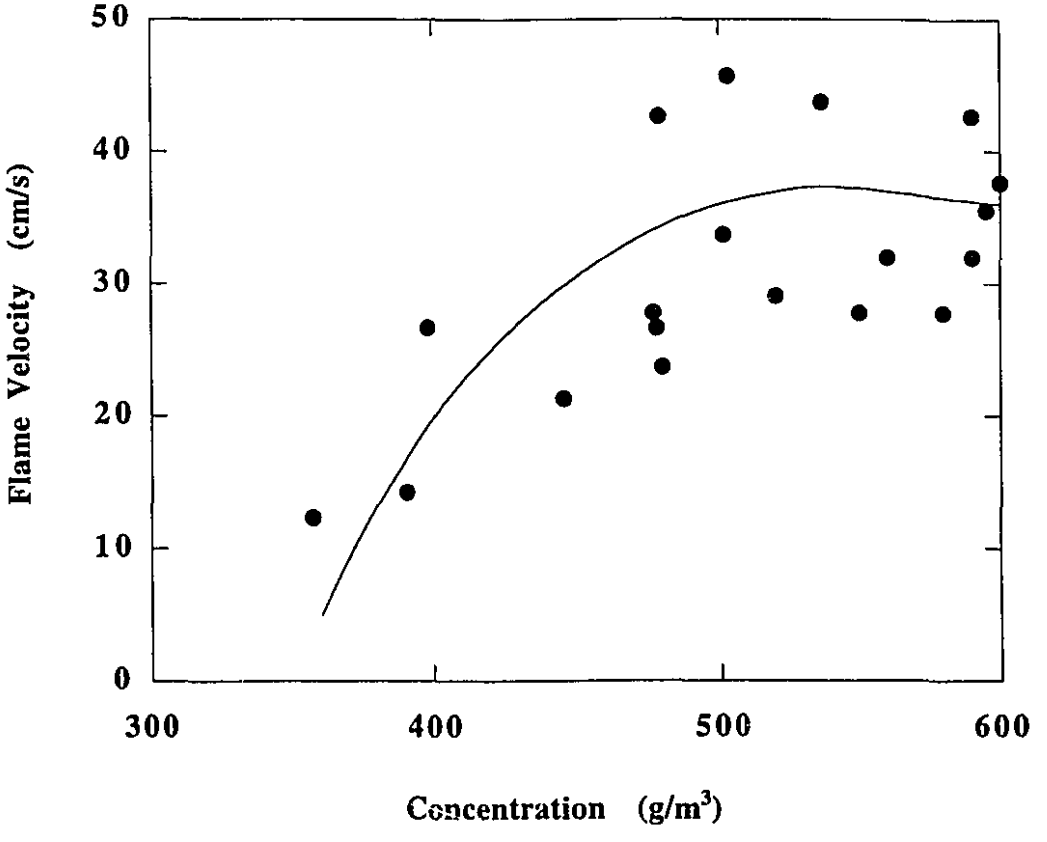

Figure 12: Experimental results of aluminum dust flame velocity for 11% initial oxygen concentration as a function of dust concentration.

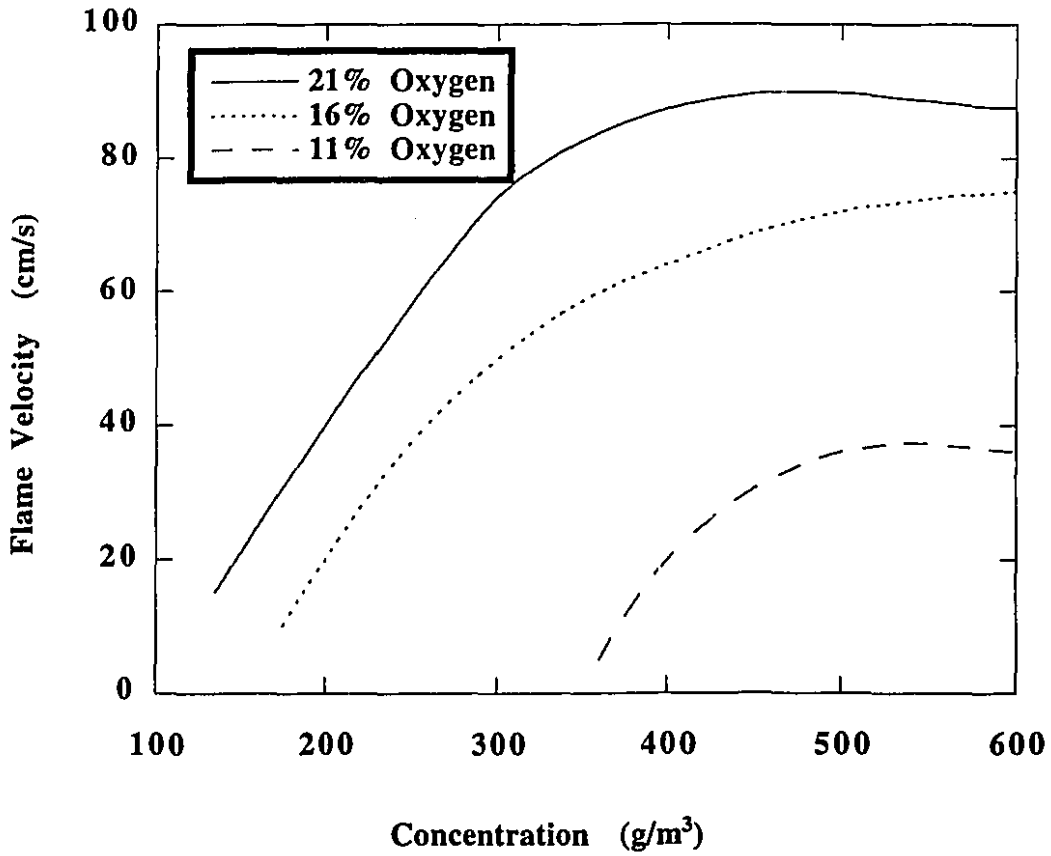

Figure 13: Experimental results of aluminum dust flame velocity for different initial oxygen concentration as a function of dust concentration.

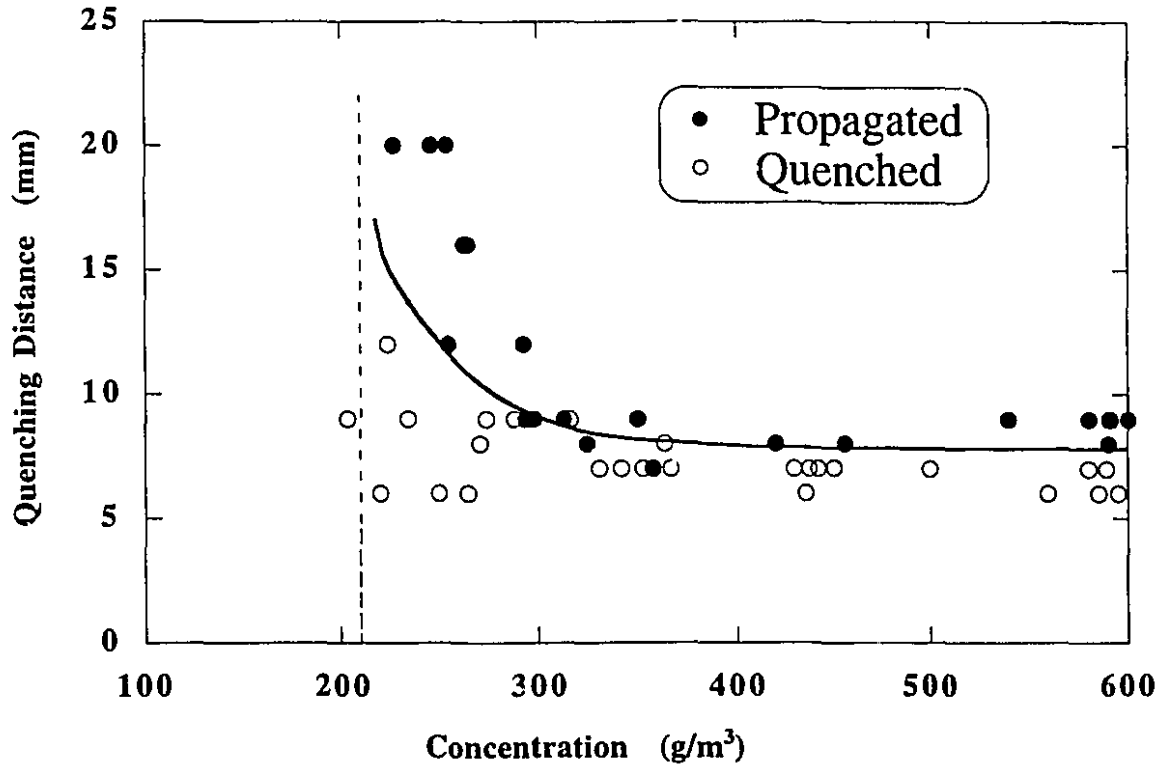

Figure 14: **Experimental results of aluminum-21% oxygen-79% helium flame quenching distance as a function of dust concentration.**

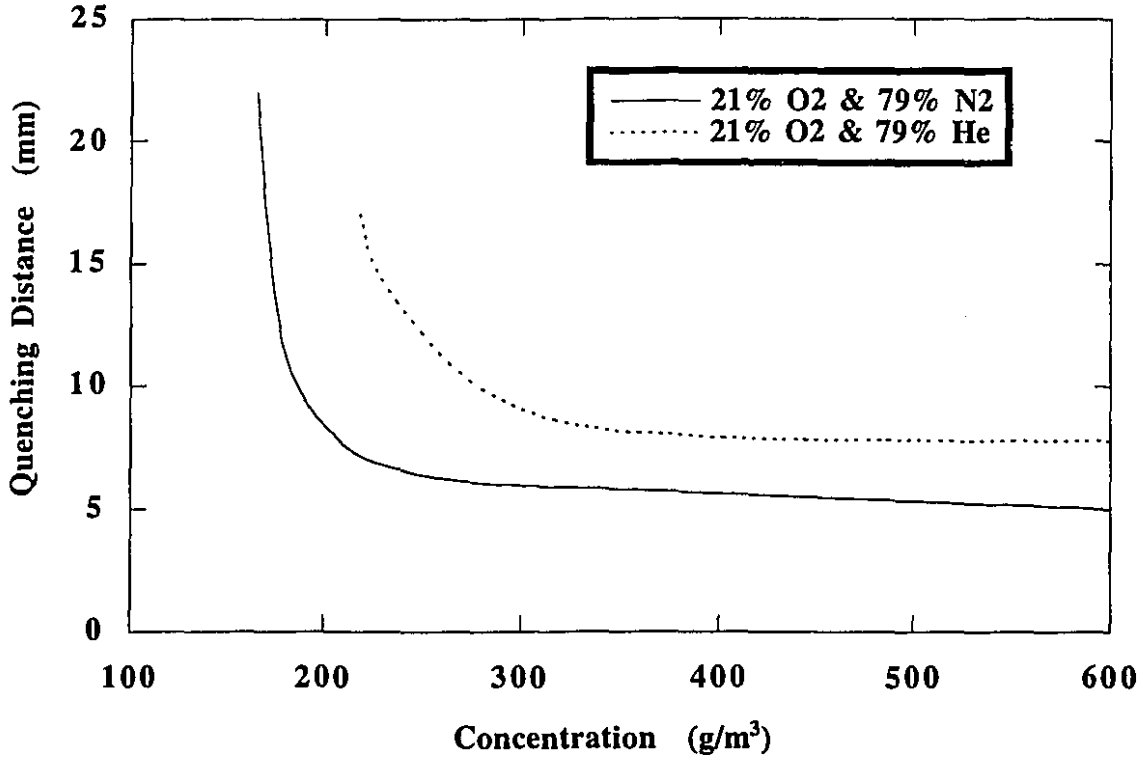

Figure 15: **Comparison of the quenching distance for different inert gases: nitrogen and helium.**

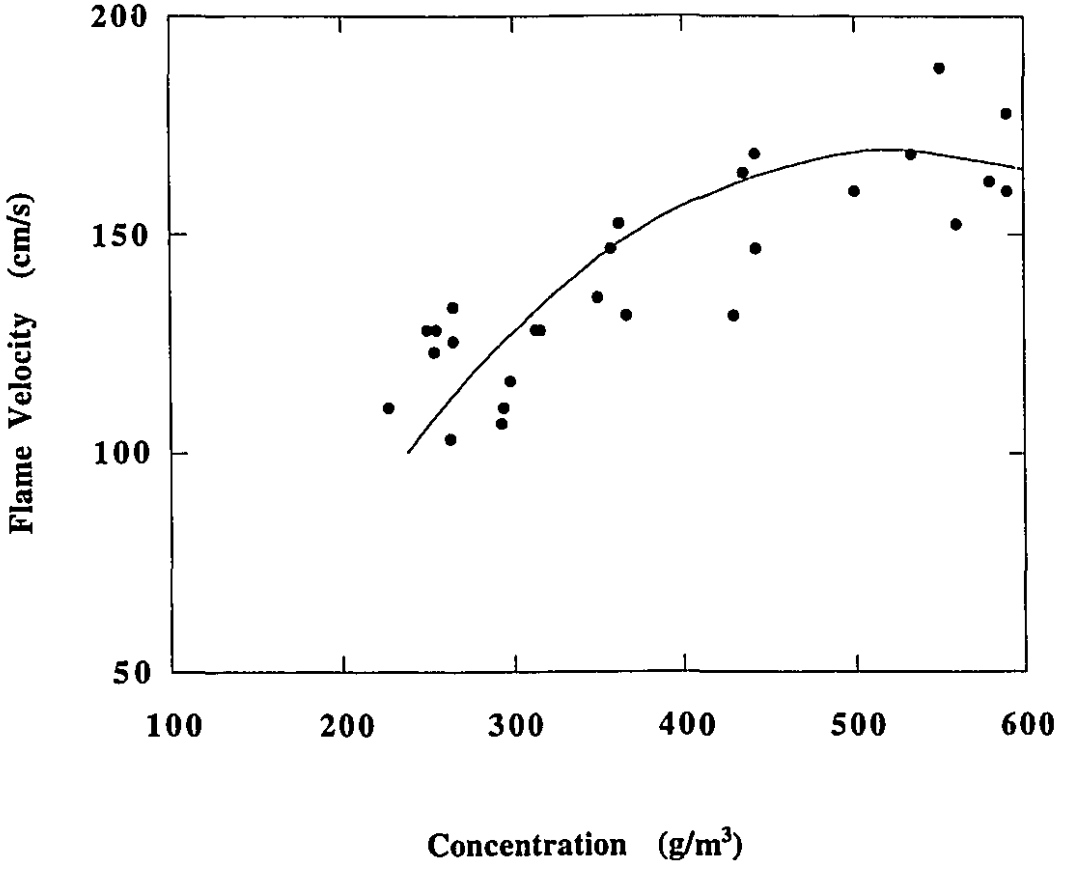

Figure 16: Experimental results of aluminum-21% oxygen-79% helium flame velocity as a function of dust concentration.

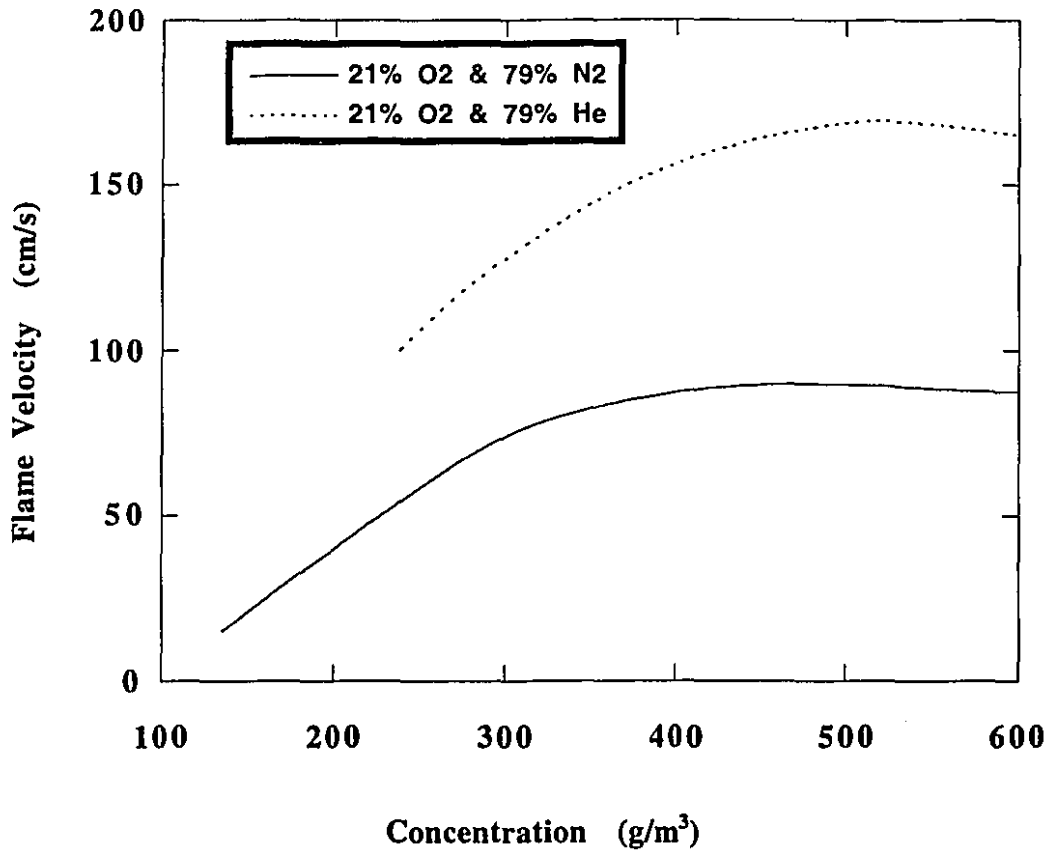

Figure 17: **Comparison of the flame velocity for different inert gas; nitrogen and helium.**

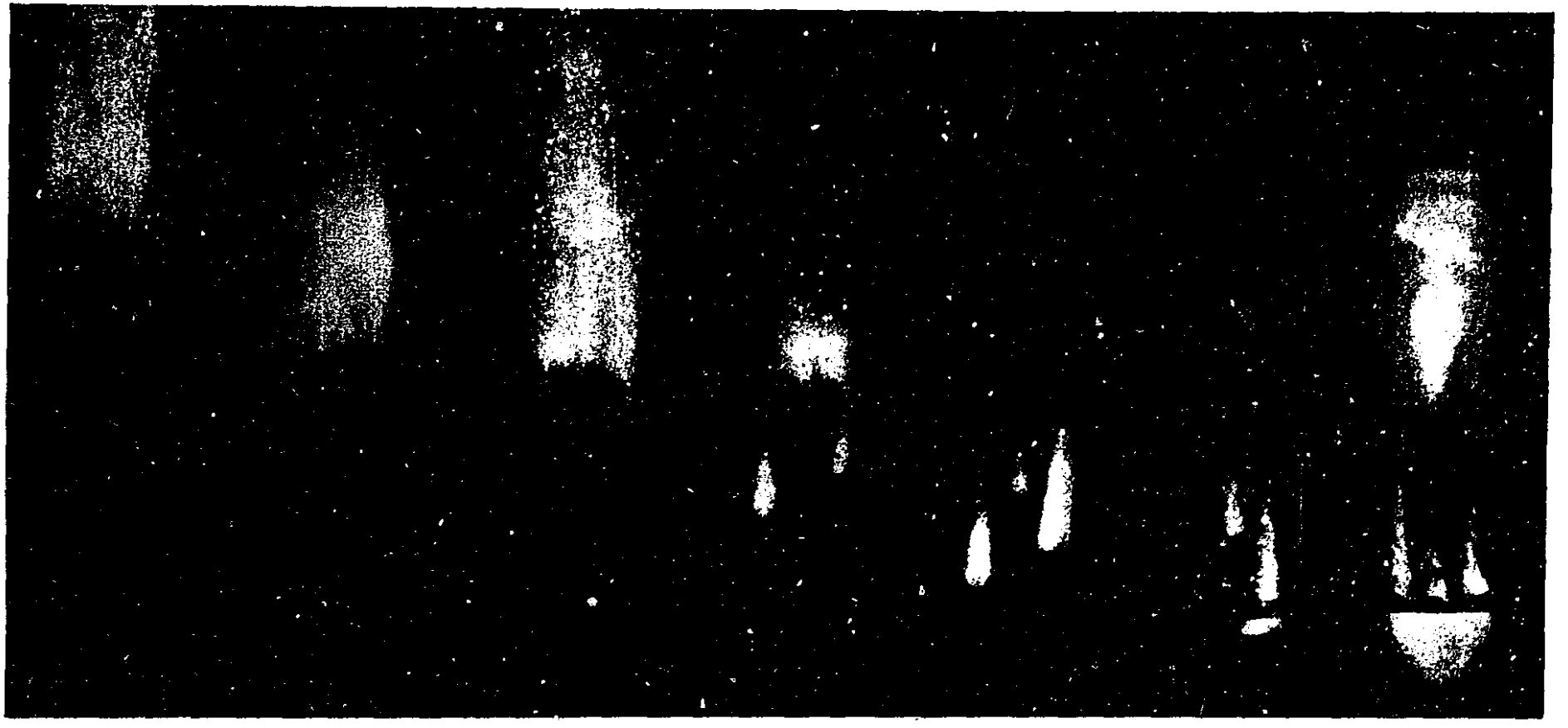

1- t=0 ms 2- t=50 ms 3- t=100 ms 4- t=150 ms 5- t=200 ms 6- t=250 ms 7- t=300 ms

2 cm

Figure 18: Photographic records of the aluminum dust-air flame propagation through quenching plates (d=9 mm, and σ = 200 gr/m^3).

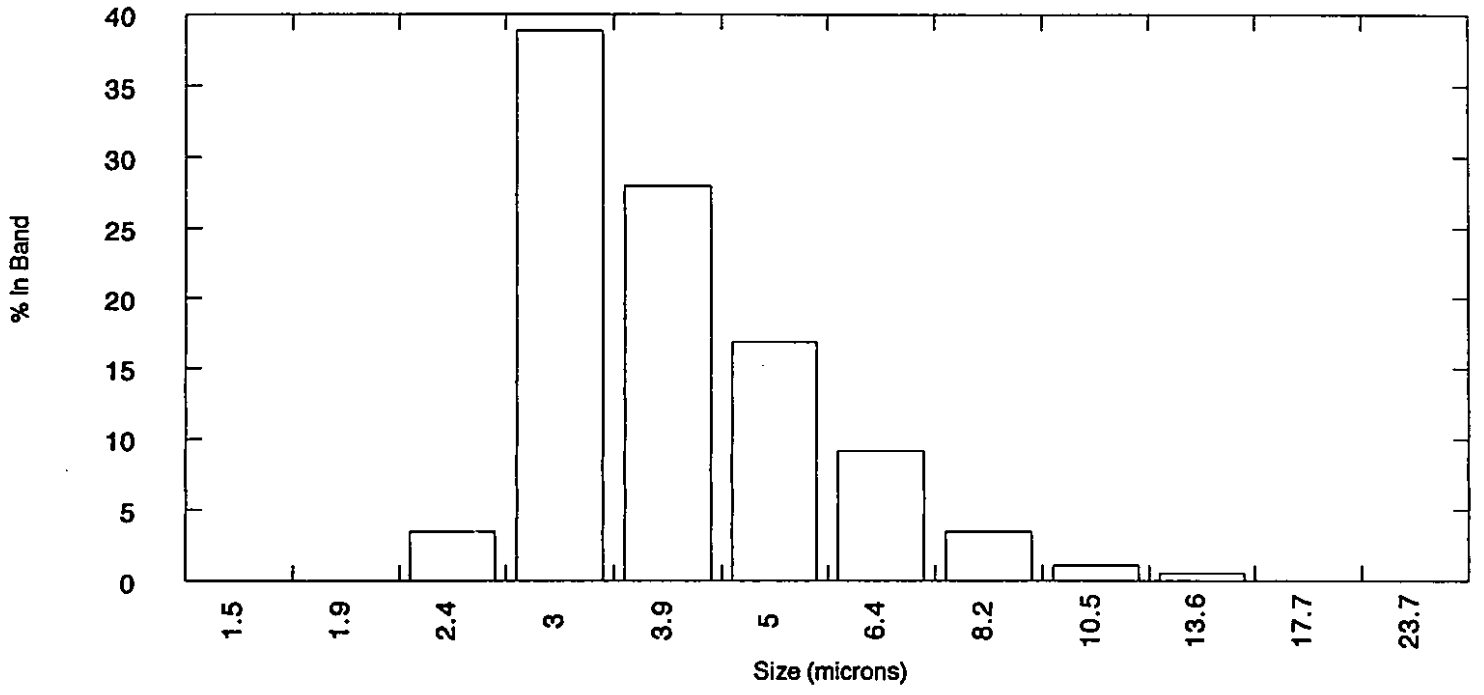

Figure 19: Number distribution of aluminum Ampal dust (Ampal 637).

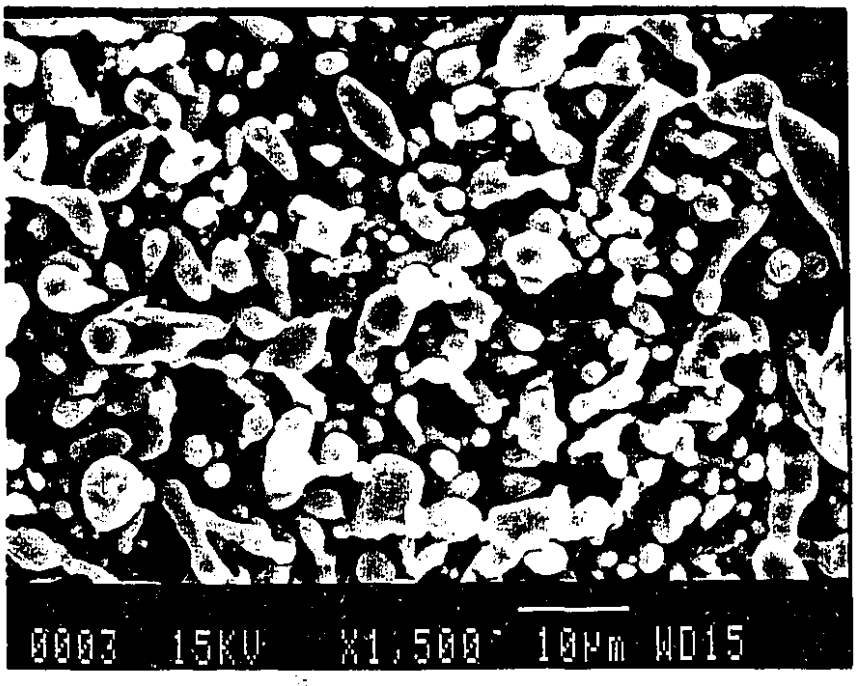

Figure 20: Scanning electron microscope photograph of the aluminum particles (Ampal 637).

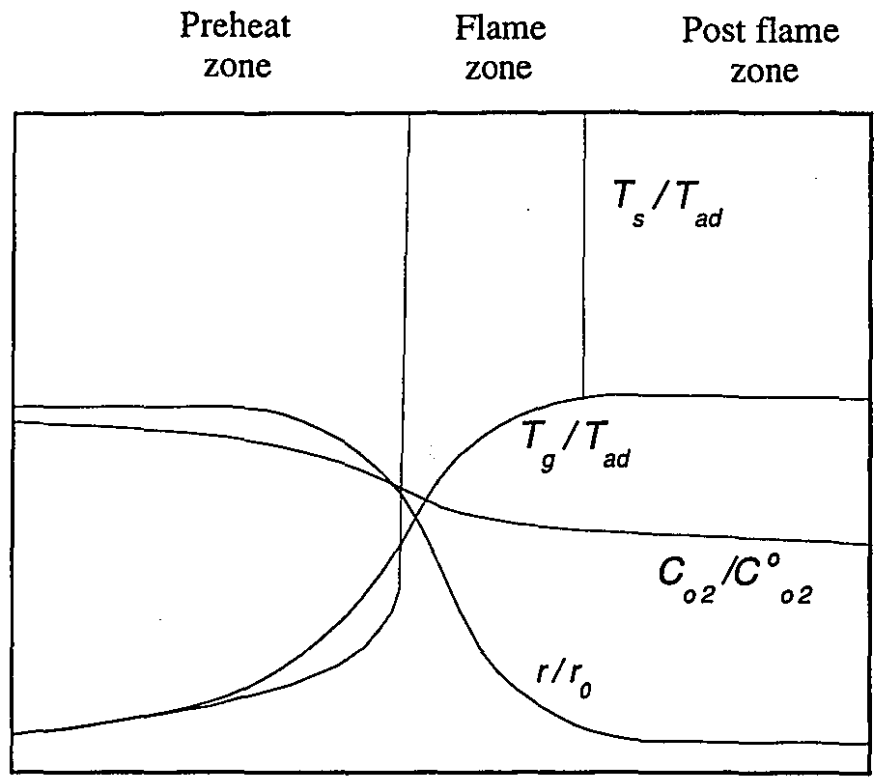

Figure 21: **Schematic illustration of the presumed flame structures of lean mixtures at adiabatic condition.**

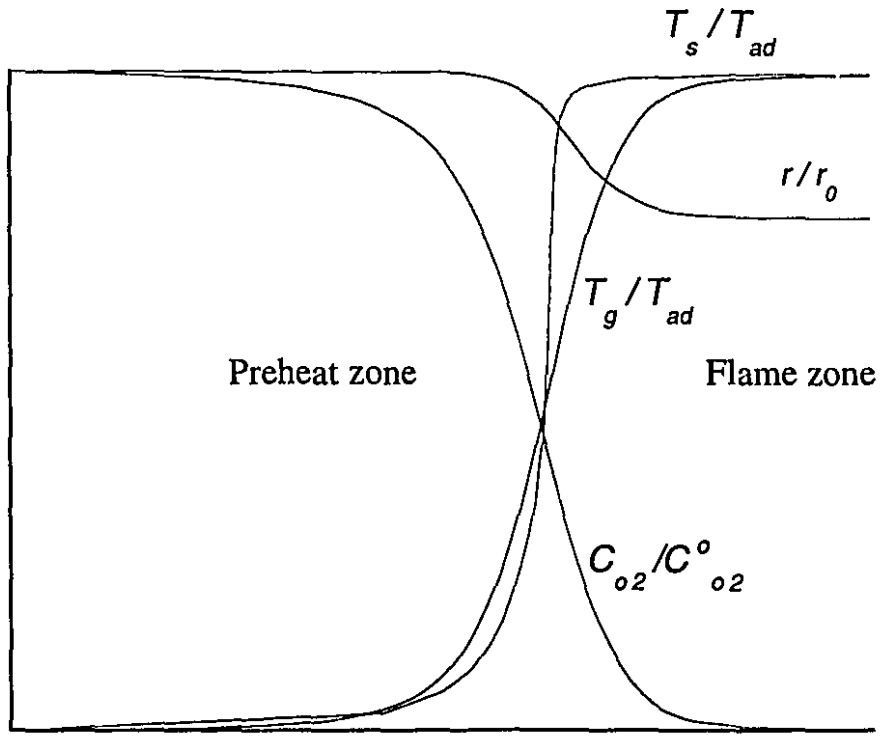

Figure 22: Schematic illustration of the presumed flame structures of rich mixtures at adiabatic condition.

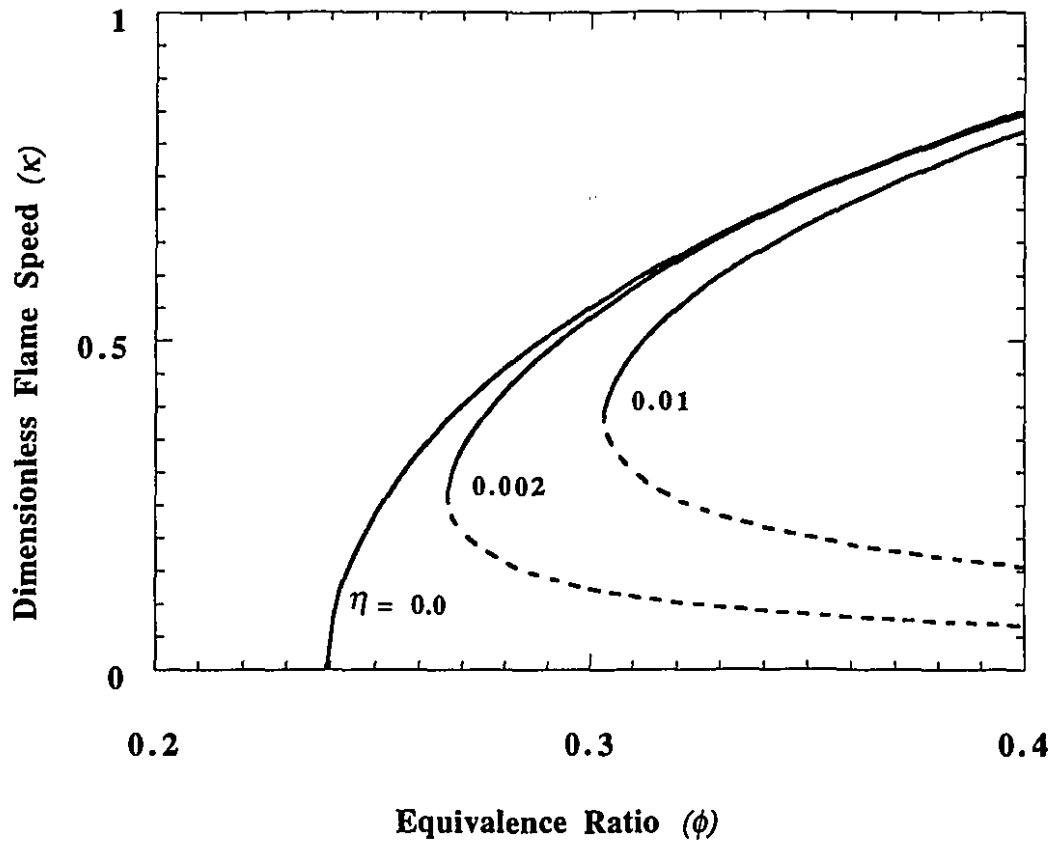

Figure 23: The dependence of dimensionless flame speed κ on fuel equivalence ratio ϕ under different values of heat loss parameters for lean mixtures.

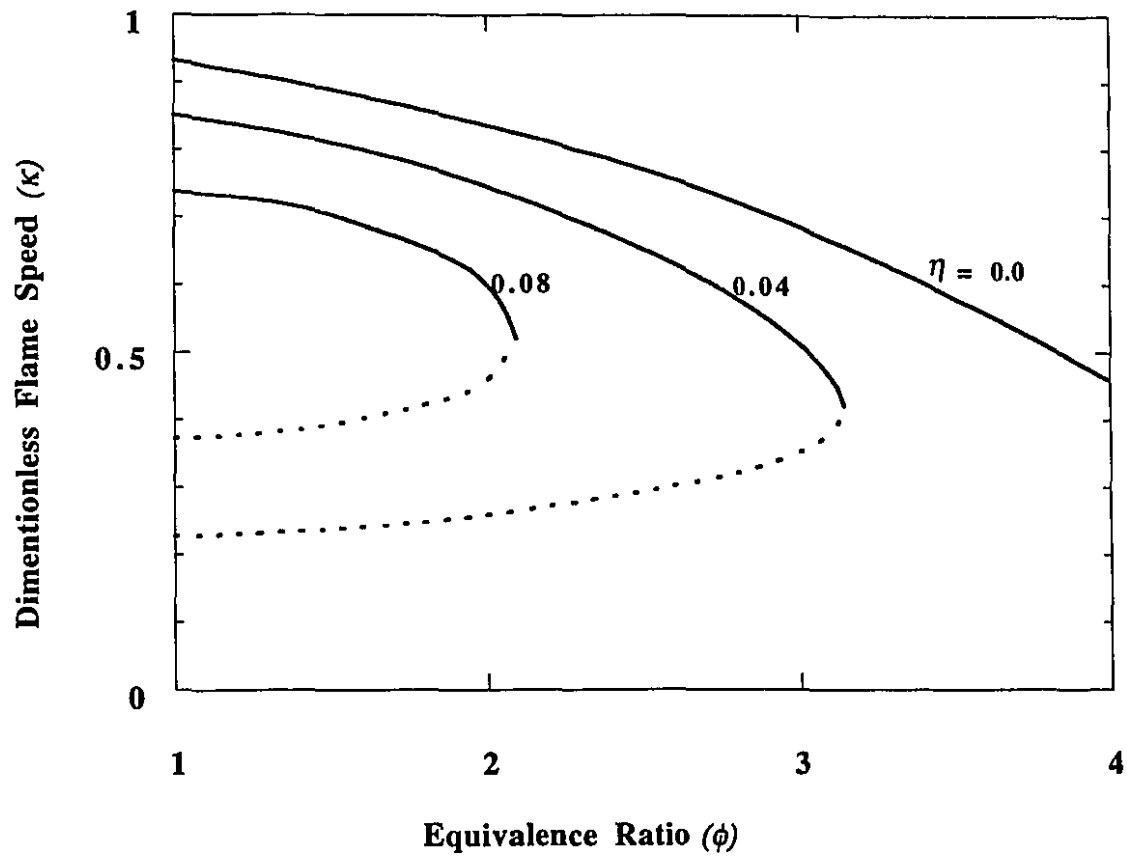

Figure 24: The dependence of dimensionless flame speed κ on fuel equivalence ratio ϕ under different value of heat loss parameters for rich mixtures.

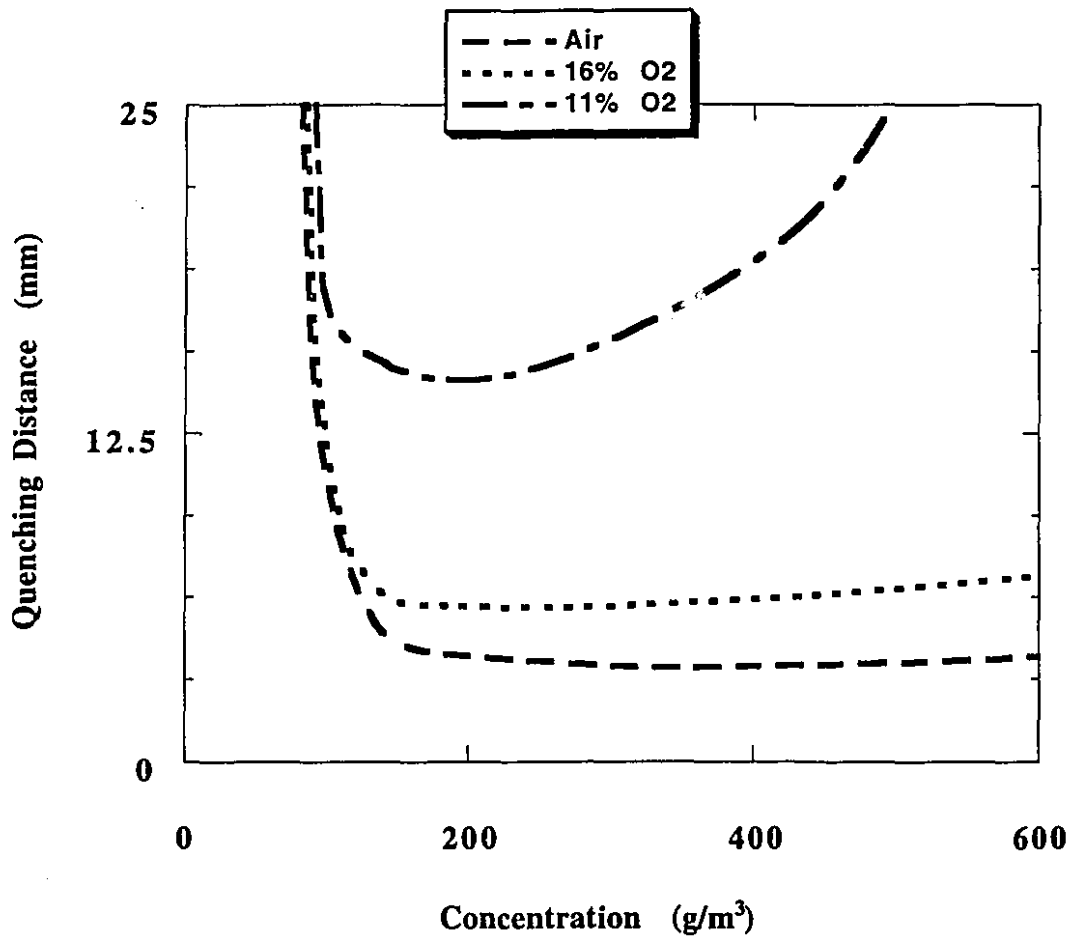

Figure 25: Theoretical results of aluminum dust flame quenching distance for different initial oxygen concentration as a function of dust concentration.

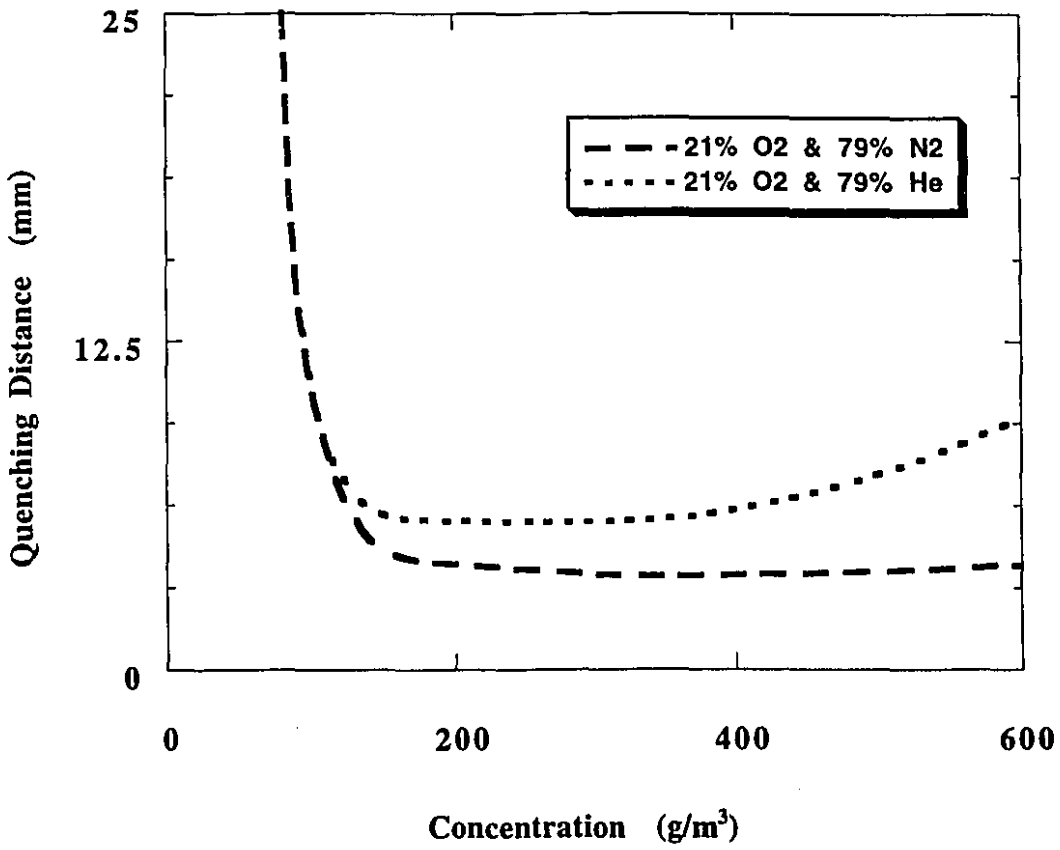

Figure 26: **Theoretical results of the comparison of quenching distance of different inert gases: nitrogen and helium.**

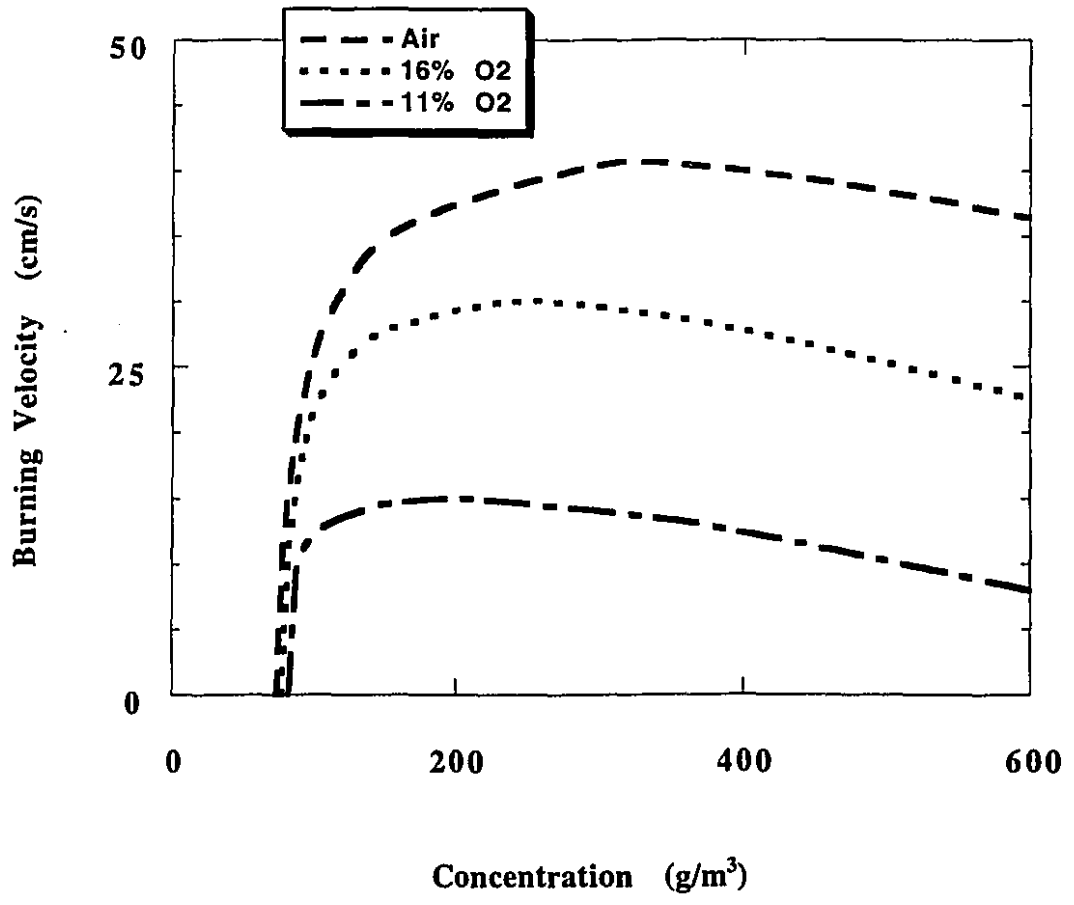

Figure 27: Theoretical results of aluminum dust flame velocity for different initial oxygen concentration as a function of dust concentration.

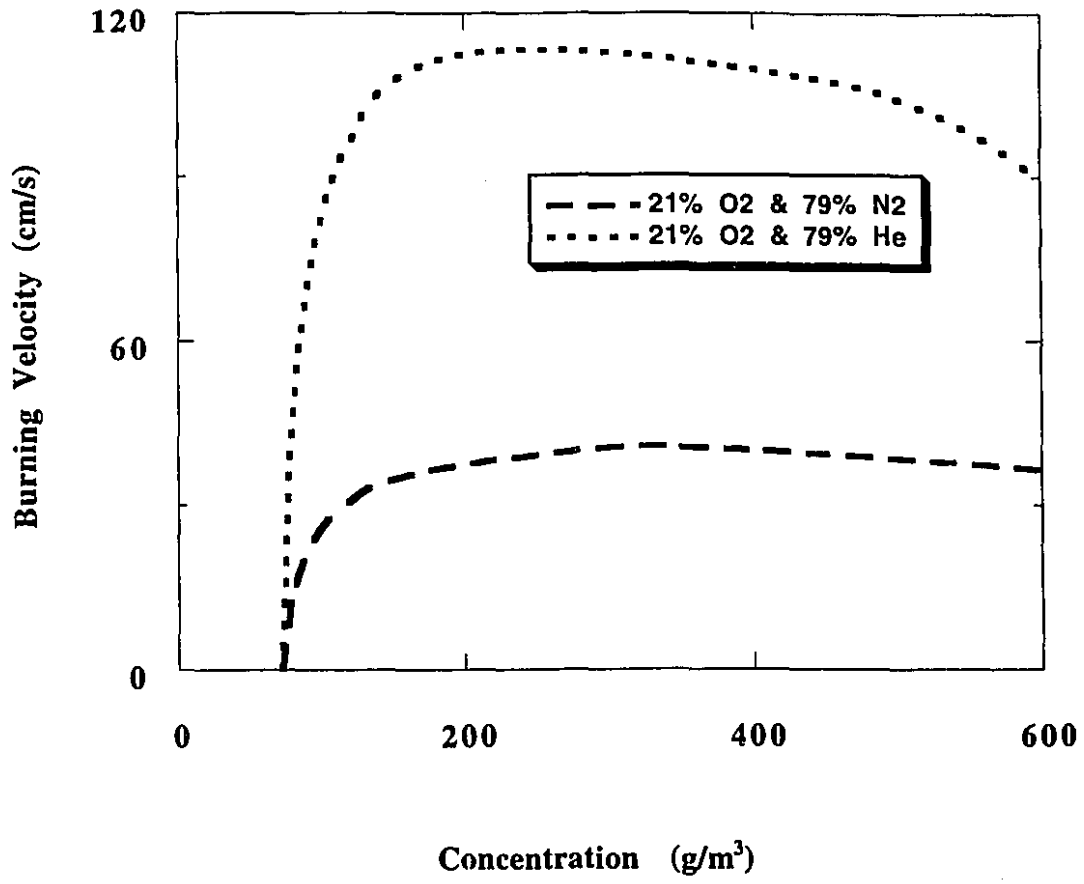

Figure 28: **Theoretical results of the comparison of the flame velocity of different inert gases: nitrogen and helium.**

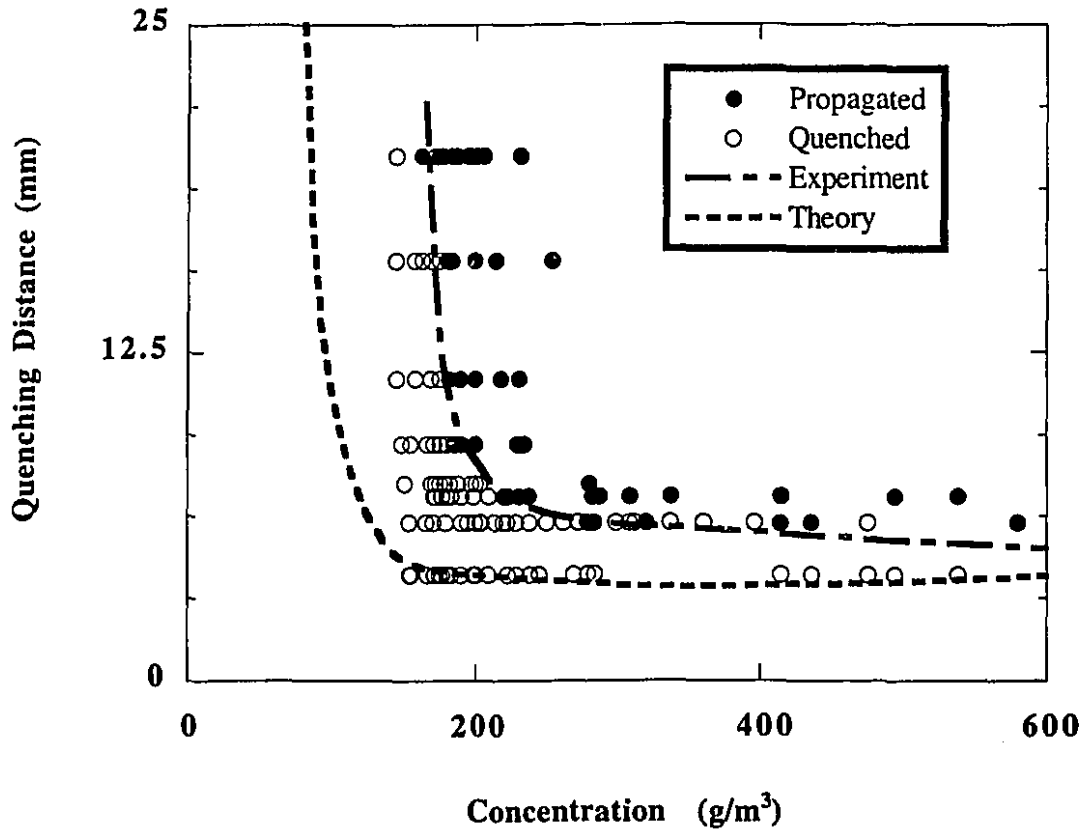

Figure 29: **Experimental and theoretical results of the quenching distance of aluminum dust-air flames.**

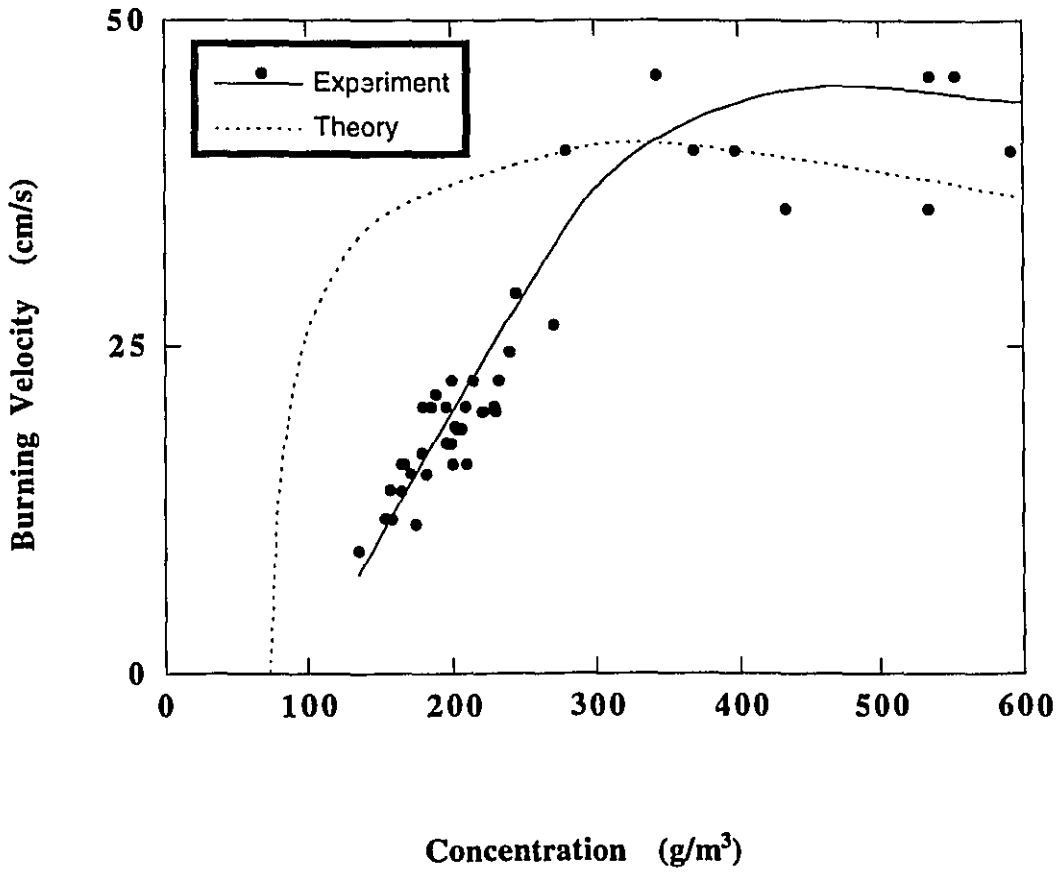

Figure 30: **Experimental and theoretical results of the burning velocity of aluminum dust-air flames.**

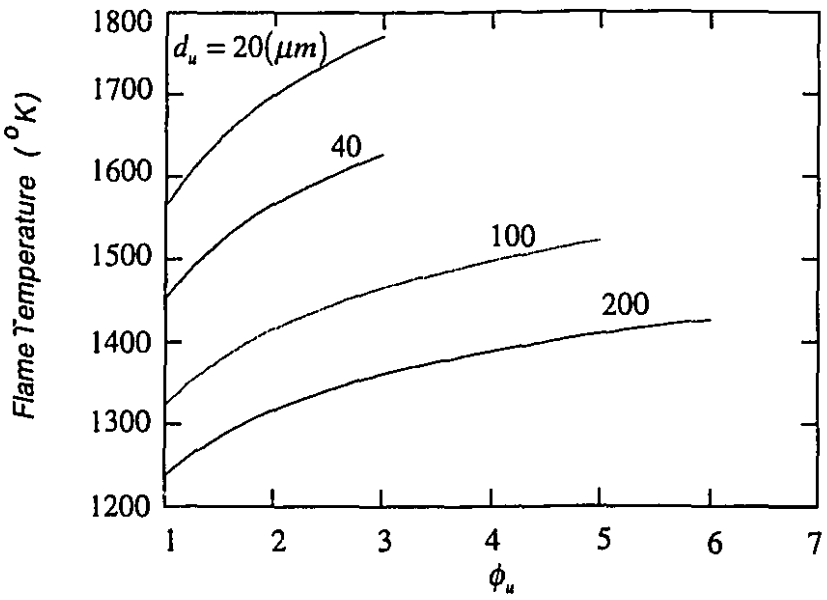

Figure 31: Calculated values of the flame temperature in the reaction zone, $T_f(^\circ K)$ at adiabatic$(\kappa' = 1)$, as a function of ϕ_u for various $d_u(\mu m)$.

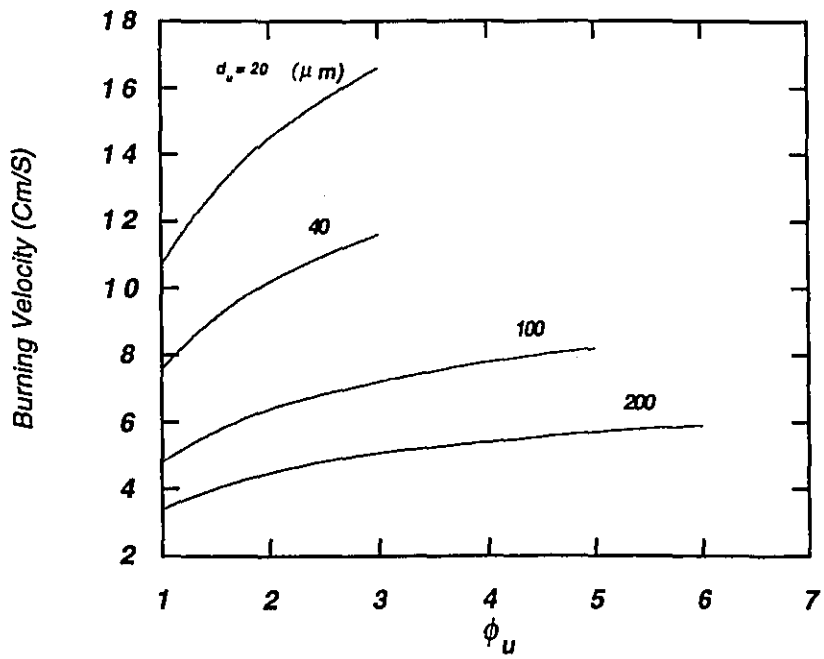

Figure 32: Calculated values of the burning velocity $v_u(cm/s)$ at adiabatic $(\kappa' = 1)$ as a function of ϕ_u for various of $d_u(\mu m)$.

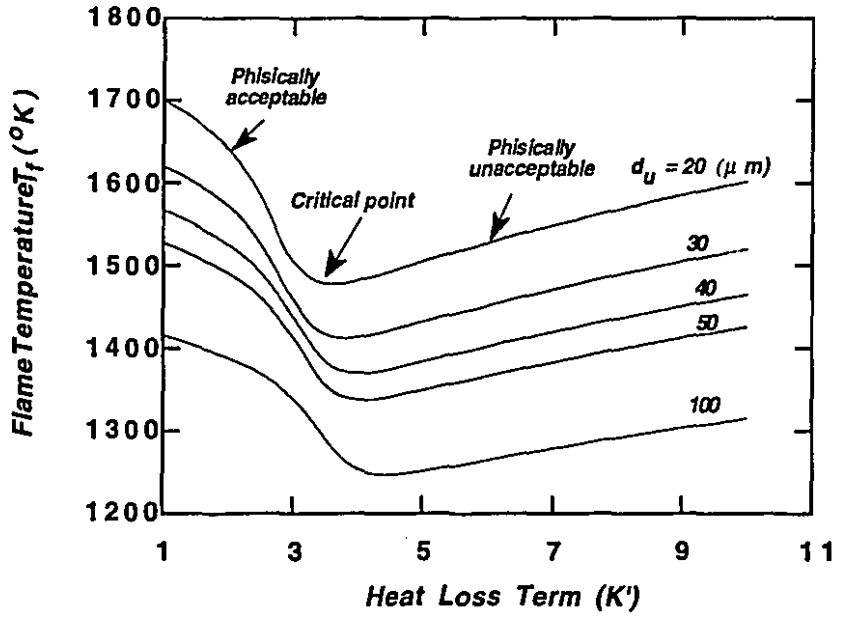

Figure 33: Calculated values of the flame temperature in the reaction zone $T_f(^{\circ}K)$ for $\phi_u = 2$ as a function of heat loss term (κ') for various of $d_u(\mu m)$.

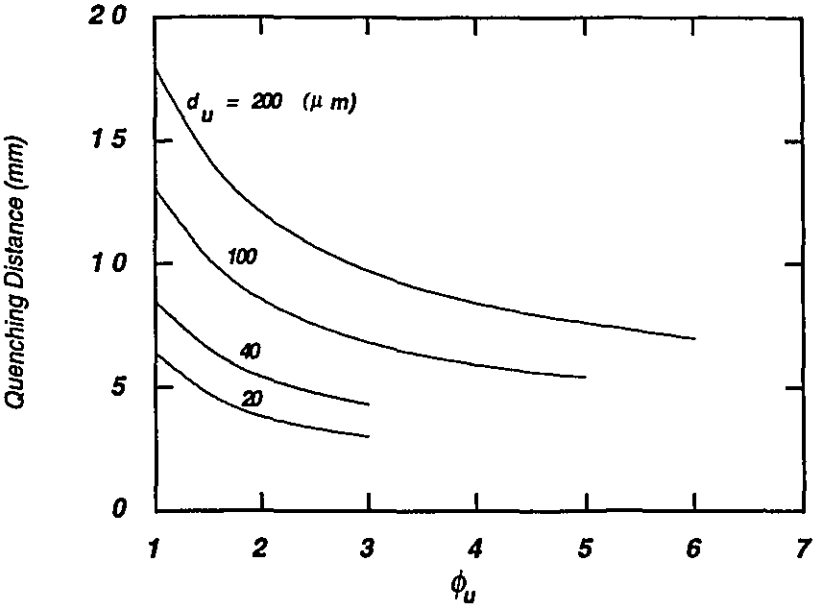

Figure 34: Calculated values of dust flame quenching distances $d_q(mm)$ as a function of ϕ_u for various $d_u(\mu m)$